FLUORIDE FIBER LASERS

by

Junfeng Wang

_____

A Dissertation Submitted to the Faculty of the

JAMES C. WYANT COLLEGE OF OPTICAL SCIENCES

In Partial Fulfillment of the Requirements
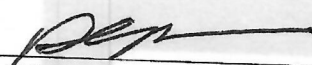
For the Degree of

DOCTOR OF PHILOSOPHY

In the Graduate College

THE UNIVERSITY OF ARIZONA

2022

THE UNIVERSITY OF ARIZONA
GRADUATE COLLEGE

As members of the Dissertation Committee, we certify that we have read the dissertation prepared by **Junfeng Wang**, titled *Fluoride Fiber Lasers* and recommend that it be accepted as fulfilling the dissertation requirement for the Degree of Doctor of Philosophy.
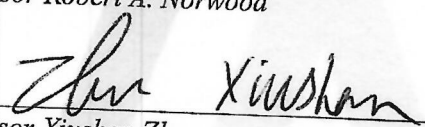
_____   Date: 6/29/22
Professor Nasser N. Peyghambarian

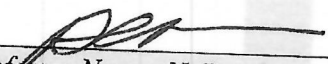_____   Date: 6/29/22
Professor Robert A. Norwood

_____   Date: 06/29/2.22
Professor Xiushan Zhu

Final approval and acceptance of this dissertation is contingent upon the candidate's submission of the final copies of the dissertation to the Graduate College.

I hereby certify that I have read this dissertation prepared under my direction and recommend that it be accepted as fulfilling the dissertation requirement.

_____   Date: 6/29/22
Professor Nasser N. Peyghambarian
Dissertation Committee Chair
Wyant College of Optical Sciences

ACKNOWLEDGEMENTS

When I finish my Ph.D program in the College of Optical Sciences, I want to acknowledge a lot of people that have been helpful to me, both in academic and non-academic aspects.

Firstly, I would like to take this opportunity to express my sincere gratitude to my academic advisor Dr. Nasser Peyghambarian who financially supported my research during my Ph.D program. Without his help I cannot conduct my research in College of Optical Sciences.

I would also like to thank my research advisor Dr. Xiushan Zhu who has been directly supervising my research and gives me tremendous help in the past years. Without his guidance and persistent support this dissertation would not have been accomplished.

I am very grateful for Dr. Robert A. Norwood serving as my dissertation committee and providing valuable suggestions.

I would like to thank Lizhu Li, Minghong Tong, Lloyd J. LaComb Jr., Leonid Kotov, Shijie Fu, Valery Temyanko, Jingwei Wu, Khawlah Al Yahyaei, Masoud Mollaee, Noah Allen Hovde, Gregory W Kaminski, Viktor Dubrovin, Qingru Wang, Yuchen Wang, Jing Zhang, Yunxiu Ma, Honglian li, Enci Chen for their help and useful discussions.

I also would like to express my thanks to Linda Schadler, Majid Behabadi and Elena Temyanko, Mark Rodriguez, Jini Kandyil for their help and important administrative work.

Important roles in my PhD life are played by many good friends outside my lab. Firstly, I would like to express my special thanks to my roommates Sifang Cui, Xuan Wang. They treat me as a family member and keep me from feeling lonely. I wish them all to have a bright future.

Finally, an immeasurable gratitude goes to my parents for their endless love, support, encouragement and sacrifice.

Table of Contents

List of Tables

List of Figures

10

Abstract

Compared to other laser platforms, fiber lasers have the advantages of outstanding heat dissipating capability, high power scalability, excellent beam quality, inherent simplicity and compactness, robust manufacturing and maintenance, and hermetically guided laser beams. Fiber lasers have seen significant progress in various aspects of laser performance, including high power/energy, short pulse duration, narrow spectral linewidths, and improved efficiency during the past sixty years. It is worth noting that most of these achievements were accomplished with silica fibers. Different from silica fibers usually producing lasers only at the 1 μm, 1.55 μm, and 2 μm wavelength regions, fluoride fibers are of great interest for generating lasers from ultraviolet to mid-infrared due to their low phonon energy and the ultra-wide transparency window of fluoride glass. In this dissertation, dysprosium (Dy^{3+}) doped fluoride fiber lasers at 3 μm and holmium (Ho^{3+}) doped fluoride fiber lasers at 1.2 μm were investigated.

To date, research activity on 3 μm fiber lasers has been focused on erbium (Er^{3+}), Ho^{3+} and Dy^{3+} doped fluoride fiber lasers. Compared to Er^{3+} and Ho^{3+} doped fluoride fiber lasers that generally produce lasers below 3 μm, Dy^{3+}-doped fluoride fiber lasers have attracted significant attention recently because Dy^{3+} has a much broader emission spectral bandwidth in the 3 μm wavelength region and is able to produce laser radiation up to 3.4 μm. However, most Dy^{3+}-doped fiber lasers have been pumped with fiber lasers or solid-state lasers at the absorption

15

peaks of Dy^{3+} at 1.1 μm, 1.3 μm, 1.7 μm, and 2.8 μm, where commercial high-power laser diodes are unavailable. We proposed to solve this problem by using Er^{3+} synthesized Dy^{3+}-doped fluoride fibers, which allow us to develop compact 3.4 μm fiber lasers pumped with low-cost high-efficiency diodes at 980 nm. In my Ph.D research, spectroscopic studies on Er^{3+}-, Dy^{3+}-, and Dy^{3+}/ Er^{3+} -doped fluoride glasses was first conducted to confirm efficient energy transfer from Er^{3+} to Dy^{3+} in the Er^{3+}/Dy^{3+} co-doped system when pumped at 980 nm. Then a custom Dy^{3+}/Er^{3+}-doped fluoride fiber was designed and fabricated and Dy^{3+}/Er^{3+}-doped fluoride fiber lasers beyond 3 μm were demonstrated with low-cost high efficiency diode laser pumps at 980 nm. Moreover, a diode-pumped wavelength tunable fiber laser with a tuning range from 2.71 to 3.37 μm was demonstrated.

In addition to 2 and 3 μm fiber lasers, Ho^{3+}-doped fluoride fibers have been demonstrated as high efficiency gain media for 1.2 μm lasers. In this dissertation, a diode-pumped mode-locked Ho^{3+}-doped fluoride fiber laser at 1.2 μm was demonstrated with a ring-cavity laser incorporated with a carbon-nanotube saturable absorber. Stable mode-locked pulses with an average power of 1 mW at a repetition rate of 18.47 MHz were obtained at a pump power of 348 mW. The pulse energy and peak power of this mode-locked laser oscillator were estimated to be about 54 pJ and 12.6 W. The pulse duration was measured to be 4.3 ps by an autocorrelator.

Chapter 1. Introduction and Background.

1.1. Fiber lasers.

"Laser" is an acronym for "Light Amplification by Stimulated Emission of Radiation", created in 1957 by Gordon Gould, although the conceptual foundation for the laser was Albert Einstein's proposal that photons could create stimulated emission of identical photons from excited atoms [1]. The term is nowadays mostly used for laser oscillator related devices generating light based on laser principles. The world's first laser was demonstrated in 1960 by Theodore H. Maiman [2,3]; a flash lamp was used to pump the ruby crystal to achieve a solid-state laser. Nearly in the same year, the first gas laser was made [4]. Since then, many different types of lasers, such as gas lasers, liquid lasers and solid-state lasers have been developed.

Typical gas lasers include CO_2 lasers [5-6], helium-neon lasers [7], excimer lasers [8] and argon ions lasers [9]. The CO_2 laser is a molecular gas laser with emission in the long-wavelength infrared spectral region (10.6 μm) and mostly used for processing machines and marking applications. The helium-neon laser is a type of gas laser whose gain medium consists of a mixture of helium and neon gases and mostly used in measurement systems with a low output. Ultraviolet lasers, excimer lasers and argon ions lasers are predominantly used in semiconductor exposure equipment.

Compared to other types of lasers, solid-state lasers are currently the most preferred for factors relating principally to their performance, reliability and minimal required maintenance. The solid-state laser efficiency is generally higher than that of the gas lasers we mentioned above. The solid-state laser output power can vary from milliwatts to kilowatts for different applications. Both continuous-wave and pulsed outputs can be readily achieved by solid state lasers.

A fiber laser is a kind of solid-state laser which uses doped optical fiber as the gain medium. A basic all-fiber configuration of a fiber laser is shown in Figure 1.1.1 (a); it consists of a doped fiber performing as the gain medium and a pair of fiber Bragg gratings (FBGs) forming the oscillation cavity. Optical fiber is a cylindrical waveguide that has a core with high refractive index and a cladding with low refractive index as shown in Figure 1.1.1 (b). It exhibits outstanding thermal performance due to its high surface to volume ratio which provides for rapid heat dissipation. The spatial distribution of the optical mode in the fiber is well-confined which ensures low cavity optical loss and good beam quality. The broad gain linewidth of rare earth doped fiber enables ultrashort pulse operation and wide wavelength tunability. An all-fiber laser system also benefits from significantly improved compactness and reduced alignment difficulty during laser operation.
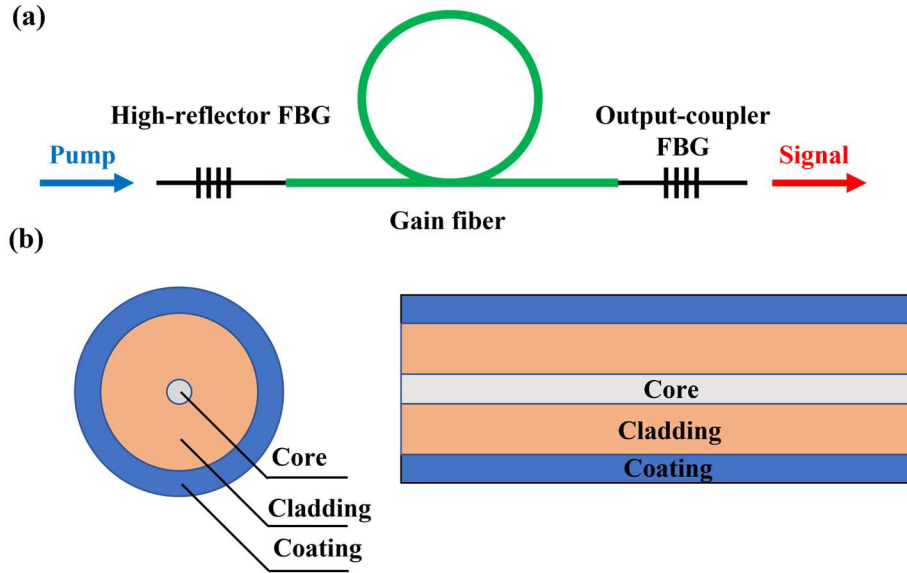
Fig. 1.1.1. (a) Basic configuration of a fiber laser. (b) Basic structure of single cladding step-index optical fiber.

The first fiber laser was demonstrated in 1964 [10], and intense research interest has been focused on fiber lasers since the work of Payne in 1985 [11,12]. Sixty years of development in fiber lasers has resulted in greatly improved laser performance and a broad range of applications. At present, the emission wavelengths of fiber lasers cover from the ultraviolet to the visible, infrared, and even to the mid-infrared region [13-19]. In 1994, micro-watt scale lasing around 381 nm has been observed in neodymium-doped fluoride glass fibers at room temperature [13]. Other than conventional laser pumping schemes to achieve lasers operating in the visible wavelength region [14], other promising techniques such as second harmonic generation and up-conversion lasing [15] have also been applied to the production of visible coherent radiation. Fiber lasers operating at infrared and mid-infrared region [16-19] also attract intense research interest due to their application to molecular spectroscopy, medical

treatment, oxygen remote sensing, noninvasive medicine and biomedical diagnostics [20-24].

In the next section, we will introduce some laser fundamentals that will help us understand both the physical mechanisms and important parameters for lasers in general.

1.2. Laser fundamental.

1.2.1. Absorption, spontaneous emission, and stimulated emission.

Particles in a quantum mechanical system can only take on certain discrete values of energy, known as energy levels. In this section, we will discuss absorption, spontaneous emission and stimulated emission based on energy level diagrams.

Absorption is the process where the optical energy of a photon is converted to the internal energy of electrons. As illustrated in Figure 1.2.1, when a photon with some specific frequency ν is absorbed, the photon energy ($h\nu$) causes an electron in the ground state (E_1) to go to a higher energy level (E_2). As specific atoms have certain energy level gaps, only photons with a certain frequency can be absorbed to raise the electrons out of the ground state, which leads directly to the observation of an absorption spectrum, where transmission is reduced at those optical frequencies corresponding to a difference in energy between the ground state and a given excited state.
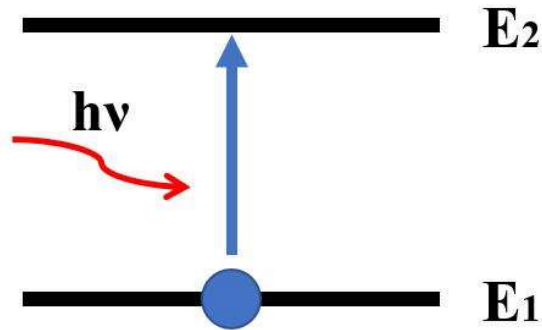
Fig. 1.2.1. Partial energy level diagram illustrating absorption of a photon.

Spontaneous emission is an energy conversion process where the excited electron in a higher energy level decays to a lower energy level without interactions with other photons and emits a photon with certain frequency as shown in Figure 1.2.2 with $E_2 - E_1 = h\nu$. The average decay time by spontaneous emission is called the spontaneous emission lifetime. The spontaneous lifetime varies from material to material, with the process usually occuring within nanoseconds, while it can take as long as seconds in some kinds of materials. Energy is conserved during the decay process; there are radiative decay channels where the energy is converted to an electromagnetic wave (photons) and non-radiative decay channels where the energy is converted to heat or molecular vibrations. Black body radiation is also a kind of spontaneous emission.
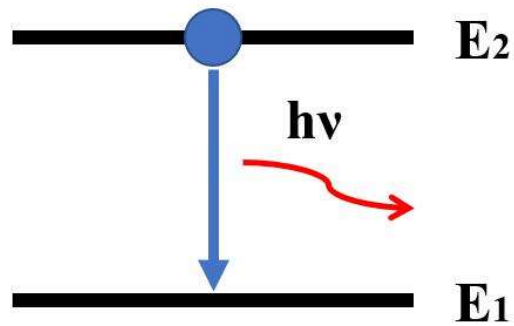
Fig. 1.2.2. Partial energy level diagram illustrating spontaneous emission of a photon.

Stimulated emission is an energy conversion process where the excited electron in a higher energy level decays to a proper lower energy level through interactions with other photons and emits a photon at a certain frequency as shown in Figure 1.2.3. The stimulated emission photon will have the same frequency, direction, phase, and electromagnetic polarization as the incoming photon which initiated the process.
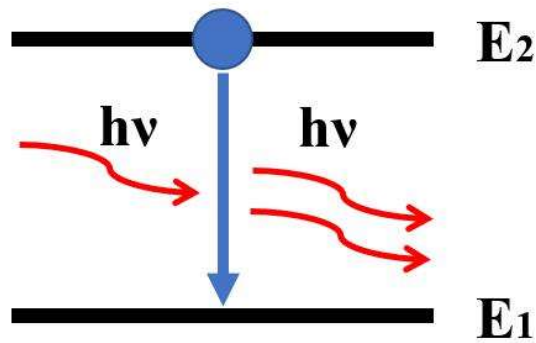
Fig. 1.2.3. Partial energy level diagram illustrating stimulated emission.

In laser physics, transition cross sections are used to quantify the probability of optically induced events. We will briefly introduce two kinds of transition cross

sections here, the absorption cross section and the emission cross section. We can measure the absorption of the material to calculate its absorption cross section and measure the fluorescence of the material to calculate its emission cross section. The absorption and emission cross sections of holmium doped ZBLAN glass is illustrated in Figure 1.2.4.   In most cases, there is a McCumber relation [25] that relates the absorption and emission cross sections.
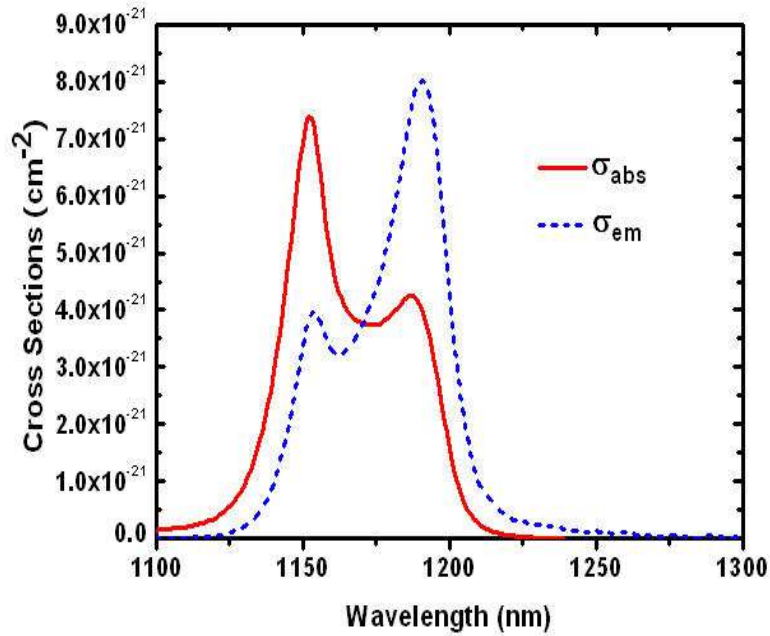
Fig. 1.2.4. Absorption and emission cross sections of holmium-doped ZBLAN glass.

1.2.2. Rate equations and population inversion.

We have discussed absorption, spontaneous emission, and stimulated emission processes in the last section, and we are going to discuss what factors determine the rate of these processes in this section.

As shown in Figure 1.2.4, assume two energy levels are involved, the lower state (E_1) is the ground state and the upper state is the excited state (E_2). The number of electrons per unit volume in the ground state is denoted as N_1 and the number of electrons per unit volume in the excited state is denoted as N_2.
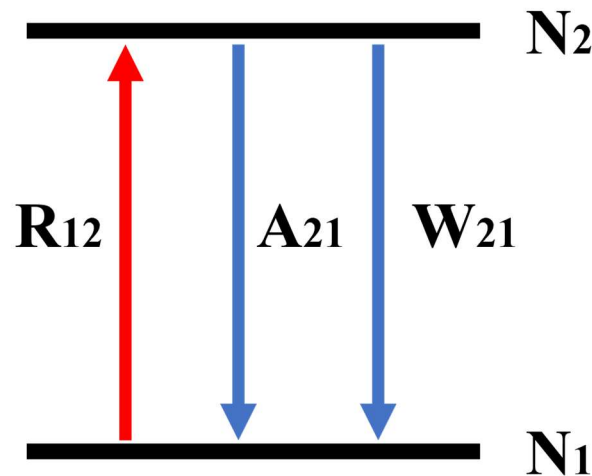
Fig. 1.2.4. Partial energy level diagram for analyzing rate equations.

The rate of the absorption process can be represented as Equation 1.1, where B is known as the Einstein B coefficient and u is related to the spectral energy density per unit bandwidth; we will discuss the process for specific cases in Chapter 2 where the coefficient R is defined. Absorption can only occur when

there are electrons in the ground state and it is proportional to the number of electrons in the ground state. Moreover, the absorption rate also depends on the number of incoming photons.

$$\frac{dN_1}{dt}\bigg|_{abs} = -B_{12}N_1u = -R_{12}N_1 \qquad\qquad (eq.\,1.1)$$

The rate of the spontaneous emission process can be represented by Equation 1.2; it clearly depends on the number of electrons in the excited state. The constant A is called the Einstein A coefficient, which is related to the lifetime of an electron in the energy level.

$$\frac{dN_1}{dt}\bigg|_{spon-emi} = A_{21}N_2 \qquad\qquad (eq.\,1.2)$$

The rate of the stimulated emission process can be represented as in Equation 1.3, it is dependent on the number of electrons in the excited state. As stimulated emission requires incoming photons, the spectral energy density per unit bandwidth also influence the process rate. We are going to discuss specific cases in Chapter 2 where the coefficient W will be defined and used.

$$\frac{dN_1}{dt}\bigg|_{sti-emi} = B_{21}N_2u = W_{21}N_2 \qquad\qquad (eq.\,1.3)$$

According to equations from eq. 1.1 to eq. 1.3, we can see that the process rate is related to the number of electrons in each energy level and the input photon densities. When a photon with a certain frequency is absorbed and the electrons are excited to a higher energy level, the number density of electrons in

the ground state decreases and the number density of the electrons in the excited state increases. After photons are emitted from the excited state, the number density of the electrons in the higher energy level decreases and the number density of the electrons in the ground state increases. Equation 1.4 represents the time rate of change of the number density of electrons in the ground state, which should ultimately be zero when the system is at steady state.

$$\frac{dN_1}{dt} = -B_{12}N_1 u + A_{21}N_2 + B_{21}N_2 u = 0 \qquad\qquad (eq.\,1.4)$$

Laser amplification can only be achieved when more than 50% of the atoms maintain electrons in the excited state; this is called population inversion. We are going to discuss rate equations with specific cases in Chapter 2 and numerical results will be analyzed there.

1.3. Fluoride fiber.

One way to increase the efficiency of a fiber laser is to increase the rare-earth doping concentration of the fiber. However, rare-earth clusters can take place at high dopant concentrations which lead to concentration quenching and photon darkening. Using fiber fabricated from special materials other than silicate glass is one method to enhance the limited doping concentration. Phosphate, germanate, chalcogenide and fluoride fibers can all serve as the host material that primarily constitutes the fiber. In this section, we will discuss the main properties of glass fibers fabricated from these different materials.

Silicate glasses are the most common hosts for rare-earth ions due to their low loss, high tunability and strength. Phosphate glasses allow very high doping concentrations of rare-earth ions and are primarily used for high gain fibers. The high gain coefficient of phosphate fiber enables an efficient fiber laser with a short oscillation cavity that delivers single frequency output [26,27]. Fluoride and chalcogenide glasses have also attracted great attention as they were found to have low phonon energy and excellent mid-infrared transparency. These glasses can perform as the rare-earth ion host for lasers operating at visible and mid-infrared region, where the emission wavelength is difficult to obtain from silicate and phosphate fiber. In the field of laser development, fluoride glasses are more popular than chalcogenide glasses as fluoride glasses have high doping concentration limits ($\sim$10 mol.%), relatively high strength and low background loss (<0.05 dB/m). Chalcogenide glasses have good performance in nonlinear frequency generation due to their high nonlinearity [28,29] although long term efforts are needed for chalcogenide fiber lasers to advance due to their low rare-earth ion doping limit ($\sim$0.1 mol.%) and large background loss (0.5-1 dB/m). In this section, we will focus mainly on fluoride glasses and fluoride fibers.

Ohsawa reported the first ZBLAN glass (ZrF_4-BaF_2-LaF_3-AlF_3- NaF) in 1981 [30] and a molar composition of 53% ZrF_4, 20% BaF_2, 4% LaF_3, 3% AlF_3 and 20% NaF was considered the most stable glass for optical fiber application. Fluoride glass is more difficult to fabricate than silicate glass because of the strict requirements for the purity of starting materials. During all synthesis processes for fluoride fiber, the absence of water and contamination prevention should be

strictly satisfied. Moreover, ZBLAN glasses can easily crystallize as the glass transition temperature and the melting point are quite close. It is important to note that the composition of ZBLAN glass can vary, as small quantities of similar materials can be added or substituted to slightly modify the glass properties and optical properties.

Compared to silica glass, ZBLAN glasses have lower bond strengths, which leads to differences in key properties. The infrared absorption edge of ZBLAN glass is at a much longer wavelength than that of silica glass, but the stability and hardness of ZBLAN glass is much lower than that of silica glass, which increases the difficulty of working with the ZBLAN fibers. Attenuation is another important parameter for fiber optic materials; the minimum loss coefficient for ZBLAN glass is predicted to be 0.01 dB/km at 2.5 μm [31] and an attenuation coefficient of less than 1dB/km has been demonstrated in ZBLAN fibers [32]. However, the background loss of all commercially available ZBLAN fibers (10-100 dB/km) is much higher than that of commercial silica fiber (0.2 dB/km), which is due to the impurities introduced during the fabrication process. A detailed comparison of the basic properties of silica and ZBLAN glasses is given in Table 1.3.1.

Table 1.3.1. Comparison of basic properties between silica and ZBLAN glasses [114].

Glass property	Silica	ZBLAN
Approximate transmission range (1 mm thickness T > 10%) (μm)	0.16–4.0	0.22–8.0
Maximum phonon energy (cm^{-1})	1100	600
Transition temperature ($^\circ$C)	1175	260
Specific heat (J/(g·K))	0.179	0.151
Thermal conductivity W/(m·K)	1.38	0.628
Expansion coefficient (10^{-6}/K)	0.55	17.2
Density (g/cm^3)	2.2	4.33
Knoop hardness (kg/mm^2)	600	225
Fracture toughness (MPam$^{1/2}$)	0.72	0.32
Poisson's ratio	0.17	0.17
Young's modulus (Gpa)	70	58.3
Shear's modulus (Gpa)	31.2	20.5
Bulk's modulus (Gpa)	36.7	47.7
Refractive index (@ 0.589 um)	1.458	1.499
Abbe number	68	76
Zero material dispersion wavelength (μm)	1.3	1.6
Nonlinear index (10^{-13} esu)	1	0.85
Thermo-optic coefficient (10^{-6}/K)	11.9	−14.75

Compared to silica fiber, fluoride fiber exhibits higher optical transmission in the mid-infrared wavelength region (beyond 2μm) because the heavy glass constituents lead to low phonon-energy (~600 cm^{-1}). Among the energy levels of rare-earth dopants, some transitions that is not presented in silicate materials are enabled because of the low phonon-energy. Some energy levels of rare-earth dopant ions in fluoride glasses also exhibit long lifetimes compared with those in silicate fiber, allowing the realization of fiber lasers in the mid-infrared region. We will discuss continuous wave laser operation based on fluoride fiber more specifically in Chapter 3.
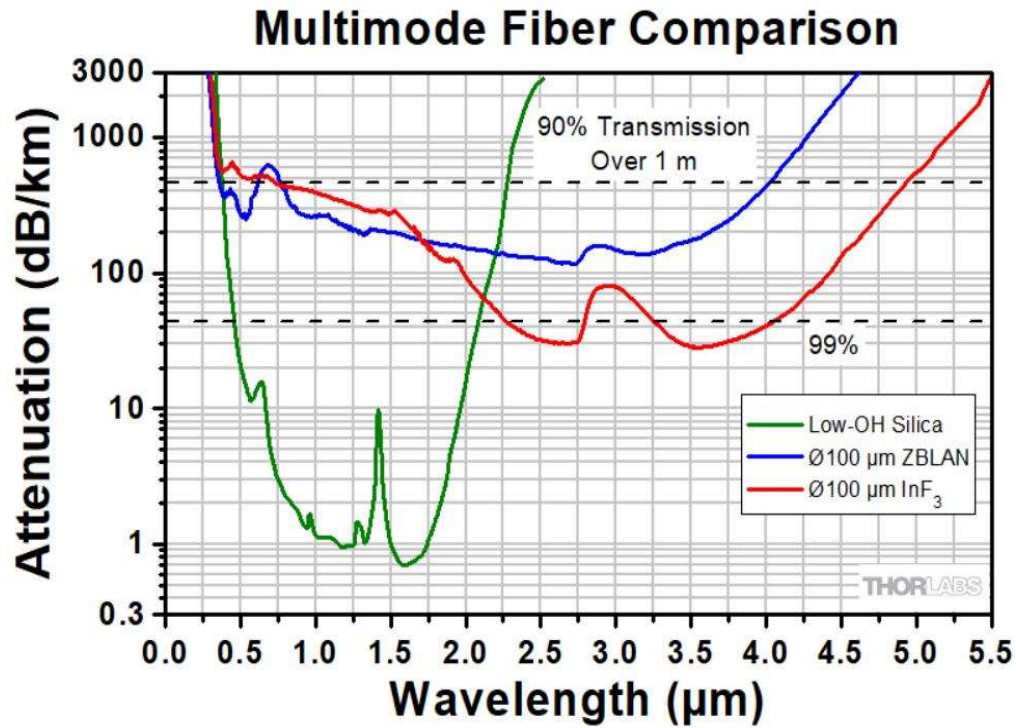
Fig. 1.3.1. Transmission of silica fiber and fluoride fiber. (From Thorlabs https://www.thorlabs.com/newgrouppage9.cfm?objectgroup_id=7062 #ad-image-0)

1.4. Pulsed fiber lasers.

Pulsed laser operation can generally be achieved by Q-switching and mode-locking techniques. Due to the broad gain bandwidth of rare-earth ion doped glass, rare-earth doped fibers have attracted great interest for laser pulse generation. Ultrafast fiber lasers with high-power output have been applied to industrial processes such as micromachining, including microscale cladding, surface texturing, welding, cutting, and drilling [33–36]. Because of the high peak power output of a pulsed laser, pulsed lasers perform as an ideal source for nonlinear photonics effects and associated applications such as optical

parametric oscillators[37-41], supercontinuum generation[42-43] and terahertz generation[44-45]. In this section, we give a brief introduction to Q-switching and mode-locking techniques.

Q-switching and mode-locking are two laser technology approaches fo achieveing pulsed lasers. Q-switching is a technique to achieve pulsed lasers by adjusting the intracavity losses and the Q-factor of the cavity. The pulses achieved by Q-switching are typically in nanosecond scale. A basic schematic of how Q-switching or mode-locking components are inserted into a laser system is illustrated in Figure 1.4.1. Various Q-switches components have been demonstrated for achieving Q-switched laser over the past decades. Q-switched fiber lasers have been demonstrated through the use of bulk or fiber coupled acoustic-optic modulators (AOM) and electro-optic modulators (EOM) [46-48], saturable absorbers [49-51], the gain switching method [52] and other Q-switched techniques [53-55].
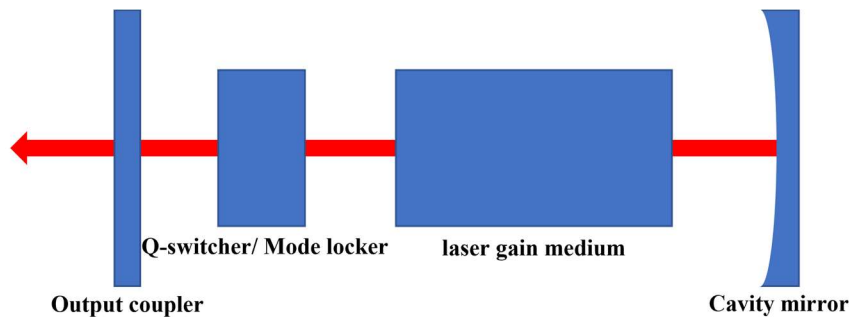
Fig. 1.4.1. Schematic of Q-switching/mode locking components in a laser system.
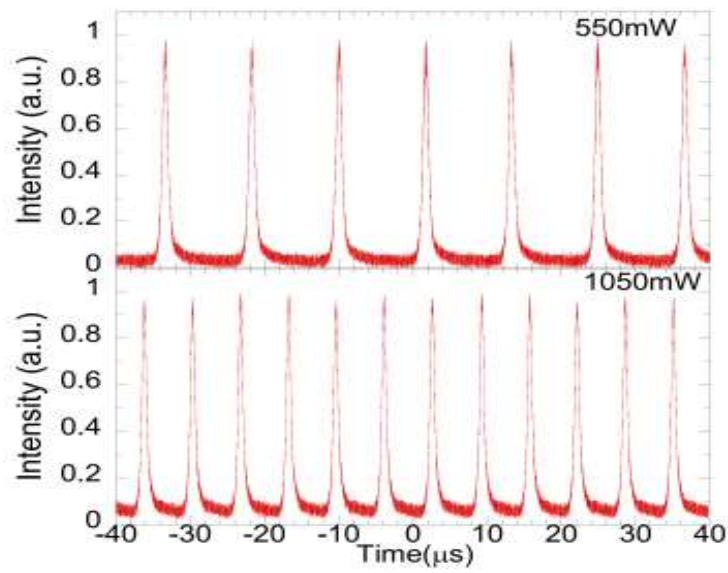
Fig. 1.4.2. Nanosecond scale pulse trains from a Q-switched laser.
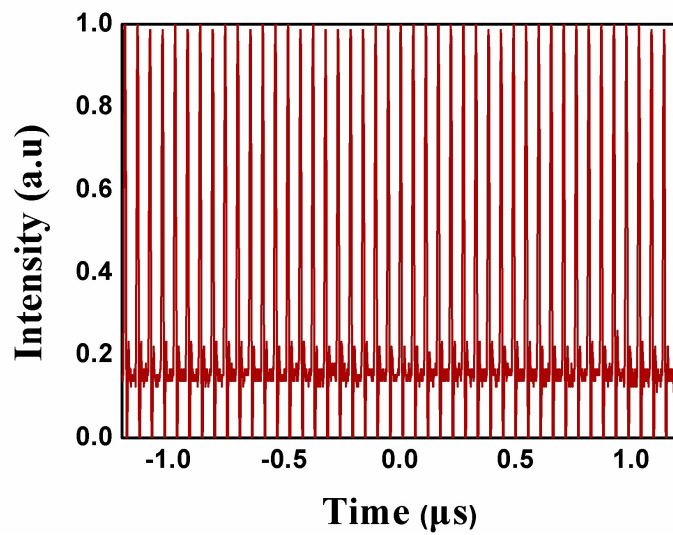
Fig. 1.4.3. Picosecond scale pulse trains from a mode-locked laser.

By locking multiple axial modes in a laser cavity, mode-locked lasers capable

of producing ultrafast laser pulses (femtosecond or picosecond pulses) with peak

powers many orders of magnitude higher than in the CW mode are of great interest. The schematic of mode-locked laser is similar with that of Q-switched laser. Mode locking components such as modulators, saturable absorbers or polarization dependent structures are usually placed in the laser cavity and lead to the formation of the ultrafast pulses. The pulses achieved by mode-locking are typically in the picosecond or femtoseconds regime[56-59]. Pulse trains from a Q-switched laser and mode-locked laser are shown in Figure 1.4.2 and Figure 1.4.3.

Besides pulsed laser in near-infrared and infrared region, various methods to achieve Q-switched lasers [60-67] and mode-locked lasers [68-77] at 3 μm are focusing on the rare-earth dopants such as erbium and holmium.

We will discuss the pulsed laser operation based on fluoride fiber more specifically in Chapter 4.

1.5 Outline of the dissertation.

Fluoride fiber lasers are of great interest for a wide range of scientific and technological applications including spectroscopy, medical surgery, free space communication, remote sensing, and material processing. In this dissertation, I report on the spectroscopic study of fluoride glasses and mid-infrared laser development based on these materials.

In Chapter 2, a spectroscopic study of rare-earth doped fluoride materials is presented. Both fluorescence spectra and lifetime of these materials have been

measured by a custom-built experimental setup and the energy transfer processes have been analyzed.

In Chapter 3, we discuss the development of mid-infrared fluoride fiber lasers based on the co-doped rare earth materials. The performance of the continuous wave operation mid-infrared laser has been analyzed and a laser tunable over a 700 nm range has been demonstrated and the results analyzed.

In Chapter 4, a diode-laser pumped carbon nanotube mode-locked Ho^{3+}-doped fluoride fiber laser at 1.2 μm is demonstrated. Stable mode-locked pulses with an average power of 1 mW at a repetition rate of 18.47 MHz were obtained at a pump power of 348 mW. The pulse energy and peak power of this mode-locked laser oscillator were about 54 pJ and 12.6 W, and increased to 2.41 nJ and 0.54 kW, respectively, for a 15-cm long Ho^{3+}-doped fluoride fiber amplifier. The pulse duration was measured to be 4.3 ps by an autocorrelator.

Chapter 2. Spectroscopic study of rare-earth-doped fluoride glass

Rare-earth doped fluoride glasses have attracted great interest for serving as a gain medium because of their specific emission wavelengths and energy levels with low phonon energy, which enable efficient emission at wavelengths that are not available in rare-earth doped silicate glasses due principally to non-radiative decay and transmission loss. In this chapter, we are going to discuss rate equations for erbium (Er^{3+}), holmium (Ho^{3+}) and dysprosium (Dy^{3+}) doped fluoride glasses. Spectroscopic properties of Er^{3+}, Ho^{3+} and Dy^{3+} singly doped fluoride glasses will be discussed, with both fluorescence and lifetime measurements accomplished by custom built experimental setups. According to the spectroscopic properties of singly doped fluoride glasses, co-doped fluoride glasses will also be investigated, and the related rate equations will be analyzed based both on simulation results and experiment results, forming a theoretical basis for the mid-infrared co-doped fluoride glass fiber laser in the next chapter.

2.1. Er^{3+}, Ho^{3+}, and Dy^{3+} singly–doped fluoride glass.

Rare-earth doped fluoride glasses with a composition of ZrF_4-BaF_2-LaF_3-AlF_3-NaF (ZBLAN) as the host glass were fabricated by FiberLabs Inc. using the conventional melting-quenching technique. 2 mol% Er^{3+}-doped, 1 mol% Ho^{3+}-doped and 1 mol% Dy^{3+}-doped glasses were prepared. Singly doped ZBLAN glass samples with a thickness of about 1 cm were cut and polished for transmission

spectrum measurements. Glass samples with a thickness of 1 mm were cut and their two large-area surfaces and one small-area surface were polished to optical quality for the fluorescence and lifetime measurements.

2.1.1. Energy-level diagrams and rate equations.

The partial energy-level diagram for Er^{3+} and the transitions related to ground state absorption and mid-IR emission are shown in Figure 2.1.1. Er^{3+} ions in the ground state can be excited to the $^4I_{11/2}$ ($^4I_{15/2} \rightarrow {}^4I_{11/2}$) level by absorbing near-IR light at 976 nm. The radiative transition from level $^4I_{11/2}$ to level $^4I_{13/2}$ generates emission in the 3 μm wavelength region and that from level $^4I_{13/2}$ to the ground level generates light in the 1.5 μm wavelength region.
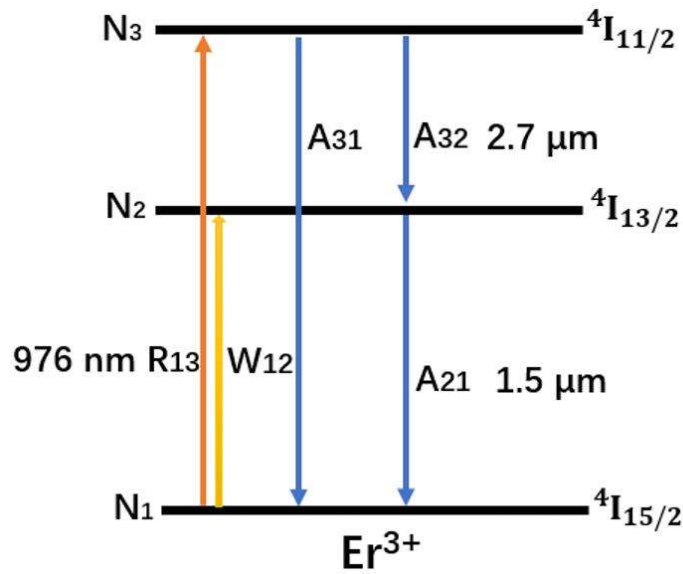
Fig. 2.1.1. Partial energy-level diagram of Er^{3+} and the transitions related to emission in the infrared region.

The steady state rate equations for Er³⁺ doped fluoride glass samples can be written as follows (eq. 2.1 ~eq. 2.4):

$$\frac{dN_3}{dt} = R_{13}N_1 - A_{31}N_3 - A_{32}N_3 = 0 \qquad (eq.\,2.1)$$

$$\frac{dN_2}{dt} = A_{32}N_3 - A_{21}N_2 = 0 \qquad (eq.\,2.2)$$

$$\frac{dN_1}{dt} = -R_{13}N_1 + A_{31}N_3 + A_{21}N_2 = 0 \qquad (eq.\,2.3)$$

$$N_{er} = N_1 + N_2 + N_3 \qquad (eq.\,2.4)$$

where, N_i is the population on the corresponding energy level of Er³⁺ in Figure 2.1.1. $R_{13}=(\sigma_{abs}P_p)/(h\nu_p A_{eff})$ is the pump rate, σ_{abs} is the absorption cross-section of Er³⁺, P_p is the laser pump power, A_{eff} is the effective area of the pump spot, h is the Plank constant, and ν is the frequency of the pump; A_{ij} is the transition rate of the spontaneous emission from level i to level j and the values of A_{ij} can be achieved according to their lifetimes and branching ratios. To have a numerical understanding of the rate equation, we need to measure the transmission of the glass sample to acquire σ_{abs}, measure the lifetime of each energy level to acquire A_{ij} and the population density N_i of each energy level will be represented by the fluorescence intensity.

In our experiment, the transmission spectra of the glass samples from 300-3300 nm were measured with a Cary 5000 spectrometer. Figure 2.1.2 shows the transmission of the 1.1 cm-thick 2 mol% Er³⁺-doped ZBLAN sample. Applying equations 2.5 and 2.6, the absorption cross-section (σ_{abs}) of Er³⁺ is calculated to

be 2×10^{-25} m^2 at 976 nm. Here, T is the transmission of the bulk sample at a specific wavelength (i.e., 976 nm), L is the length of the bulk sample, α is the absorption coefficient at the measurement wavelength and the N is the doping concentration.

$$T = \exp(-\alpha L) \qquad\qquad (eq.\,2.5)$$

$$\alpha = \sigma_{abs} N \qquad\qquad (eq.\,2.6)$$
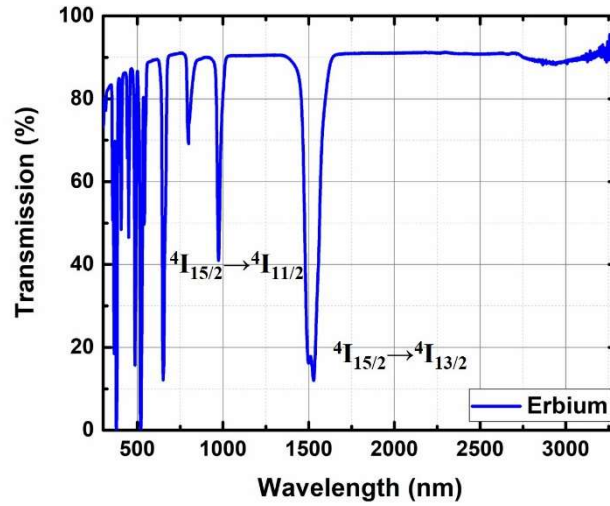
Fig. 2.1.2. Measured transmission spectra of 1.1 cm-thick 2 mol% Er^{3+}-doped ZBLAN glass samples.

Ho^{3+} ions have a near-IR absorption band at 1150 nm and the ground state absorption ($^5I_8{\rightarrow}^5I_6$) at this wavelength can populate the upper laser level $^5I_6$ for 3 μm emission ($^5I_6 \rightarrow {}^5I_7$). The radiative transition from level $^5I_7$ to the ground state level $^5I_8$ generates light in the 2 μm wavelength region. The partial energy-level diagram for Ho^{3+} and the transitions related to ground state absorption and mid-IR emission are shown in Figure 2.1.3.
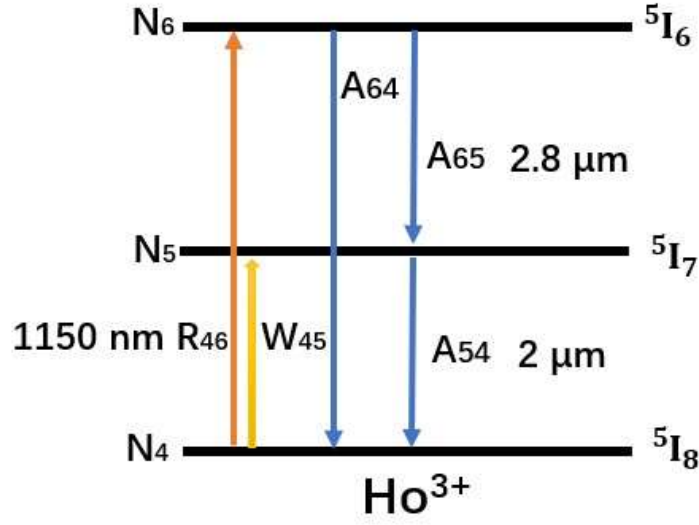
Fig. 2.1.3. Partial energy-level diagram for Ho^{3+} and the transitions related to emission in the infrared region.

The steady state rate equations of Ho^{3+} doped fluoride glass can be written as follows (eq. 2.7 ~eq. 2.10):

$$\frac{dN_6}{dt} = R_{46}N_4 - A_{64}N_6 - A_{65}N_6 = 0 \qquad (eq.\,2.7)$$

$$\frac{dN_5}{dt} = A_{64}N_6 - A_{54}N_5 = 0 \qquad (eq.\,2.8)$$

$$\frac{dN_4}{dt} = -R_{46}N_4 + A_{64}N_6 + A_{54}N_5 = 0 \qquad (eq.\,2.9)$$

$$N_{ho} = N_4 + N_5 + N_6 \qquad (eq.\,2.10)$$

Figure 2.1.4 shows the transmission of a 0.75 cm-thick 1 mol% Ho^{3+}-doped ZBLAN sample from which the absorption cross-section can also be calculated.
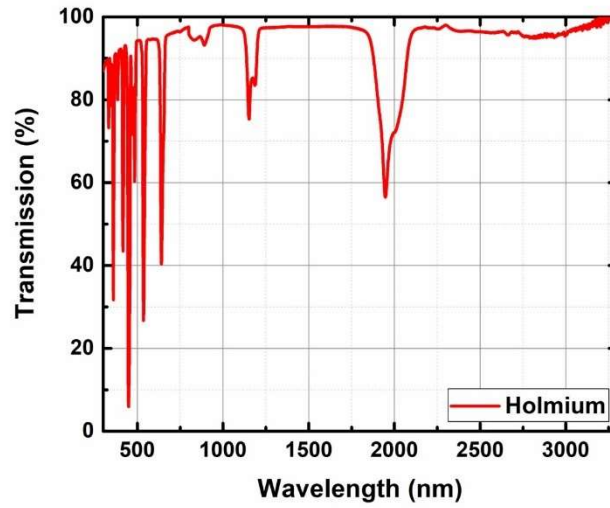
Fig. 2.1.4. Measured transmission spectra of 0.75 cm-thick 1 mol% Ho^{3+}-doped ZBLAN sample

Dy^{3+} ions have three near-IR absorption bands at 1090 nm, 1300 nm, and 1700 nm. The 3 μm emission can be produced by the radiative transition from level $^6H_{13/2}$ to level $^6H_{15/2}$. The partial energy-level diagrams of Dy^{3+} and the transitions related to the ground state absorption and mid-IR emission are shown in Figure 2.1.5.
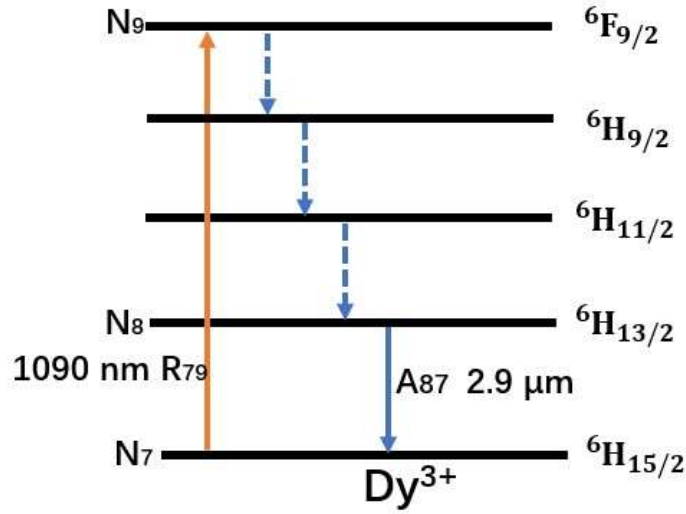
Fig. 2.1.5. Partial energy-level diagram of Dy^{3+} and the transitions related to emission in the infrared region.

The steady state rate equations (steady states) of Dy^{3+} doped fluoride glass samples can be written as follows (eq. 2.11~eq. 2.13):

$$\frac{dN_8}{dt} = R_{79}N_7 - A_{87}N_8 = 0 \qquad\qquad (eq.\,2.11)$$

$$\frac{dN_7}{dt} = -R_{79}N_7 + A_{87}N_8 = 0 \qquad\qquad (eq.\,2.12)$$

$$N_{dy} = N_7 + N_8 \qquad\qquad (eq.\,2.13)$$

Figure 2.1.6 shows the transmission of a 1 cm-thick 1 mol% Dy^{3+}-doped ZBLAN glass sample; the absorption cross-section can also be calculated.
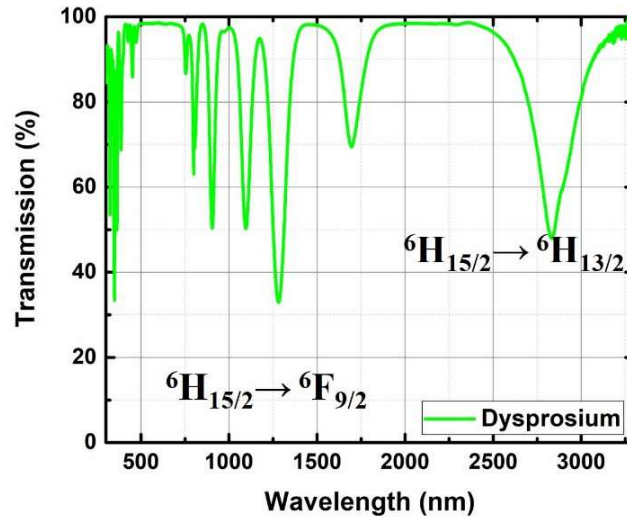
Fig. 2.1.6. Measured transmission spectrum of a 1 cm-thick 1 mol% Dy^{3+}-doped ZBLAN sample

2.1.2. Fluorescence measurement

Fluorescence is emitted when the rare-earth ion doped material is pumped with light at at specific wavelengths. For rare-earth ion doped material, the electrons of the dopant ions will be excited from the ground state to excited states when the material is pumped at wavelengths with large absorption cross-sections. For electrons in excited states, radiative decay occurs and spontaneous emission will be observed which is known as fluorescence. The intensity of the fluorescence is related to the population density on the excited state energy level and the emission wavelength is generally dependent on difference in energy between the excited state and the ground state; fluorescence can also occur between two excited state energy levels. The study of the fluorescence helps us to determine the emission wavelength of lasers based on the material. In this section, a

conventional method to measure the fluorescence of rare-earth doped materials will be introduced and the experimental setup will be applied to measure the infrared fluorescence of Er^{3+}, Ho^{3+} and Dy^{3+} doped ZBLAN glasses.

A conventional measurement technique with the experimental setup is depicted in Figure 2.1.7.   A well-polished glass sample was fixed by a tweezer with the mechanic stage, the pump source was launched into the glass sample at a small region close to the edge of the polished surface. Once the electrons in the ground state were raised to excited states, spontaneous emission occurs and fluorescence emission results. The fluorescence emitting from the glass sample was collected by a collimating lens at 90 degrees to the direction of the pump light. The continuous wave fluorescence was modulated by a mechanical chopper at A low frequency (typically a few hundred Hertz), after which another focusing lens was applied after the chopper to collect the light into the monochromator (ORIEL Instruments, Model 77702). The fluorescence intensity was measured by the lock-in detection technique with a lock-in amplifier (Princeton Applied Research, Model 5209) to detect the modulated signal received by the detector of the monochromator. LabVIEW software was used to control the monochromator and record the fluorescence spectrum.

Near-infrared continuous-wave laser sources at absorption peaks were used as the pumps to excite Er^{3+}, Ho^{3+}, and Dy^{3+}.   To ensure a system compatible with both infrared and mid-infrared emission, a black diamond aspheric lens (Thorlabs C036TME-E) was selected to work as the collimation lens and a CaF_2 plano-convex lens (Thorlabs LA5370) was selected to work as the focusing lens.

Scattered pump light sometimes influenced the fluorescence measurement results while the pump is focused on the test samples. To filter the scattered pump light and fluorescence of no interest, long-pass filters with cut-off wavelengths at 2500 nm (Spectrogon LP-2500nm) and 1250 nm (Thorlabs FEL1250) were used for the fluorescence measurement in the 3 μm and near-IR wavelength regions, respectively.
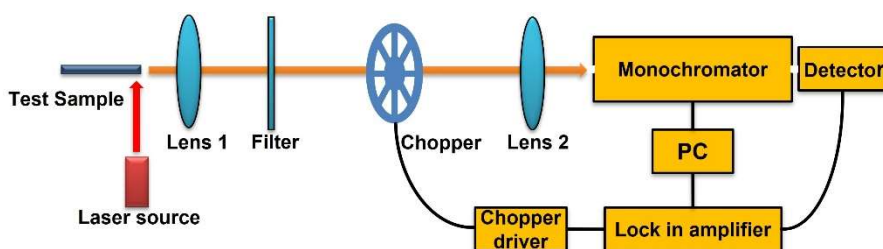
Fig. 2.1.7. Fluorescence measurement setup.

Energy level diagrams of Er^{3+}, Ho^{3+} and Dy^{3+} doped ZBLAN glass samples have been discussed in Section 2.1.1 and we can determine the optimum pump wavelength for these three glasses, respectively. A 976 nm source was used as the pump for Er^{3+}, a 1150 nm source as the pump for Ho^{3+} and a 1090 nm source as the pump for Dy^{3+}. The fluorescence spectra of singly Er^{3+}-, Ho^{3+}-, and Dy^{3+}-doped ZBLAN glass in the 3 μm wavelength region were measured and are shown in Fig. 2.1.8.
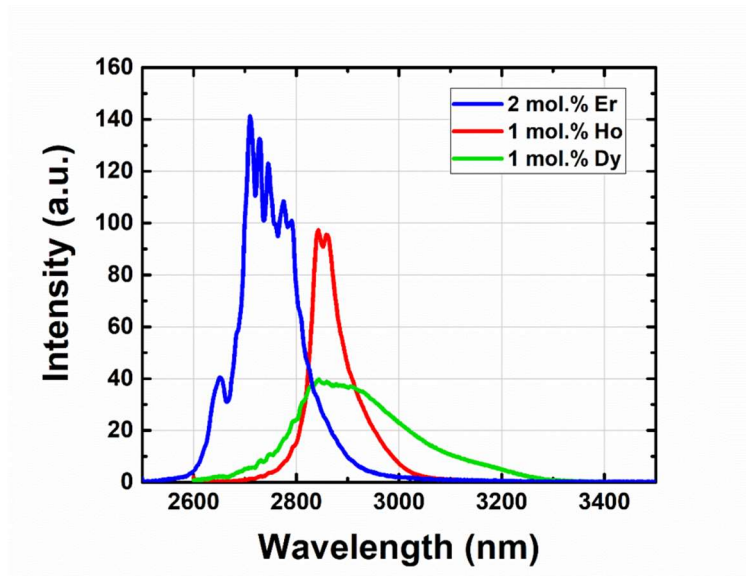
Fig. 2.1.8. Measured fluorescence spectra of the 2 mol% Er^{3+}-, 1 mol% Ho^{3+}-, and 1 mol% Dy^{3+}-doped ZBLAN glasses in the 3 μm wavelength region.

The Er^{3+}-doped ZBLAN sample was pumped by a 976 nm source and has a fluorescence emission ranging from 2500 nm to 3000 nm with a peak at 2740 nm. Small dips around 2740 nm are due to the absorption of the water vapor in the measurement setup. The Ho^{3+}-doped ZBLAN sample was pumped by a 1150 nm source and the fluorescence has a peak at 2850 nm with the long wavelength emission extending to 3100 nm. The Dy^{3+}-doped ZBLAN sample was pumped by a 1090 nm source and has a very broad fluorescence ranging from 2600 nm to 3400 nm.

2.1.3. Lifetime measurement

In addtion to a material's fluorescence spectrum, excited state lifetime is also an important factor that will influence laser performance. The lifetime refers to how

45

long the electrons can stay a given excited state, with longer lifetime making it easier to achieve population inversion. For rare-earth materials, lifetimes can be as short as a few microseconds, or as long as a few milliseconds. In this section, we introduce the experimental setup we used to measure the lifetime and investigate the lifetime of Er^{3+}, Ho^{3+} and Dy^{3+} doped ZBLAN glasses.

The lifetime measurement setup is shown in Figure 2.1.9. A nanosecond pulse optical parametric oscillator (OPO) source with a pulse duration of 10 ns at a repetition rate of 10 Hz (Continuum Surelite) was used as the pump source. Like the fluorescence spectrum measurement setup, the fluorescence emitting from the glass sample was collected and focused onto a detector (Thorlab PDA 20H) by two aspheric black diamond lenses (Thorlab C036TME-E). An oscilloscope (Tektronics TDS 1012) was connected to the detector to record the fluorescence decay curve. A set of filters were used to obtain the fluorescence only corresponding to the transition of interest from a specific energy level. The lifetime of an energy level was determined by fitting the fluorescence decay curve with an exponential decay function. The lifetimes of level $^4I_{11/2}$, level $^5I_6$, and level $^6H_{13/2}$ of singly Er^{3+}-, Ho^{3+}-, and Dy^{3+}-doped ZBLAN glass in the 3 μm wavelength region were measured to be 6.9 ms, 3.76 ms, and 0.512 ms, respectively, as shown in Fig. 2.1.10.
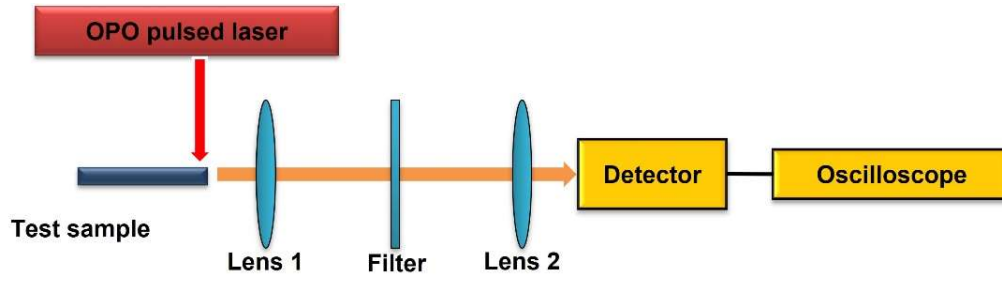
Fig. 2.1.9. Lifetime measurement setup.

Fig. 2.1.10. Measured 3 μm fluorescence decay curves and fitting curves of (a) 2 mol% Er^{3+}-doped, (b) 1 mol% Ho^{3+}-doped, and (c) 1 mol% Dy^{3+}-doped ZBLAN glasses.

2.2. Er^{3+}/Dy^{3+} and Ho^{3+}/Dy^{3+} co-doped fluoride glass.

In Section 2.1, we have discussed the fluorescence spectrum, lifetime and the associated measurement systems required. The fluorescence spectrum and lifetime of singly Er^{3+}, Ho^{3+} and Dy^{3+} doped ZBLAN glasses have been studied and analyzed. In this section, co-doped ZBLAN glasses will be studied and energy transfer process among the doping ions will be investigated and analyzed.

2 mol% Er^{3+}/1 mol% Ho^{3+} co-doped, and 2 mol% Er^{3+}/1 mol% Dy^{3+} co-doped ZBLAN glasses were prepared using the conventional melt-quenching technique. The partial energy diagrams of the co-doped ZBLAN samples are shown in Figure

47

2.2.1. According to the energy diagram, we assumed that energy transfer (ET) processes from Er^{3+} to Ho^{3+} (ET_{2-5}, ET_{3-6}) and from Er^{3+} to Dy^{3+} (ET_{2-8}, ET_{3-9}) will occur. We will use fluorescence and lifetime measurement results to verify our assumption here.
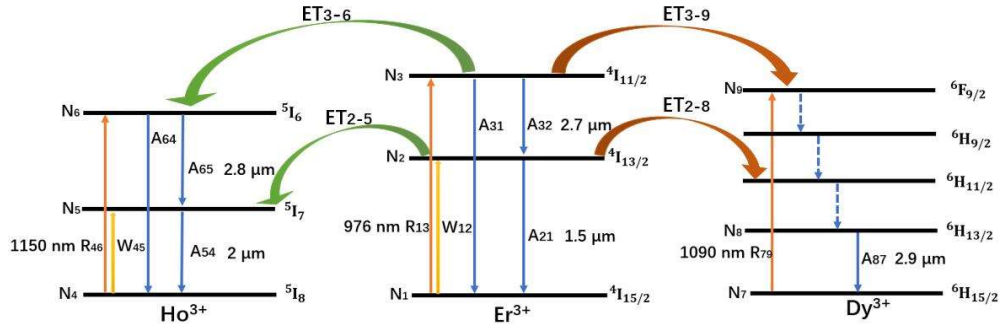
Fig. 2.2.1. Partial energy-level diagrams of Er^{3+}, Ho^{3+}, and Dy^{3+} and the transitions and energy transfer processes related to emission in the mid-IR.

The fluorescence spectra of the 2 mol% Er^{3+}, 2 mol% Er^{3+}/1 mol% Dy^{3+}, and 2 mol% Er^{3+}/1 mol% Ho^{3+} doped ZBLAN glass samples pumped with a 976 nm diode laser at a power level of 316 mW were measured from 1400 to 2200 nm and from 2500 to 3500 nm; the spectra are shown in Figure 2.2.2. Figure 2.2.2(a) and (b) show the fluorescence spectra of the singly Er^{3+}-doped ZBLAN glass with peaks at 1540 nm and 2740 nm, corresponding to the transitions $^4I_{13/2} \rightarrow {}^4I_{15/2}$ and $^4I_{11/2} \rightarrow {}^4I_{13/2}$, respectively. The fluorescence spectra of the Er^{3+}/Ho^{3+} co-doped ZBLAN glass in the near-IR and the 3 μm wavelength regions are shown in Figure 2.2.2(c) and (d), respectively. Besides the fluorescence of Er^{3+} in the 1.5 μm wavelength region, the Er^{3+}/Ho^{3+} co-doped ZBLAN glass has fluorescence emission with a peak at 1950 nm, corresponding to the Ho^{3+}

transition from $^5I_7$ to $^5I_8$. Moreover, the fluorescence of the Er^{3+}/Ho^{3+} co-doped ZBLAN glass in the 3 μm wavelength region exhibits the combined features of the fluorescence of singly Er^{3+}- and Ho^{3+}-doped ZBLAN samples. Because Ho^{3+} ions don't have absorption at 976 nm, these results clearly prove that energy transfer from level $^4I_{13/2}$ of Er^{3+} to level $^5I_6$ of Ho^{3+} occurs in ZBLAN as illustrated by the ET_{3-6} process in Figure 2.2.1. The fluorescence spectra of the Er^{3+}/Dy^{3+} co-doped ZBLAN glass in the 1.5 μm and 3 μm wavelength regions are shown in Figure 2.2.2(e) and (f), respectively. The fluorescence spectrum of the Er^{3+}/Dy^{3+} co-doped ZBLAN at 3 μm is almost the same as that of the singly Dy^{3+}-doped ZBLAN, showing that very efficient energy transfer from level $^4I_{11/2}$ of Er^{3+} to level $^6F_{9/2}$ of Dy^{3+} occurs as illustrated by the ET_{3-9} process in Figure 2.2.1. The fluorescence of the Er^{3+}/Dy^{3+} co-doped ZBLAN at 1.54 μm, however, is much smaller than that of the singly Er^{3+} doped ZBLAN, also indicating most energy is transferred from Er^{3+} to Dy^{3+}.
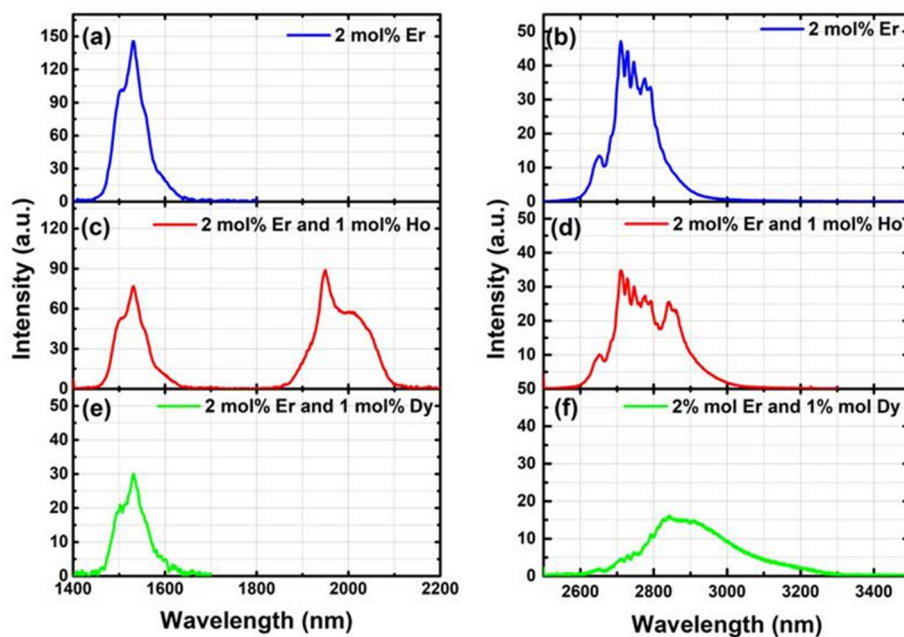
Fig. 2.2.2. Fluorescence spectra of the 2 mol% Er^{3+}-doped, 2 mol% Er^{3+}/1 mol% Ho^{3+} co-doped, and 2 mol% Er^{3+}/1 mol% Dy^{3+} co-doped ZBLAN glass samples measured at 1400-2200 nm and 2500-3500 nm when they were pumped at 976 nm.

We have established the proposed energy transfer processes via the fluorescence results. The co-doped ZBLAN samples only absorb the 976 nm pump light, located at the one of absorption peaks of Er^{3+}, while exhibiting the emission fluorescence properties of Ho^{3+} and Dy^{3+}. We now further verify these energy transfer processes through lifetime measurements.

The energy transfer from Er^{3+} to Ho^{3+} and Dy^{3+} was also confirmed by measuring the 3 μm fluorescence decay from level $^4I_{11/2}$ of Er^{3+} in the co-doped glass samples using the lifetime measurement setup shown in Figure 2.1.9. The glass samples were pumped with a 10 ns second pulsed laser at 976 nm. The fluorescence decay curves of the 3 μm fluorescence of Er^{3+}/Ho^{3+} and Er^{3+}/Dy^{3+} co-

doped ZBLAN samples were measured by using filters to remove the light below 2.5 μm and are shown in Fig. 2.2.3(a) and (b), respectively. The decay time of the 3 μm fluorescence of the 2 mol% Er^{3+}/1 mol% Ho^{3+} co-doped ZBLAN sample is 6.15 ms, which is smaller than that of the singly Er^{3+}-doped ZBLAN, indicating that energy transfer from Er^{3+} to Ho^{3+} occurs. The decay time of the 3 μm fluorescence of the 2 mol% Er^{3+}/ 1 mol% Dy^{3+} co-doped ZBLAN sample is only 0.84 ms, which is significantly reduced due to the efficient energy transfer from Er^{3+} to Dy^{3+}. It is worth noting that the fluorescence decay times are consistent with the measured fluorescence spectra. In the Er^{3+}/Ho^{3+} co-doped ZBLAN, the energy transfer from Er^{3+} to Ho^{3+} is not significant, so the fluorescence decay time is close to the lifetime of level $^4I_{11/2}$ of Er^{3+} and the fluorescence spectrum exhibits the combined features of the fluorescence of Er^{3+} and Ho^{3+}. The energy transfer from Er^{3+} to Dy^{3+} is very efficient in the Er^{3+}/Dy^{3+} co-doped ZBLAN, so the fluorescence decay time is close to the lifetime of level $^6H_{13/2}$ of Dy^{3+} and the fluorescence spectrum is almost the same as that of the singly Dy^{3+}-doped ZBLAN.

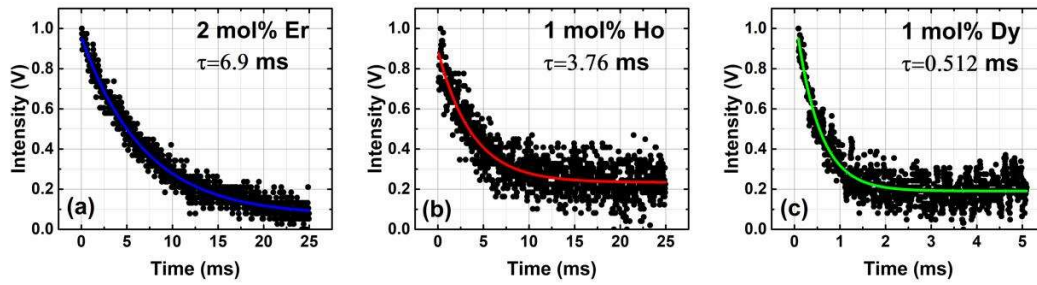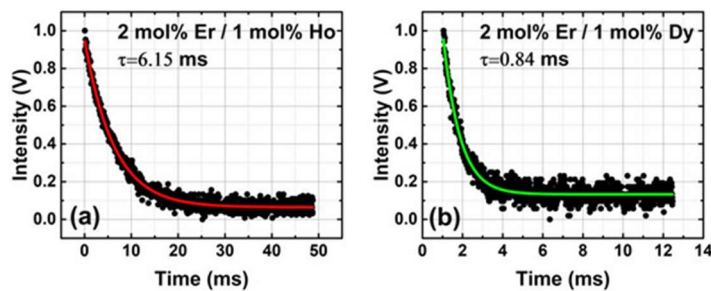
Fig. 2.2.3. Measured 3 μm fluorescence decay curves and fitting curves of (a) 2 mol% Er^{3+}/1 mol% Ho^{3+} co-doped and (b) 2 mol% Er^{3+}/1 mol% Dy^{3+} co-doped ZBLAN glasses in the 3 μm wavelength region.

In addition to the energy transfer processes from level $^4I_{11/2}$ of Er^{3+} to Ho^{3+} and Dy^{3+} (ET_{3-6} and ET_{3-9} processes shown in Figure 2.2.1), the energy transfer processes from level $^4I_{13/2}$ of Er^{3+} to level $^5I_7$ of Ho^{3+} (ET_{2-5}) and level $^6H_{11/2}$ of Dy^{3+} (ET_{2-8}) also occur in the co-doped ZBLANs and were confirmed by the measured fluorescence spectra and the reduced lifetime of level $^4I_{13/2}$ of Er^{3+} when they were pumped at 1480 nm. The fluorescence of Er^{3+}/Ho^{3+} co-doped ZBLAN sample pumped by a 1480 nm diode laser was measured and is shown in Figure 2.2.4(a). Besides the fluorescence of Er^{3+} at the 1.55 μm wavelength region, the fluorescence of Ho^{3+} with a peak at 1950 nm was also measured although Ho^{3+} ions don't have any absorption at 1480 nm, indicating that energy transfer from $^4I_{13/2}$ of Er^{3+} to level $^5I_7$ of Ho^{3+} occurs. Figure 2.2.4(b) shows the fluorescence of Er^{3+}/Dy^{3+} co-doped ZBLAN sample pumped by a 1480 nm diode laser. Besides the fluorescence of Er^{3+} at the 1.55 μm wavelength region, the fluorescence of Dy^{3+} with a peak at 2850 nm was also measured, confirming the energy transfer from level $^4I_{13/2}$ of Er^{3+} to level $^6H_{11/2}$ of Dy^{3+}. The 1.55 μm fluorescence decay curves of the three ZBLAN glass samples pumped at 1480 nm were also measured and are shown in Figure. 2.2.5. The lifetime of level $^4I_{13/2}$ of the Er^{3+}/Ho^{3+} co-doped ZBLAN was calculated to be 3.18 ms and that of the Er^{3+}/Dy^{3+} co-doped ZBLAN was calculated to 0.462 ms. Both lifetimes are much smaller than that of the singly Er^{3+}-doped ZBLAN (10.92 ms), again proving the efficient energy transfer from level $^4I_{13/2}$ of Er^{3+} to level $^5I_7$ of Ho^{3+} and level $^6H_{11/2}$ of Dy^{3+}, respectively.
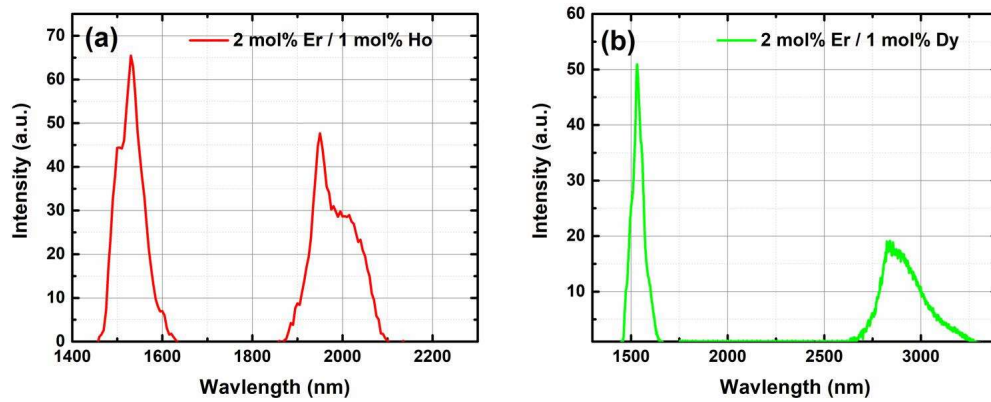
Fig. 2.2.4. Measured fluorescence spectra of (a) Er^{3+}/Ho^{3+} and (b) Er^{3+}/Dy^{3+} co-doped ZBLAN samples pumped at 1480 nm.
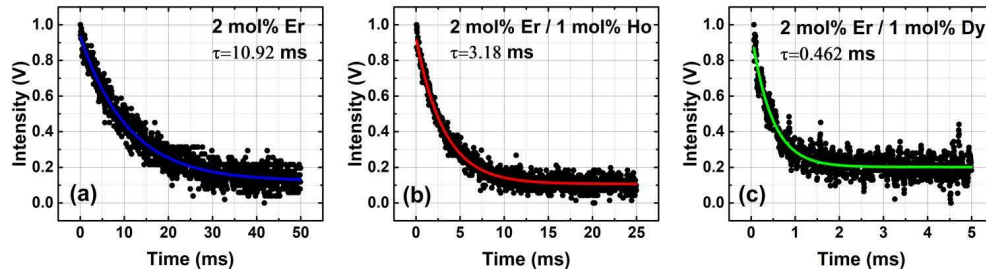
Fig. 2.2.5. Measured 1.55 μm fluorescence decay curves and fitting curves of (a) 2 mol% Er^{3+}-doped, (b) 2 mol% Er^{3+}/1 mol% Ho^{3+} co-doped, and (c) 2 mol% Er^{3+}/1 mol% Dy^{3+} co-doped ZBLAN glasses pumped at 1480 nm.

The backward energy transfer from Dy^{3+} and Ho^{3+} to Er^{3+} was also investigated in our experiment. The fluorescence spectrum of the Er^{3+}/Ho^{3+} co-doped ZBLAN sample pumped at 1150 nm was measured at 1400-2200 nm and is shown in Figure 2.2.6(a). In addition to the 2 μm emission from Ho^{3+}, a very weak fluorescence at 1.55 μm from Er^{3+} was measured and is shown in Figure 2.2.6(a), indicating that the backward energy transfer from Ho^{3+} to Er^{3+} occurs but the energy transfer probability is very low.   The fluorescence spectrum of the Er^{3+}/Dy^{3+} co-doped ZBLAN sample pumped at 1090 nm was measured at

1000-2000 nm and is shown in Figure 2.2.6(b). The fluorescence at 1.55 μm from Er^{3+} was not measured, indicating that the backward energy transfer from Dy^{3+} to Er^{3+} is negligible.
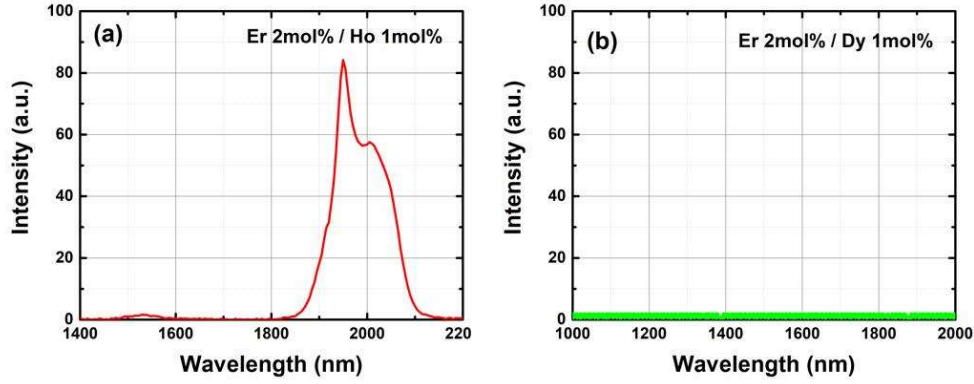
Fig. 2.2.6. (a) Fluorescence spectrum of 2 mol% Er^{3+}/1 mol% Ho^{3+} co-doped ZBLAN pumped at 1150 nm measured at 1400-2200 nm and (b) Fluorescence spectrum of 2 mol% Er^{3+}/1 mol% Dy^{3+} co-doped ZBLAN pumped at 1090 nm measured at 1000-2000 nm.

In this section, we have proved the energy transfer process between Er^{3+}, Ho^{3+} and Dy^{3+} according to their fluorescence and lifetime results. In the next section, we are going to complete the numerical analysis by rate equations and determine the energy transfer coefficient.

2.3 Rate equations for Er^{3+}/Dy^{3+} and Er^{3+}/Ho^{3+} co-doped systems.

The parameters of energy transfer processes (k_{25}, k_{36}, k_{28}, k_{39}) can be obtained by solving the rate equations for Er^{3+}/Dy^{3+} and Er^{3+}/Ho^{3+} co-doped ZBLAN samples to calculate the populations on the corresponding energy levels and fitting the

measured fluorescence spectra. The rate equations for Er^{3+}/Ho^{3+} co-doped ZBLAN pumped at 976 nm can be written as follows:

$$\frac{dN_3}{dt} = R_{13}N_1 - A_{31}N_3 - A_{32}N_3 - k_{36}N_3N_4 = 0 \qquad (eq.\,2.14)$$

$$\frac{dN_2}{dt} = A_{32}N_3 - A_{21}N_2 - k_{25}N_2N_4 = 0 \qquad (eq.\,2.15)$$

$$\frac{dN_1}{dt} = -R_{13}N_1 + A_{31}N_3 + A_{21}N_2 + k_{25}N_2N_4 + k_{36}N_3N_4 = 0 \quad (eq.\,2.16)$$

$$N_1 + N_2 + N_3 - N_{Er} = 0 \qquad (eq.\,2.17)$$

$$\frac{dN_6}{dt} = k_{36}N_3N_4 - A_{64}N_6 - A_{64}N_6 = 0 \qquad (eq.\,2.18)$$

$$\frac{dN_5}{dt} = k_{25}N_2N_4 + A_{65}N_6 - A_{54}N_5 = 0 \qquad (eq.\,2.19)$$

$$\frac{dN_4}{dt} = k_{25}N_2N_4 - k_{36}N_3N_4 + A_{64}N_6 + A_{54}N_5 = 0 \qquad (eq.\,2.20)$$

$$N_4 + N_5 + N_6 - N_{Ho} = 0 \qquad (eq.\,2.21)$$

Where, N_i is the population on the corresponding energy level of Er^{3+} and Ho^{3+} shown in Figure 2.2.1; $R_{13}=(\sigma_{abs}P_p)/(h\nu_pA_{eff})$ is the pump rate, σ_{abs} is the absorption cross-section of Er^{3+}, which is 2×10^{-25} m^2 at 976 nm, P_p is the laser pump power, A_{eff} is the effective area of the pump spot, h is the plank constant, and ν is the frequency of the pump; A_{ij} is the transition rate of the spontaneous emission from level i to level j and the values of A_{ij}s can be achieved according to their lifetimes and branch ratios; and k_{ij} is the parameter for the energy transfer process from level i to level j between Er^{3+} and Ho^{3+}.

Figure 2.3.1(a) shows the measured 3 μm fluorescence spectra of the Er³⁺/Ho³⁺ co-doped ZBLANs pumped by the 976 nm diode laser at 120 mW and 316 mW and their fitting curves.   The parameters k_{36} and k_{25} were calculated to be 6.24×10^{-19} cm³/s and 1.03×10^{-18} cm³/s, respectively, by fitting the fluorescence spectra of the Er³⁺/Ho³⁺ co-doped ZBLANs with the fluorescence spectra of the singly Er³⁺- and Ho³⁺-doped ZBLANs. Clearly, the energy transfer rate from level $^4I_{11/2}$ of Er³⁺ to level $^5I_6$ of Ho³⁺ is smaller than that from level $^4I_{13/2}$ of Er³⁺ to level $^5I_7$ of Ho³⁺.   It should be noted that, the parameter k_{25} can be also obtained by fitting the fluorescence spectrum of the Er³⁺/Ho³⁺ co-doped ZBLAN pumped at 1480 nm that is shown in Fig. 2.3.1(a).

The rate equations for Er³⁺/Dy³⁺ co-doped ZBLAN pumped at 976 nm can be written as follows.

$$\frac{dN_3}{dt} = R_{13}N_1 - A_{31}N_3 - A_{32}N_3 - k_{39}N_3N_7 = 0 \qquad (eq.\,2.22)$$

$$\frac{dN_2}{dt} = A_{32}N_3 - A_{21}N_2 - k_{28}N_2N_7 = 0 \qquad (eq.\,2.23)$$

$$\frac{dN_1}{dt} = -R_{13}N_1 + A_{31}N_3 + A_{21}N_2 + k_{28}N_2N_7 + k_{39}N_3N_7 = 0 \quad (eq.\,2.24)$$

$$N_1 + N_2 + N_3 - N_{Er} = 0 \qquad (eq.\,2.25)$$

$$\frac{dN_8}{dt} = k_{39}N_3N_7 + k_{28}N_2N_7 - A_{87} = 0 \qquad (eq.\,2.26)$$

$$N_7 + N_8 - N_{Dy} = 0 \qquad (eq.\,2.27)$$

The 3 μm fluorescence spectra of the Er^{3+}/Dy^{3+} co-doped ZBLAN pumped with the 976 nm diode laser at 120 mW and 316 mW and their fitting curves are shown in Figure 2.3.1(b). The parameters k_{28} and k_{39} were calculated to be 2.24×10^{-20} cm^3/s and 2.86×10^{-18} cm^3/s, respectively, by fitting the fluorescence spectra of the Er^{3+}/Dy^{3+} co-doped ZBLANs with the fluorescence spectra of the singly Er^{3+}- and Dy^{3+}-doped ZBLANs. Clearly, the energy transfer rates from Er^{3+} to Dy^{3+} are much larger than that from Er^{3+} to Ho^{3+}. This is consistent with the fluorescence and lifetime measurement results. The parameter k_{28} of 2.24×10^{-20} cm^3/s was also obtained by fitting the fluorescence spectrum of the Er^{3+}/Dy^{3+} co-doped ZBLAN pumped at 1480 nm shown in Figure. 2.3.1(b).
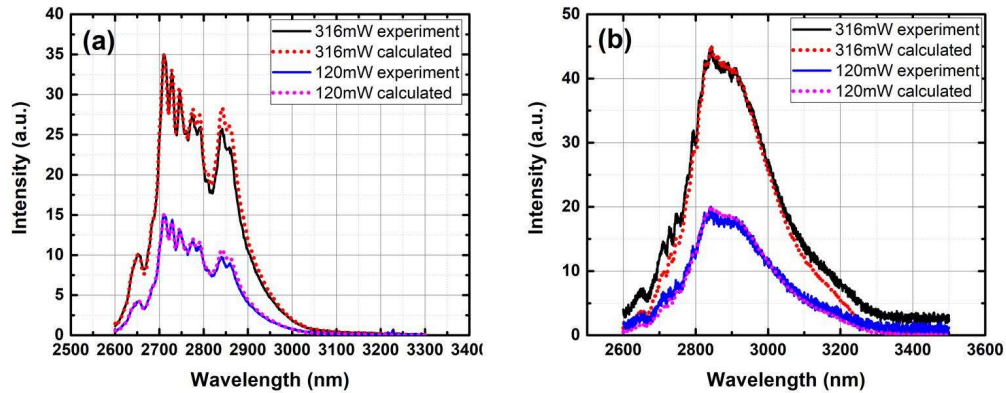
Fig. 2.3.1. Measured 3 μm fluorescence spectra and their fitting curves for (a) Er^{3+}/Ho^{3+} co-doped ZBLAN and (b) Er^{3+}/Dy^{3+} co-doped ZBLAN pumped with 120 mW and 316 mW 976 nm laser.

Spectroscopic properties of Er^{3+}-, Ho^{3+}-, Dy^{3+}-, Er^{3+}/Ho^{3+}-, and Er^{3+}/Dy^{3+}-doped ZBLAN glasses were studied and energy transfer from Er^{3+} to Ho^{3+} and Dy^{3+} ions in ZBLAN were confirmed with the experimental results. The parameters for energy transfer processes from level $^4I_{13/2}$ of Er^{3+} to level $^5I_7$ of Ho^{3+} and level $^6I_{13/2}$ of Dy^{3+} were estimated to be 6.24×10^{-19} cm^3/s and 2.86×10^{-18} cm^3/s, respectively.

This discovery opens a new path to design and develop high power diode-pumped Ho^{3+}- and Dy^{3+}-doped fiber lasers at 3 μm.

2.4. Chapter summary.

In this chapter, we applied energy level diagram, fluorescence, and lifetime measurement to analyze to rare-earth singly doped fluoride glass samples and co-doped fluoride glass samples. Both setups for fluorescence and lifetime measurement were introduced. The efficient energy transfer process between Er^{3+}, Ho^{3+} and Dy^{3+} doped fluoride glasses was verified and analyzed, which builds the theoretical foundation for mid-infrared co-doped fiber laser we are going to discuss in the next chapter.

Chapter 3. 3 μm Er/Dy co-doped ZBLAN fiber lasers.

3.1 3 μm fiber lasers.

Lasers in the mid-infrared (mid-IR) spectral region are of great interest for a wide range of scientific and technological applications including spectroscopy, medical surgery, free space communication, remote sensing, and material processing [78-82]. Compared to other laser platforms, optical fiber lasers have many well-known advantages such as excellent beam quality, high power scalability, outstanding heat dissipation capability, simplicity, and compactness. ZBLAN (ZrF_4-BaF_2-LaF_3-AlF_3-NaF) fibers have been widely used as the host media for rare-earth ions for mid-IR fiber lasers and the nonlinear media for high-efficiency ultra-broad band supercontinuum generation due to their low intrinsic loss, wide transparency window, and small phonon energy [83]. Rare-earth (Er^{3+}, Ho^{3+}, and Dy^{3+}) doped ZBLAN fiber lasers operating in the 3 μm wavelength region have attracted considerable interest because their emissions cover the fundamental rovibrational absorption lines of molecules containing C-H, N-H, and O-H chemical bonds, and they can be used for a lot of practical applications, such as medical diagnosis and surgery, remote sensing for gas and vapor, and material processing [84-87].

The first demonstration of rare-earth-doped ZBLAN fiber laser at 3 μm can be dated back to 1988 [88] and thereafter considerable investigations on Er^{3+}-doped ZBLAN fiber lasers have been completed due to the readily available diode lasers at the 790 nm and 980 nm absorption peaks of Er^{3+}[89,90]. Several watt-level Er^{3+}-doped ZBLAN fiber lasers have been reported in late 1990s [89-91]. In 2007, Zhu and Jain reported the first 10-W-level 3 μm fiber laser, which was demonstrated with a 4-m 6 mol% Er^{3+}-doped double-clad ZBLAN fiber and a high-power diode pump laser at 976 nm [92]. A slope efficiency of 21.3% was obtained by taking the advantage of energy transfer up-conversion process between Er^{3+} and Er^{3+} ions [92].   Since then, several 10-watt-level Er^{3+}-doped ZBLAN fiber lasers with higher output powers have been reported [93-95]. In 2015, a 30-W Er^{3+}-doped all-fiber laser operating at 2938 nm was demonstrated by using ZBLAN fiber Bragg gratings to form the all-fiber laser cavity and combining several high-power laser diodes near 980 nm to provide a total pump power of 188 W [96].

Compared to Er^{3+}-doped ZBLAN fiber lasers, Ho^{3+}- and Dy^{3+}-doped ZBLAN fiber lasers can operate at a wavelength beyond 3 μm and even at 3.380 μm [97], where compact diode-pumped high power laser sources are in great demand for most of the applications mentioned above. However, high efficiency high power (10s-watt or even > 100 watts) diode lasers at the near-infrared (near-IR) absorption peaks of Ho^{3+} (885 nm and 1150 nm) and Dy^{3+} (1090 nm, 1300 nm, and 1700 nm) are still not available. So far, the maximum output power of a Ho^{3+}-doped ZBLAN fiber laser at 3 μm was 2.5 W, which was pumped with a 1100 nm

Yb^{3+}-doped silica fiber laser [98]. The maximum output power of a Dy^{3+}-doped ZBLAN fiber laser pumped at near-IR was 180 mW [99]. Most recently, in-band pumping of the Dy^{3+}-doped ZBLAN fiber lasers with a Er^{3+}-doped ZBLAN fiber laser at 2.8 μm was proposed and an efficiency as high as 73% was obtained [100]. A 10-W Dy^{3+}-doped ZBLAN fiber laser in all-fiber configuration was also demonstrated recently by in-band pumping with an Er^{3+}-doped all-fiber laser at 2.83 μm [101]. All these demonstrations motivate us to design and fabricate Er^{3+} incorporated Ho^{3+}- and Dy^{3+}-doped ZBLAN fibers that can be used to develop compact all-fiber lasers above 3 μm directly pumped with readily available high power, high efficiency diode lasers near 980 nm.

The fluorescence spectra of 1 mol.% Dy^{3+}-doped and 1mol.% Er-doped ZBLAN in the 3 μm wavelength region were measured and are shown in Figure 3.1.1.   It is clear that Dy^{3+}-doped ZBLAN has a much broader emission band and much longer wavelength emission, extending to 3.4 μm.   Dy^{3+}-doped ZBLAN fiber lasers at 2.96 μm, 3.15 μm, and 3.24 μm have already been demonstrated [99-101].   The ultra-broadband emission also allows us to develop a tunable fiber laser with wide tuning range and ultrashort pulse fiber lasers [102] [103].
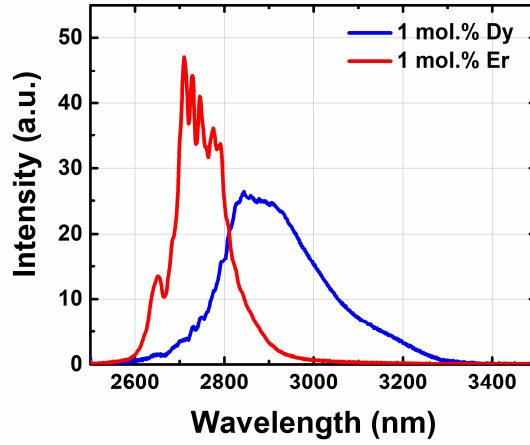
Fig. 3.1.1.   Measured fluorescence spectra of 1 mol.% Dy^{3+}-doped and 1 mol.% Er^{3+}-doped ZBLAN samples in the 3 μm wavelength region.

However, most Dy^{3+}-doped fiber lasers have been pumped with fiber lasers or solid-state lasers at the pump absorption peaks of Dy^{3+}. The partial energy-level diagram of Dy^{3+} is shown in Figure 3.1.2. The 3 μm laser is produced through the transition from the first excited state $^6H_{13/2}$ to the ground state $^6H_{15/2}$. The Dy^{3+}-doped ZBLAN has near-IR and mid-IR absorption bands at 1.1 μm, 1.3 μm, 1.7 μm, and 2.8 μm and fiber lasers have also been demonstrated with different pump sources at the four absorption bands. Compared to other pump wavelengths, Dy^{3+}-doped ZBLAN fiber lasers pumped at 2.8 μm have exhibited high efficiency and power scalability.   A 10-watt Dy^{3+}-doped ZBLAN fiber laser pumped by an Er^{3+}-doped ZBLAN fiber at 2.83 μm was reported recently [101]. A slope efficiency of 58% was obtained. Although a fiber laser pumped at 2.8 μm can be developed in an all-fiber configuration, the output power is still limited by the available pump power of an Er^{3+}-doped ZBLAN fiber laser. There is great interest in developing diode-pumped Dy^{3+}-doped fiber lasers at 3 μm so that a

more compact and robust laser source can be developed. However, high power

diode lasers at the four wavelengths are still not available. This matter can be

addressed by co-doping Dy^{3+} with other rare-earth ions that have strong

absorption peaks at the wavelengths of commercially available high power diode

pumps. In 2019, a Dy^{3+}/Tm^{3+} co-doped ZBLAN fiber laser pumped with a laser

diode at the Tm^{3+} 800 nm absorption peak of was demonstrated and an output

power of 12 mW at 3.23 μm was obtained at a pump power of 6.3 W [104]. In this

chapter, we report the demonstration of Dy^{3+}/Er^{3+} co-doped ZBLAN fiber lasers

pumped at the Er^{3+} 976 nm absorption peak , where low-cost high-power high-

efficiency pump diodes are readily available. An output power of 260 mW was

obtained with a 3.6-m Dy^{3+}/Er^{3+} co-doped ZBLAN fiber at a pump power of 7.5 W.
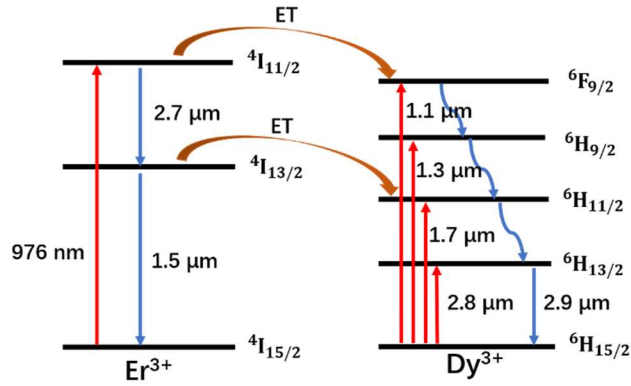
Fig. 3.1.2. Partial energy-level diagrams of Er^{3+} and Dy^{3+} and the transitions and energy transfer processes related to the laser emission at 3 μm.

Pumping Ho^{3+}- and Dy^{3+}-doped ZBLAN at the absorption bands of Er^{3+} via

energy transfer processes was proposed and has already been recently

demonstrated with comprehensive spectroscopic studies and numerical

simulations of Ho^{3+}/Er^{3+} and Dy^{3+}/Er^{3+} co-doped ZBLAN glasses [105]. The partial energy level diagrams of Er^{3+} and Dy^{3+} and the transitions related to energy transfer processes are shown in Figure 3.1.2. Er^{3+} ions can be excited from the ground state ($^4I_{15/2}$) to the excited state ($^4I_{11/2}$) by 976 pump light. Efficient energy transfer from Er^{3+} to Dy^{3+} occurs because the lifetime of state $^6F_{9/2}$ of Dy^{3+} (6 ns) is much smaller than that of state $^4I_{11/2}$ of Er^{3+} (6.9 ms) and their energy levels are close. As a result, Dy^{3+} ions are excited to state $^6F_{9/2}$ and populate state $^6H_{13/2}$ via rapid nonradiative decays. Therefore, it is possible to develop a Dy^{3+}/Er^{3+} co-doped ZBLAN fiber laser at 3 μm pumped with 976 nm pump diodes. Compared to the Dy^{3+}/Tm^{3+} co-doped fiber laser pumped at 800 nm, an Dy^{3+}/Er^{3+} co-doped fiber laser pumped at 976 nm could have higher efficiency due to the larger Stokes efficiency. Moreover, the output power and efficiency of current fiber-coupled commercial diodes at 976 nm are higher than at 800 nm, while the cost is much lower. It should be noted that, a Dy^{3+}/Er^{3+} co-doped fiber laser can also be pumped at 1.5 μm via the energy transfer process between state $^4I_{13/2}$ of Er^{3+} and state $^6H_{11/2}$ of Dy^{3+} [105], resulting in a Stokes efficiency as high as 50%. In this research, we focused on Dy^{3+}/Er^{3+} codoped fiber lasers pumped at 976 nm, where high power laser diodes are readily available and are much more efficient than 1.5 μm diodes.

3.2 Er³⁺/Dy³⁺ co-doped fluoride fiber design.

To design a Dy^{3+}/Er^{3+} co-doped fiber that can perform as the gain medium to achieve 3 μm fiber lasing when pumped by a 976 nm diode, we have studied the spectroscopic properties of some rare-earth fluoride glasses in Chapter 2 and verified that the energy transfer process between Er^{3+} and Dy^{3+} would happen. In this section, we are going to determine the gain medium for the co-doped fiber laser.

3.2.1 Fiber geometry.

Optical fibers are a type of cylindrical optical waveguide and in most cases are made of glass; most fibers used in laser development maintain a fiber core with higher index than the surrounding cladding materials. The refractive index difference between the core and the cladding is related to the numerical aperture (NA) as defined in equation 3.1. The NA determines how well the light is guided in the fiber and how much light will be coupled into the fiber.

$$NA = \sqrt{n_{core}^2 - n_{cladding}^2} \qquad (eq. 3.1)$$

There are several types of the host materials for fabricating optical fiber, with most fibers fabricated for telecommunication for operation at 1550 nm where silicate glasses are an excellent choice. In this Chapter, as we are going to discuss fiber lasers in the mid-infrared region, where fluoride fiber is our choice as low phonon energy is an advantage of fluoride glasses.

Single cladding fiber and double cladding fiber are shown in Figure 3.2.1 corresponding to the two primary pumping methods (core pump and cladding pump). In fiber laser technology, a light source is always needed for pumping the gain fiber. For single cladding fiber, the refractive index of the core is higher than that of the cladding, the pump source is guided in the core because of the total internal reflection (TIR) and the effective area of the pump light is illustrated with the red dash circle in Figure 3.2.1. For double cladding fiber, the refractive index of the core is still higher than that of the first cladding, which is higher than the second cladding, while the pump source is guided in the first cladding due to the TIR between the first cladding and the second cladding. Typically, the output power of single-mode laser diodes is restricted to 1W. In order to maintain higher pump power, multimode laser diodes are applied. However, the coupling efficiency from a multimode laser diode to single cladding fiber is quite low due to the huge difference in mode size. Heat dissipation can also be an issue when coupling a high power pump into the single cladding fiber. Under this circumstance, the double cladding fiber is more suitable for a high power pump. Sometimes, we can also increase the interaction between the pump light and the fiber core by specially designed fiber such as D-shaped fiber in Figure 3.2.1. The D-shape design reduce the skew rays in the first cladding and leads to improvements in laser efficiency.
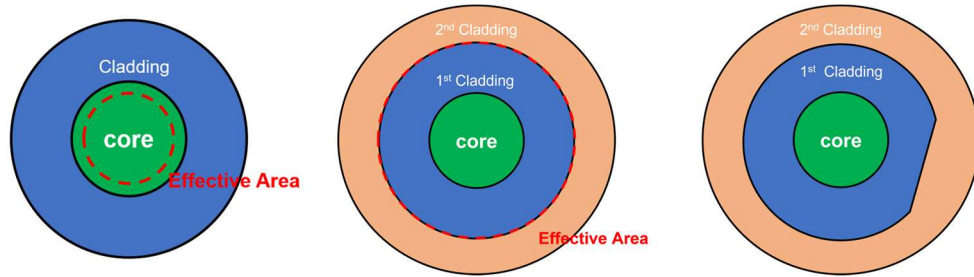
Fig. 3.2.1 Single cladding fiber (left); Double cladding fiber (middle); D-shaped fiber (right).

There are also some disadvantages to double cladding fiber, as the overlap between the pump mode distribution and the core of the double cladding fiber is much lower than that for a single cladding fiber, which leads to low absorption efficiency. Consequently, greater double cladding fiber length is generally needed to achieve the same gain as for a single cladding fiber of a given length. To increase the absorption efficiency, many types of double cladding fiber have been designed, such as off-centered core fiber, D-shaped inner cladding fiber, elliptical inner cladding fiber and hexagonal inner cladding fiber.

3.2.2 Rare-earth dopant concentrations.

In order to achieve a Dy^{3+}/Er^{3+} co-doped fiber we need to decide not only on the structure of the fiber, but also on the doping concentrations. The doping concentration refers to how many Dy^{3+} and Er^{3+} ions are doped into the fluoride fiber per unit volume and spectroscopic studies are needed as well. As we did in Chapter 2, we have studied the spectroscopic properties of 1-mm thick singly Dy^{3+}-doped and Dy^{3+}/Er^{3+} co-doped ZBLAN glass samples at different concentrations.

Measured with the setup shown in Figure 2.1.9, the lifetimes of state $^6H_{13/2}$ (3 μm transition) of Dy^{3+}-doped ZBLAN with different doping concentration (0.25 mol.%, 0.5 mol.%, 1 mol.%, and 2 mol.%) were obtained by measuring the fluorescence decay and are shown in Fig. 3.2.2. The lifetime of state $^6H_{13/2}$ decreases from 0.63 ms to 0.5 ms as the Dy^{3+} concentration increases from 0.25 mol.% to 2 mol.%. This phenomenon is because of concentration quenching, as sometimes the doping ions will form clusters at high concentrations. The clusters allow undesirable energy transfer between doping ions and decrease the power efficiency. Different host materials have different maximum doping concentrations without clustering.

The fluorescence spectra of the four singly Dy^{3+}-doped ZBLAN glass samples pumped with a 1090 nm laser at the same pump power were measured by the setup in Figure 2.1.9. The fluorescence spectra normalized by the Dy^{3+} concentration are shown in Figure 3.2.3. It is clear that fluorescence emission efficiency decreases with increasing Dy^{3+} doping level, which is another manifestation of concentration quenching. Therefore, lower Dy^{3+} concentration could result in more efficient laser emission at 3 μm and we need to keep the doping concentration of Dy^{3+} no higher than 0.25 mol.%.
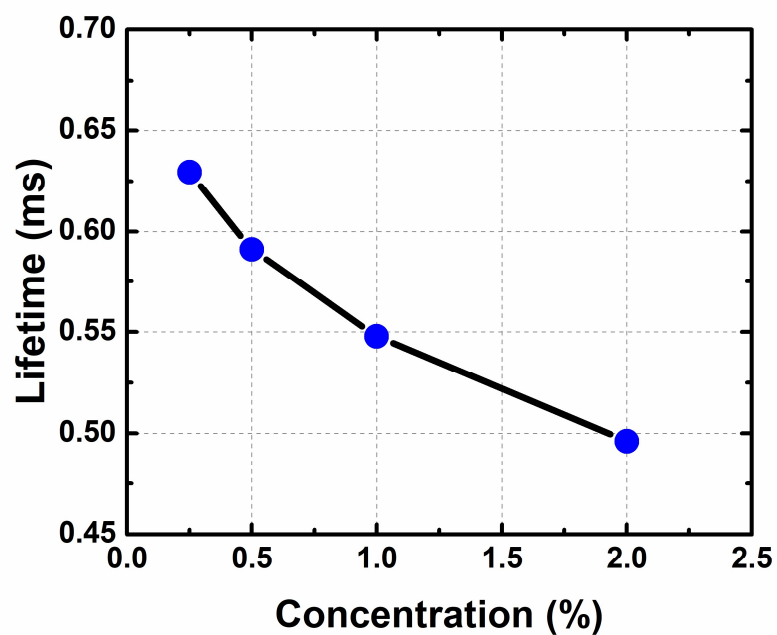
Fig. 3.2.2. Measured lifetimes of level $^6H_{13/2}$ for 1-mm thick Dy^{3+}-doped ZBLAN glass samples of various concentrations.
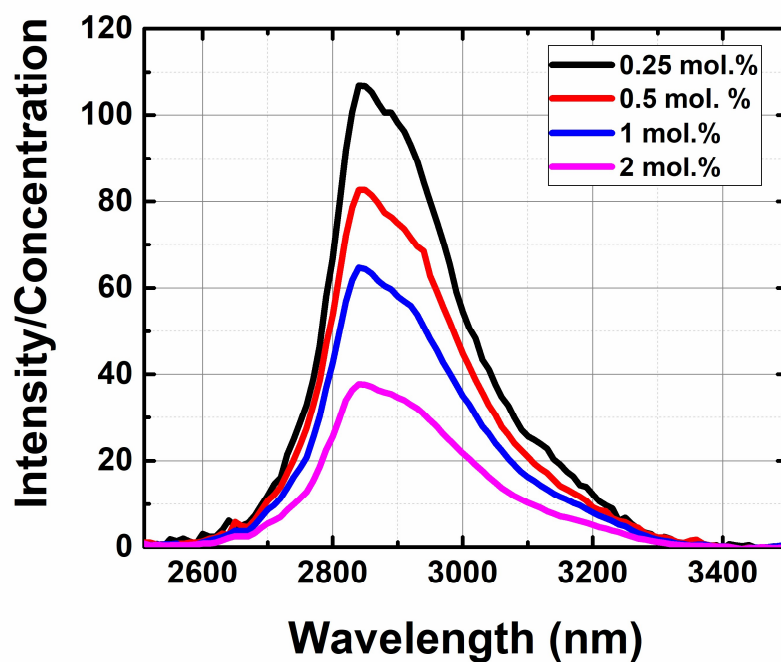
Fig. 3.2.3. Measured fluorescence spectra of 1-mm thick different concentration Dy^{3+}-doped ZBLAN glass samples normalized to the Dy^{3+} concentrations.

We also completed a similar spectroscopic study on singly doped Er^{3+} ZBLAN glass samples and no quenching effects were observed as long as the doping concentration of Er^{3+} was less than 6 mol.%. Furthermore, we need to study the doping concentration dependence of co-doped samples and determine the optimum doping concentration for developing lasers.

The fluorescence spectra of 0.25 mol.% Dy^{3+}-doped ZBLAN co-doped with 2 mol.%, 4 mol.%, and 8 mol.% Er^{3+} ions were measured with a monochromator and are shown in Figure 2.1.9. As a comparison, the fluorescence spectrum of 2 mol.% Er-doped ZBLAN is also plotted (black curve). A 976 nm multimode diode laser was applied to pump the samples and the four ZBLAN glass samples were pumped with a 976 nm diode laser at the same pump power. The fluorescence results are illustrated in Figure 3.2.4. We have proved that energy transfer occurs in Dy^{3+}/Er^{3+} co-doped ZBLAN glass samples. It is clear that Dy^{3+}/Er^{3+} co-doped ZBLAN glass samples emit ultra-broad band fluorescence extending to 3.4 μm due to efficient energy transfer from Er^{3+} to Dy^{3+}. In Figure 3.2.4 (a), the fluorescence intensity of the glass sample synthesized with 4 mol.% Er^{3+} is much larger than that of the glass sample synthesized with 2 mol.% Er^{3+}. However, the fluorescence intensity of the glass sample synthesized with 8 mol.% Er^{3+} is comparable to that of the glass sample synthesized with 4 mol.% Er^{3+}, although the absorbed pump power is doubled. Moreover, the fluorescence of the glass synthesized with 8 mol.% Er^{3+} at 2.7-2.8 μm is even smaller than that of the glass sample synthesized with 4 mol.% Er^{3+} due to Er^{3+} concentration quenching.

According to the results in Figure 3.2.4(a), we determine the optimum Er^{3+} doping concentration to be 4 mol.%. We are going to decide the best Dy^{3+} doping concentration as the next step. The fluorescence spectra of 0.1 mol.%, 0.25 mol.% and 0.5 mol.% Dy^{3+}-doped ZBLAN synthesized with 4 mol.% Er^{3+} ions were also measured at the same pump power at 976 nm and are shown in Figure 3.2.4(b). The fluorescence of the 0.1 mol.% Dy^{3+}/4 mol.% Er^{3+} co-doped glass sample exhibits high intensity at 2.7-2.8 μm, indicating that energy transfer from Er^{3+} to Dy^{3+} does not take place efficiently due to the relatively low concentration ratio between Dy^{3+} and Er^{3+}. As the Dy^{3+} concentration increases to 0.25 mol.%, the fluorescence intensity at 2.7-2.8 μm decreases significantly while the fluorescence intensity beyond 2.9 μm increases. As the Dy^{3+} concentration increases to 0.5 mol.%, the fluorescence intensity at 2.7-2.8 μm further decreases with a large magnitude but the fluorescence intensity beyond 2.9 μm does not increase due to Dy^{3+} ion concentration quenching.
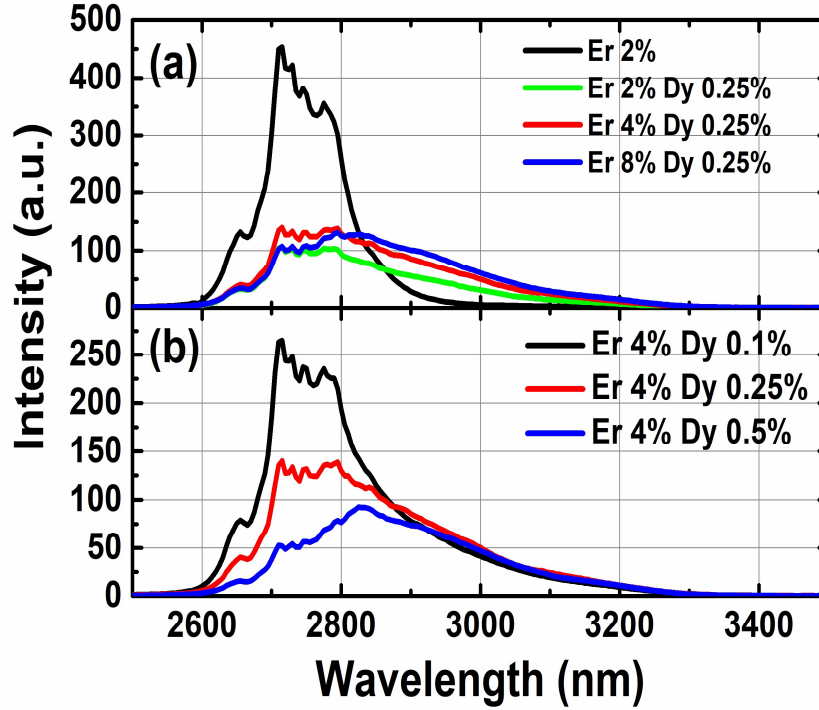
Fig. 3.2.4. Measured fluorescence spectra of (a) 2 mol% singly Er^{3+}-doped ZBLAN and 0.25 mol% Dy^{3+}-doped ZBLAN synthesized with different Er^{3+} concentrations and (b) 4 mol.% Er^{3+}-doped ZBLAN synthesized with different Dy^{3+} concentrations.

The fluorescence results shown in Fig. 3.2.4 tell us that low Dy^{3+} concentration could lead to low energy transfer efficiency while high Dy^{3+} concentration could lead to strong quenching effects. Therefore, a good compromise between energy transfer and concentration quenching needs to be engaged in the fiber design for an efficient Dy^{3+}/Er^{3+} co-doped ZBLAN fiber laser. Based on the spectroscopic study, we selected 0.25 mol.% $Dy^{3+}/4$ mol.% Er^{3+} as the dopant concentrations of the first gain fiber for our laser demonstration in the next section.

3.3 Er³⁺/Dy³⁺ co-doped fluoride fiber laser construction.

In Section 3.2, we have analyzed the fiber structure and the doping concentration we need for a mid-infrared fiber laser. In this section, we are going to develop the mid-infrared fiber laser using the parameter we determined.

3.3.1 Laser gain medium: fluoride fiber.

A custom designed 0.25 mol.% Dy³⁺/4 mol.% Er³⁺ co-doped double-clad ZBLAN fiber was fabricated by FiberLabs Inc. A microscopic image of this fiber end-facet is shown in Figure 3.3.1. The Dy³⁺/Er³⁺ co-doped fiber core has a diameter of 18 μm and numerical aperture (NA) of 0.14. The cutoff wavelength can found by calculating the V parameter, which determines whether the fiber operation is single mode (V<2.405), and dependes on the operating wavelength, fiber radius and the numerical aperture according to

$$V = \frac{2\pi}{\lambda} \, aNA \qquad\qquad (eq.\,3.1)$$

Based on our parameters, a cutoff wavelength of 3.29 μm can be calculated, which means single mode operation can be achieved if the laser wavelength is longer than 3.29 μm.
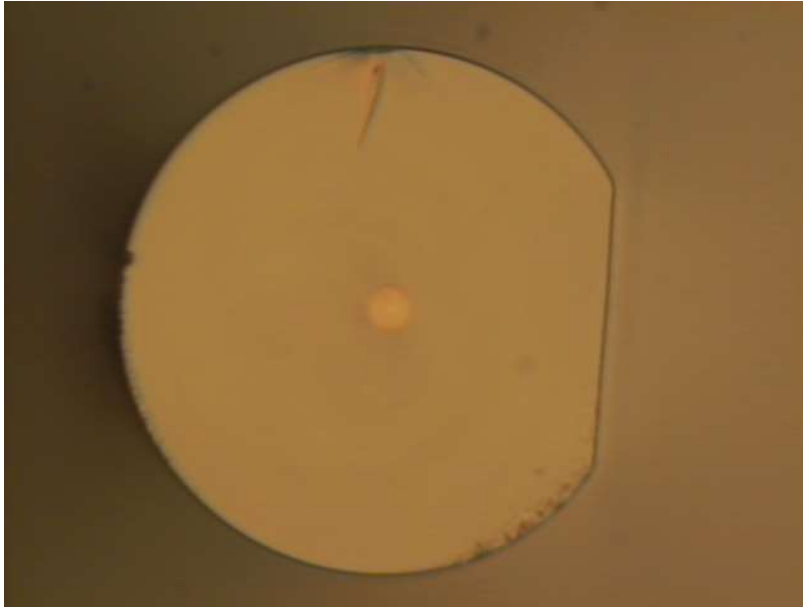
Fig. 3.3.1. Microscopic image of the gain fiber end facet.

As for the cladding, the fiber has a D-shaped inner cladding with a cross section of 250 μm × 200 μm and an NA of 0.5. As we discussed in Section 3.1, the double cladding structure will benefit when we couple high power pump light into the fiber from a multimode diode laser. The D-shaped inner cladding design has increased pump absorption compared to the circular inner cladding of a regular double-clad fiber. The pump absorption was measured to be about 2.67 dB/m by a cutback experiment. The background loss of this fiber at 3 μm is about 0.1 dB/m.

3.3.2 Laser cavity: dichroic mirror.

In order to build a mid-infrared fluoride fiber laser, we need the doped fluoride fiber as the gain medium and we also need to build an oscillation cavity for the

laser operating at 3 μm. For cavity mirrors, we need one reflector and one output coupler. The reflector should have high reflection (>95%) around 3 μm and the output coupler should have a partial reflection (25%~80%) around 3 μm. Both output coupler and reflector need high transmission at 976 nm as we don't want residual pump light, whose wavelength is at the absorption peak of Er^{3+} ions, trapped in our cavity. We chose to apply dichroic mirrors as our cavity mirrors here, and we have measured the transmissions of the dichroic mirrors by a Cary 5000 spectrometer.

Many dichroic mirrors were tested and the transmission spectra of four of them (DC0 to DC3) are shown in Figure 3.3.2 and Figure 3.3.3.
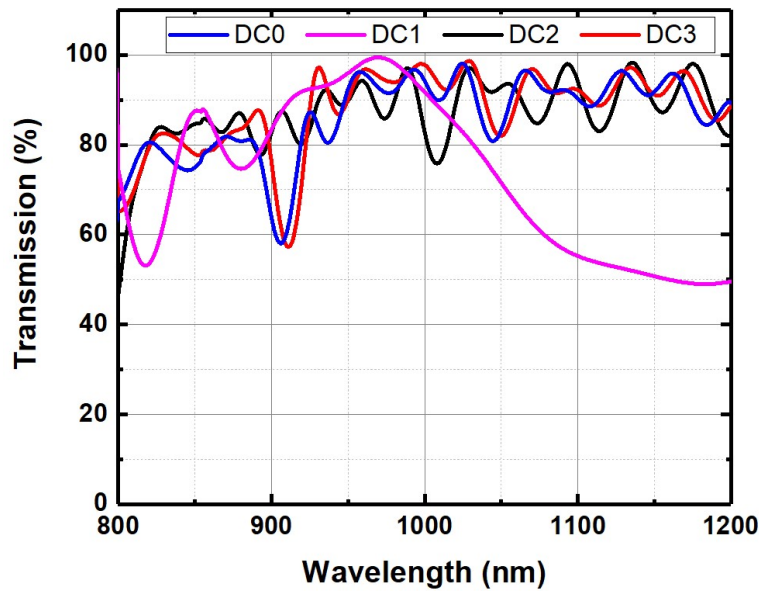
Fig. 3.3.2. Transmission spectra of dichroic mirrors in the near-infrared region (0.8~1.2 μm).
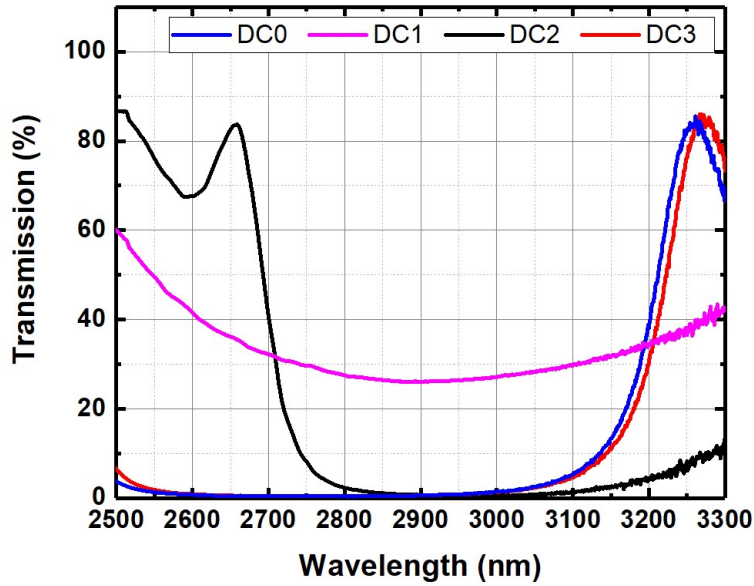
Fig. 3.3.3. Transmission spectra of dichroic mirrors in the mid-infrared region (2.5~3.3 μm).

If we need to choose an output coupler for the 3 μm mid-infrared fiber laser, DC 1 would be a good choice, since the transmission at 3 μm is 25% (reflection is nearly 75%) and the transmission at 976 nm is larger than 95%. For the cavity mirror, DC2 would be a good choice with high reflection at 3 μm and high transmission at 976 nm.

3.3.3 Laser setup.

The schematic of the 3-μm Dy^{3+}/Er^{3+} co-doped ZBLAN fiber laser is shown in Fig. 3.3.4. A commercial 976 nm multimode diode laser was used as the pump source. A CaF_2 lens was used to collimate the pump light and another CaF_2 lens was used to couple the pump light into the D-shaped inner cladding of the Dy^{3+}/Er^{3+} co-

doped ZBLAN fiber. The reason that we choose CaF_2 here is that the CaF_2 lens has a high transmission covering wavelengths from visible light to 3 μm.

Both ends of the gain fiber were flat cleaved. A dichroic mirror with a reflectivity of 70% at 3 μm and transmission of 85% above 976 nm was butt-coupled to the front end of the gain fiber to act as an output coupler. Another dichroic mirror with a reflectivity of 95% above 3 μm and 55% at 976 nm was butt-coupled to the rear end of the gain fiber to act as the cavity mirror, thereby constituting the oscillator cavity for the 3 μm laser.
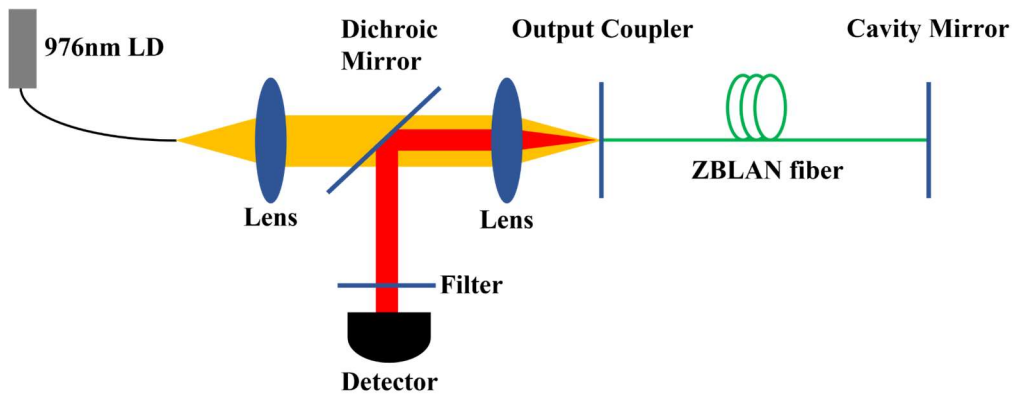
Fig.3.3.4. Schematic of the 3-μm Er^{3+}/Dy^{3+} co-doped ZBLAN fiber laser pumped by a 976 nm laser diode.

A dichroic mirror with high reflection at 3 μm and high transmission at 976 nm was oriented at 45 degrees to axis of the laser oscillator and placed between the collimating lens and the focusing lens to deliver the laser beam to the detector. An 1850 nm long pass filter was placed before the detector to make sure that only the 3 μm laser was detected. A thermal detector (Thorlabs S415C) and an optical

spectrum analyzer (Yokogawa, AQ6376) were used to measure the output power and optical spectrum.

3.3.4 Laser results.

In our experiment, fiber lasers with gain fiber lengths of 2 m, 3.6 m, and 9 m were investigated. The output power as a function of the launched pump power was measured for the three fiber lasers and shown in Figure 3.3.5.　The threshold and slope efficiency of the 3.6-m fiber laser are about 3.24 W and 5.73%, respectively. An output power of 260 mW was obtained with the 3.6-m fiber laser at a maximum launched power of 7.5 W. Further increase of the pump power could result in fluctuation of the output power or even fiber damage due to the fiber holder being heated by uncoupled pump light. The output power of this laser can be further increased by improving the pump coupling efficiency, employing effective thermal management, or building the laser in an all-fiber configuration using ZBLAN fiber Bragg gratings. For the 2-m fiber laser, only 158 mW output power was obtained at a launched power 7.5 W. The threshold and slope efficiency of this laser are about 3.1 W and 3.57%, respectively. As the gain fiber length increased to 9 m, the threshold of the fiber laser increased to 3.59 W while the slope efficiency decreased to 1.7% due to the increased propagation loss of the fiber cavity.　An output power of 66 mw was obtained at the maximum launched power.
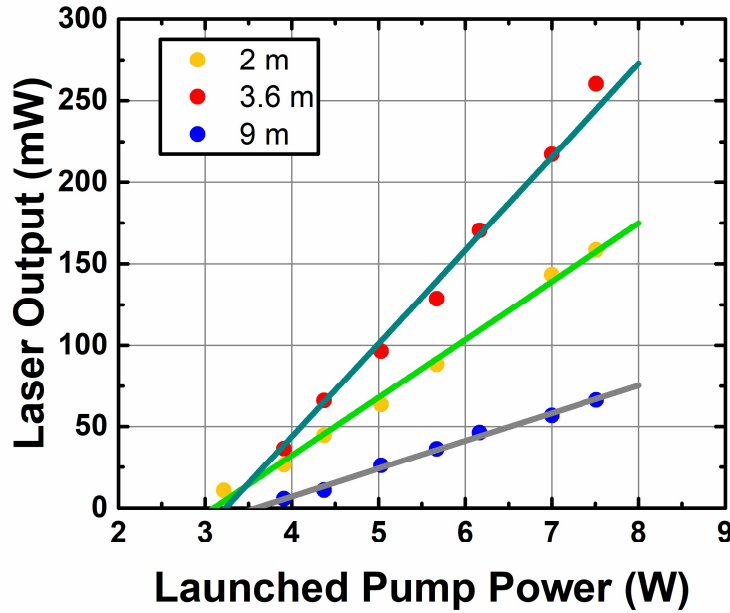
Fig. 3.3.5. Total output power as a function of the 976 nm pump power for the 2-m, 3.6-m, and 9-m Dy^{3+}/Er^{3+} co-doped fiber lasers.

Since there is no wavelength selective element inside the fiber laser cavity, the operating wavelength of the Dy^{3+}/Er^{3+} co-doped ZBLAN fiber lasers was not stable and the optical spectrum generally exhibited multiple peaks.   Figure. 3.3.6 shows a typical optical spectrum of the 9-m fiber laser at a pump power of 4.4 W. In addition to a laser peak at 3.34 μm, broadband amplified stimulated emission (ASE) at 2.5-3.2 μm was also observed on the optical spectrum analyzer at a resolution of 2 nm. The optical spectra of the 2-m, 3.6-m, and 9-m fiber lasers were measured at a pump power of 7.5 W and are shown in Fig. 3.3.7. When the gain fiber length is 2 m, the laser peak is at 3.23 μm.   As the gain fiber length increases to 3.6 m, the laser peak shifts to about 3.27 μm. The laser peak further shifts to 3.35 μm as the gain fiber length is 9 m. Due to signal re-absorption, a red

shift of the laser peak with increasing gain fiber length is observed, which is a general aspect of fiber lasers having broadband gain.
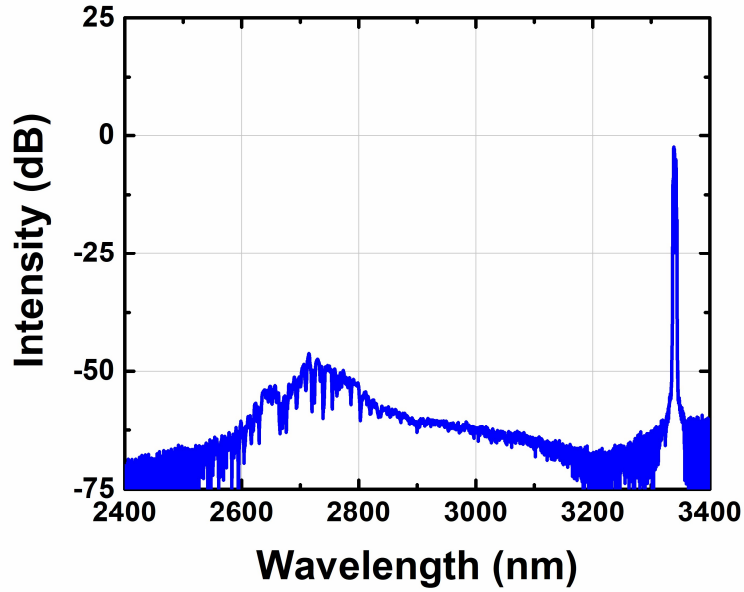
Fig. 3.3.6. Optical spectrum of the 9-m Dy^{3+}/Er^{3+} co-doped fiber laser measured over a wavelength range of 2400-3400 nm.
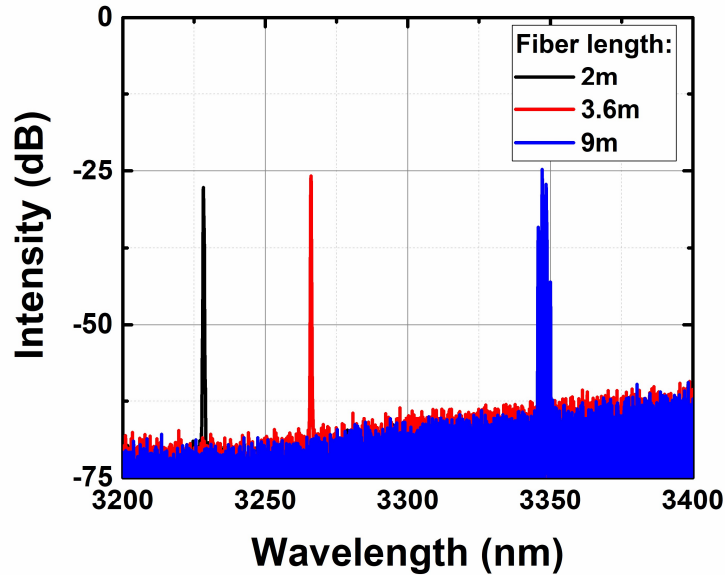
Fig. 3.3.7. Optical spectra of the 2-m, 3.6-m and 9-m Dy^{3+}/Er^{3+} co-doped fiber lasers measured at a pump power of 7.5 W.

It should be noted that the efficiencies of the three Dy^{3+}/Er^{3+} co-doped ZBLAN fiber lasers are lower than those of singly Dy^{3+}-doped ZBLAN fiber lasers pumped at 1.1 μm because 0.25 mol.% Dy^{3+} and 4 mol.% Er^{3+} may not be the optimal doping levels for the Dy^{3+}/Er^{3+} co-doped ZBLAN fiber laser. Much higher efficiency for a Dy^{3+}/Er^{3+} co-doped ZBLAN fiber laser can be obtained by further optimizing the concentrations of both dopants to reduce concentration quenching and improve the energy transfer. The green up-conversion light during the experiment like shown in Figure 3.3.8 may also be a reason, i.e., the energy upconversion process in highly Er^{3+}-doped ZBLAN [87].
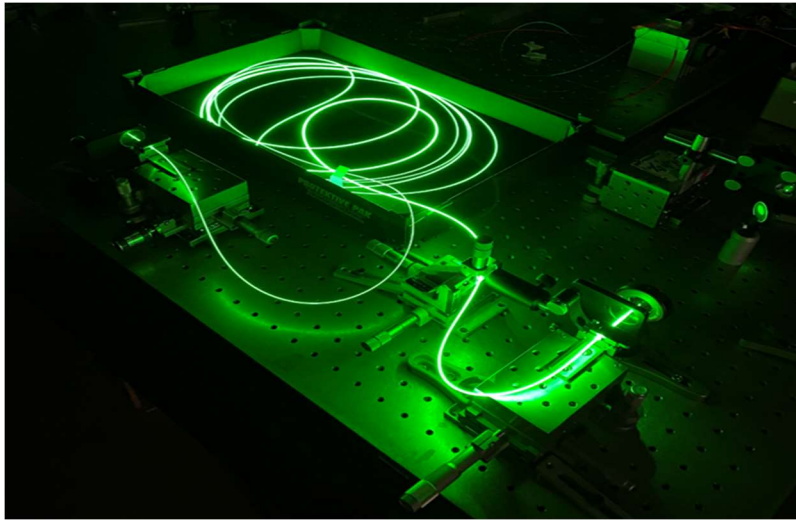
Fig. 3.3.8. Picture of experimental setup of the 3-μm Er^{3+}/Dy^{3+} co-doped ZBLAN fiber laser (up-conversion).

In this section, Dy^{3+}/Er^{3+} co-doped ZBLAN fiber lasers pumped at the 980 nm absorption band of Er^{3+} were demonstrated. A maximum output power of 260 mW at 3.27 μm with a slope efficiency of 5.73% was obtained with a 3.6-m 0.25 mol.% Dy^{3+}/ 4mol.% Er^{3+} co-doped fiber directly pumped by a 976 nm laser diode.

The ASE of the co-doped fiber is quite broad as shown in Figure 3.3.6, so it may have the potential to be the gain medium of the tunable laser, which will be discussed in the next section.

3.4 Wavelength tunable Er³⁺/Dy³⁺ co-doped fluoride fiber laser.

In this section, wavelength tunable dysprosium-erbium (Dy³⁺/Er³⁺) co-doped ZBLAN (ZrF$_4$-BaF$_2$-LaF$_3$-AlF$_3$-NaF) fiber lasers pumped at 980 nm were developed with a bulk grating blazed at 3.1 μm in the Littrow configuration and their performances were investigated. A wavelength tunable range of 674.4 nm (2709.2 nm -3373.6 nm) was achieved with a 4.5-m 0.25 mol.% Dy³⁺/ 4 mol.% Er³⁺ co-doped ZBLAN fiber. Our experiments demonstrated that either Er³⁺ or Dy³⁺ can be lasing individually in a Dy³⁺/Er³⁺ co-doped ZBLAN fiber and that a fiber laser with a wavelength tunable range from 2.7 μm to 3.4 μm or longer wavelengths can be achieved with proper fiber and cavity design.

3.4.1 3 μm wavelength tunable fiber lasers.

Wavelength tunable lasers have been developed with almost all types of current laser technologies because of their extensive practical applications in spectroscopy, optical communications, frequency metrology, hyperspectral imaging, device characterization, and remote sensing, among other areas. Wavelength tunable lasers in the mid-infrared (MIR) have attracted significant interest because most molecules have intense fundamental vibrational

absorptions in this region, which are more than 3-orders of magnitude stronger than those in the near-infrared, offering tremendously improved molecule detection sensitivity and accuracy. Nonlinear wavelength convertors such as optical parametric oscillators (OPOs) and difference-frequency generators (DFGs) have been widely used to achieve wavelength tunable mid-IR lasers [106-109]. However, OPOs and DFGs always have low efficiency and require complex manufacturing and frequent maintenance. Direct mid-IR laser generation based on rare-earth or transition-metal doped materials and semiconductor materials provides a simple and high-efficiency approach to achieve wavelength tunable mid-IR lasers. For example, Cr^{2+}:ZnSe and Fe^{2+}:ZnSe crystals have been used to develop wavelength tunable lasers with tuning ranges of 2.1-2.8 μm and 3.7-5 μm, respectively [110-111]. Recently, advances in quantum cascade lasers (QCLs) and interband cascade lasers (ICLs) have enabled very compact and high-efficiency wavelength tunable laser sources covering 3-12 μm or even longer wavelengths [112-113]. However, the output power levels of crystal and semiconductor lasers are generally limited by thermal management issues. Due to outstanding heat dissipation capability and excellent output beam quality, rare-earth doped fluoride fiber lasers are promising platforms for wavelength tunable lasers at 3 μm, where erbium (Er^{3+}), holmium (Ho^{3+}), and dysprosium (Dy^{3+}) have efficient emissions while ICLs still have low efficiency and low output power [114].

The first wavelength tunable fiber laser at 3 μm was demonstrated with a 2 mol. % Er^{3+}-doped ZBLAN (ZrF_4-BaF_2-LaF_3-AlF_3-NaF) fiber in 2000 [115]. A wavelength tunable range of 2.71-2.83 μm with output power < 5 mW was

achieved. In 2007, a watt-level wavelength tunable fiber laser was demonstrated with highly Er^{3+}-doped and Er^{3+}/Pr^{3+} co-doped ZBLAN fibers [116]. Due to the improved laser efficiency of highly Er^{3+}-doped ZBLAN, a 10-watt-level wavelength tunable fiber laser with tuning range of 170 nm (2.71-2.82 μm) was demonstrated [117]. Since Ho^{3+} has a transition with an emission wavelength greater than Er^{3+} in the 3 μm wavelength region, a Ho^{3+}/Pr^{3+} co-doped ZBLAN fiber laser with wavelength tuning range from 2.83 μm to 2.9 μm was demonstrated in 2011 [118]. A 42 nm wavelength tuning (2923 ～ 2965 nm) from the Ho^{3+} doped self-Q-switched all-fiber laser is achieved by applying a novel loss-adjusting technique [119]. Compared to Er^{3+}- and Ho^{3+}-doped ZBLAN fiber lasers, Dy^{3+}-doped ZBLAN fiber lasers have recently attracted more attention as a wavelength tunable laser source because the $^6H_{13/2} \rightarrow ^6H_{15/2}$ transition in Dy^{3+} has a very broad emission band (2.6-3.4 μm). In 2016, a Dy^{3+}-doped ZBLAN fiber laser with wavelength tunable range of 2.95 - 3.35 μm was demonstrated by in-band pumping at 2.8 μm [120]. By changing the pump source to a 1.7 μm Raman fiber laser, the wavelength tunable range of the Dy^{3+}-doped ZBLAN fiber laser was increased to nearly 600 nm (2.8-3.38 μm) [121]. In this section, we report the study of wavelength tunable Dy^{3+}/Er^{3+} co-doped ZBLAN fiber lasers using a grating blazed at 3.1 μm in the Littrow configuration. A wide wavelength tunable range of 674.4 nm (2709.2 nm -3373.6 nm) was achieved with a 4.5-m 0.25 mol.% Dy^{3+}/4 mol.% Er^{3+} co-doped ZBLAN fiber exhibiting laser operation of both Dy^{3+} and Er^{3+} ions in the co-doped system.
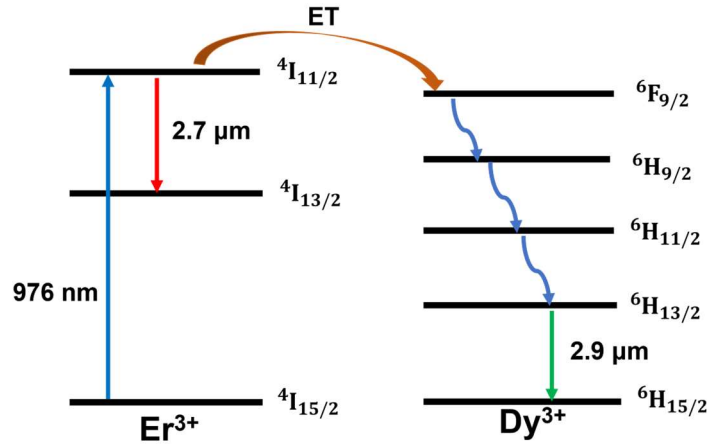
Fig. 3.4.1. Partial energy-level diagrams of Er^{3+} and Dy^{3+} and transitions/energy transfer processes related to the laser emission at 3 μm.

Dy^{3+}/Er^{3+} co-doped ZBLAN was originally proposed for lasers at 3 μm that could be pumped at Er^{3+} absorption bands, where commercial high-power high-efficiency diodes are readily available [105]. When Dy^{3+}/Er^{3+} co-doped ZBLAN is pumped at 980 nm, Er^{3+} ions are excited from the ground state ($^4I_{15/2}$) to the excited state ($^4I_{11/2}$). Because the energy of the $^6F_{9/2}$ state of Dy^{3+} is close to that of the $^4I_{11/2}$ state of Er^{3+}, which has a long lifetime (6.9 ms) in ZBLAN, efficient energy transfer from Er^{3+} to Dy^{3+} can occur. This has been verified by both spectroscopic study and fiber laser demonstration [105, 122]. A Dy^{3+}/Er^{3+} co-doped ZBLAN fiber laser at 3.27 μm pumped by a 980 nm diode has recently been successfully demonstrated [122]. In addition to the energy transfer, the electrons in the $^4I_{11/2}$ state of Er^{3+} are also depleted via light emission at 2.7 μm through transitions from $^4I_{11/2}$ to $^4I_{13/2}$, resulting in very broad emission due to the contributions of both Er^{3+} and Dy^{3+} emissions. Figure 3.4.2 shows the 3 μm fluorescence spectra of a 1 mol.% Er^{3+}-doped ZBLAN glass pumped at 980 nm, a

1 mol.% Dy^{3+}-doped pumped at 1090 nm, and a 0.25 mol.% Dy^{3+}/4 mol.% Er^{3+} co-doped ZBLAN glass pumped at 980 nm. It is clear that the emission bandwidth of the Dy^{3+}/Er^{3+} co-doped ZBLAN is enhanced compared to that of singly Dy^{3+}-doped or Er^{3+}-doped ZBLAN. Although Dy^{3+}-doped ZBLAN has broad fluorescence spanning from 2.6 μm to 3.4 μm, it is difficult to obtain laser operation below 2.8 μm because the emission cross-section of Dy^{3+} is smaller than the absorption cross-section in this band. Because emission from the $^4I_{11/2}$ - $^4I_{13/2}$ transition is still very strong in 0.25 mol.% Dy^{3+}/ 4 mol.% Er^{3+} co-doped ZBLAN, laser operation below 2.8 μm can still be achieved by forcing Er^{3+} ions to lase. The amplified spontaneous emission (ASE) spectrum of a 4.5-m 0.25 mol.% Dy^{3+}/4 mol. % Er^{3+} co-doped ZBLAN fiber pumped at 980 nm was measured and is shown in Figure 3.4.3. As a comparison, the ASE spectrum of singly Dy^{3+}-doped ZBLAN fiber pumped at 1090 nm and singly Er^{3+}-doped ZBLAN fiber pumped at 980 nm were also measured and are shown in Fig. 3.4.3. Much broader ASE covering 2.5-3.6 μm was measured with the Dy^{3+}/ Er^{3+} co-doped fiber. The ASE from Er^{3+} in Dy^{3+}/ Er^{3+} co-doped fiber at 2.7-2.8 μm is 5 dB higher than that of Dy^{3+} at 3 μm, showing the potential for laser operation based on Er^{3+} transitions at 2.7-2.8 μm in the co-doped system and allowing us to achieve a wide wavelength tunable fiber laser with a tuning range of 2.7-3.4 μm.
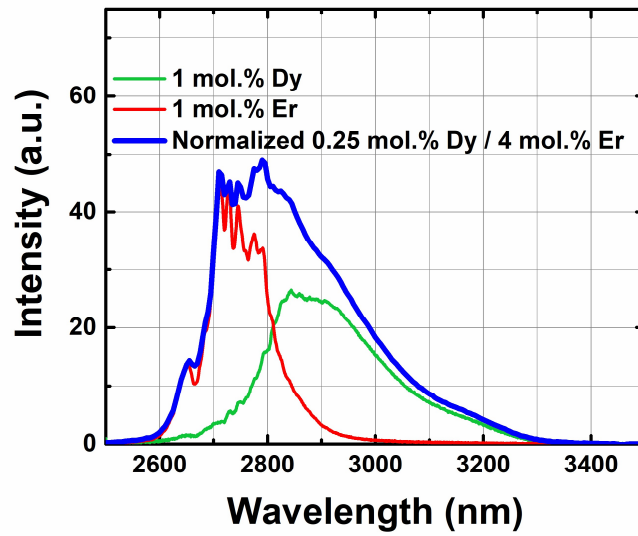
Fig. 3.4.2. Measured fluorescence spectra of 1 mol.% Dy^{3+}-doped, 1 mol.% Er^{3+}-doped, 0.25 mol.% Dy^{3+}/ 4 mol.% Er^{3+} co-doped ZBLAN samples in the 3 μm wavelength region

.
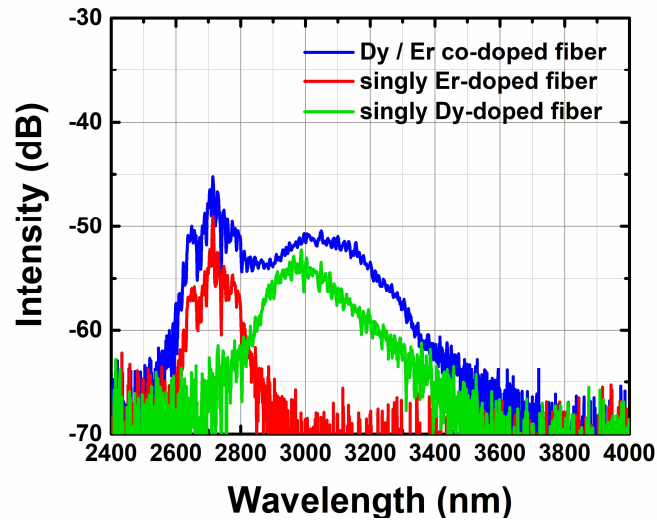
Fig. 3.4.3. Measured ASE spectra of Dy^{3+}/ Er^{3+} co-doped, singly Er^{3+-} doped, and singly Dy^{3+}-doped ZBLAN fibers.

In this section, we used the 0.25 mol.% Dy^{3+}/ 4 mol.% Er^{3+} co-doped ZBLAN fiber to demonstrate widely wavelength tunable Dy^{3+}/Er^{3+} ZBLAN fiber lasers and investigate their performance. Continuous wavelength tunable emission from

2.71 μm to 3.38 μm was obtained due to the laser operation of both Er^{3+} and Dy^{3+} ions in the co-doped system.

3.4.2 Experimental setup.
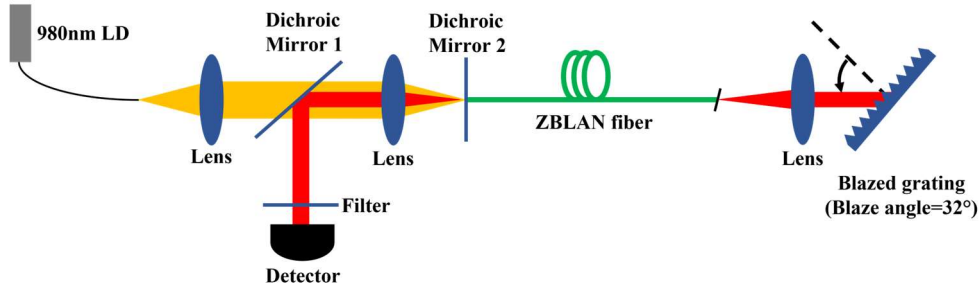
Fig. 3.4.4. Schematic of tunable 3-μm Dy^{3+}/ Er^{3+} co-doped ZBLAN fiber laser pumped by a 980 nm laser diode.

The schematic of the wavelength tunable Dy^{3+}/ Er^{3+} co-doped ZBLAN fiber laser is shown in Figure 3.4.4. The core of the Dy^{3+}/Er^{3+} co-doped fiber has a diameter of 18 μm and numerical aperture (NA) of 0.14. Its inner cladding has a D-shaped cross section of 250 μm × 200 μm and an NA of 0.5, which enhances the pump absorption by deflecting the skew rays through the fiber core. A commercial 980 nm laser diode was used as the pump source, and a pair of CaF_2 lenses with a focal length of 2.54 cm were used to collimate the pump light and couple the pump into the D-shape inner cladding of Dy^{3+}/Er^{3+} co-doped ZBLAN fiber. A dichroic mirror (Dichroic Mirror 2) with reflectivity of 70% at 3 μm and high transmission at 980 nm was butt-coupled to the flat cleaved front end of the gain fiber and used as an output coupler. Another CaF_2 lens was placed after the angle cleaved rear end of the gain fiber to collimate the 3 μm emission light. A blazed grating (Thorlabs GR1325-45031) was placed at 3 cm after the collimating CaF_2 lens to reflect the

diffracted beam at a specific wavelength back into the core of the gain fiber, working as the wavelength selective cavity mirror. Another dichroic mirror (Dichroic Mirror 1) with high reflection around 3 μm and high transmission at 980 nm was placed between the collimating lens and focusing lens at 45° to the laser beam to deliver the 3 μm laser beam to the detector. An 1850 nm long pass filter was placed before the detector to make sure that only the 3 μm laser was detected. A thermal detector (Thorlabs S415C) and an optical spectrum analyzer (Yokogawa, AQ6376) were used to measure the output power and optical spectrum, respectively.

3.4.3 Experimental results and discussion

In our experiment, the performance of wavelength tunable Dy^{3+}/Er^{3+} co-doped ZBLAN fiber lasers with different gain fibers was investigated. Figure 3.4.5 shows the optical spectra of the wavelength tunable fiber laser with 3.5-m gain fiber operating at different wavelengths. Wavelength tunable laser operation from 2708 nm to 3296.8 nm was achieved. It should be noted that the wavelength tunable range of the 3.5-m fiber laser was limited by the onset of parasitic lasing at 2930 nm, which can be suppressed by using optical components with highly anti-reflective coatings to reduce the reflections inside the cavity. Using long gain fiber is an alternative approach to conquer the parasitic lasing at 2930 nm and extend the laser operating wavelength because a longer gain fiber can usually produce higher gain at long wavelength, where the emission cross-section of the gain medium is small. To extend the tunable wavelength range of a Dy^{3+}/Er^{3+} co-

doped ZBLAN fiber laser beyond 3.3 μm, 4.5 m and 6 m gain fibers were then used in our experiment. The optical spectra of the 4.5-m Dy^{3+}/Er^{3+} co-doped ZBLAN fiber laser operating at different wavelengths are shown in Figure 3.4.6.   A wavelength tuning range of 2709.2-3373.6 nm was achieved. Figure 3.4.7 shows the optical spectra of the 6-m Dy^{3+}/Er^{3+} co-doped ZBLAN fiber laser operating at different wavelengths beyond 3.2 μm. The longest operation wavelength achieved with the 6-m gain fiber was 3.38 μm. Further tuning the blazed grating didn't result in laser operation at a longer wavelength but rather onset of parasitic lasing at 3240 μm. Because the ASE of a Dy^{3+}/Er^{3+} co-doped ZBLAN fiber can extend to 3.6 μm as shown in Figure 3.4.3, it is very possible to achieve laser operation beyond 3.4 μm if the parasitic lasing is suppressed and a longer gain fiber is used.
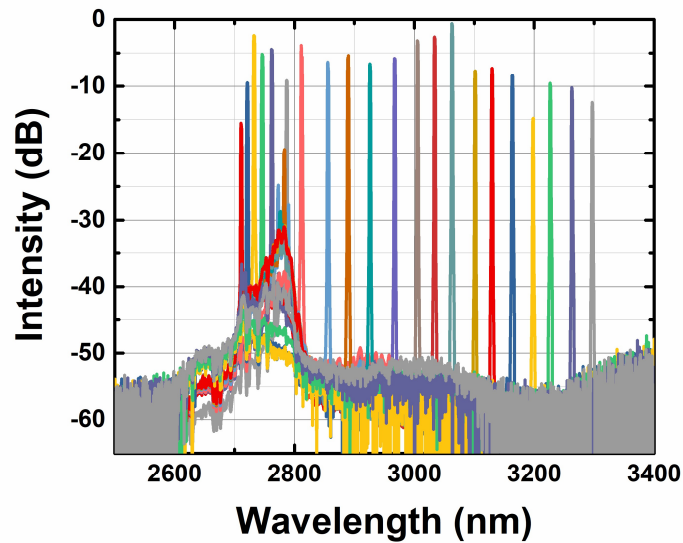
Fig. 3.4.5. Measured optical spectra of wavelength tunable Dy^{3+}/Er^{3+} co-doped ZBLAN fiber laser with gain fiber length of 3.5 m operating at different wavelengths.
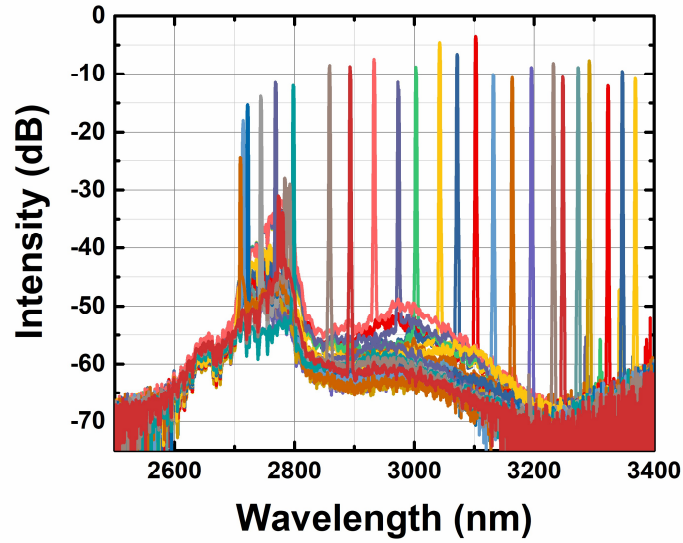
Fig. 3.4.6. Measured optical spectra of wavelength tunable Dy^{3+}/Er^{3+} co-doped ZBLAN fiber laser with gain fiber length of 4.5 m operating at different wavelengths.
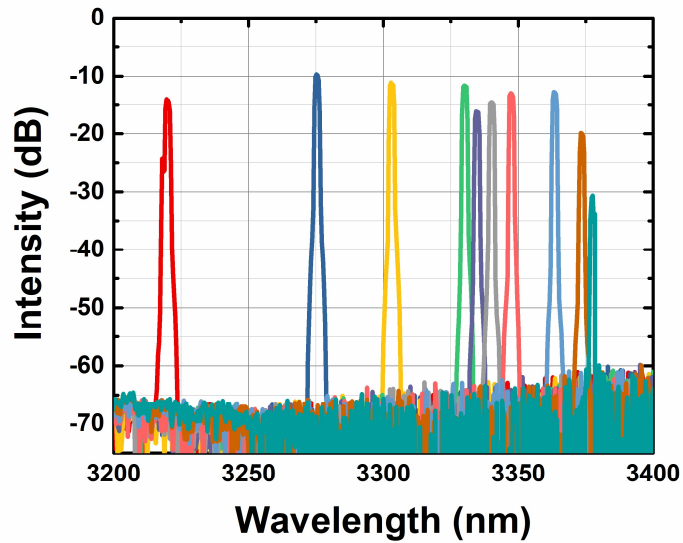
Fig. 3.4.7. Measured optical spectra of wavelength tunable Dy^{3+}/Er^{3+} co-doped ZBLAN fiber laser with gain fiber length of 6 m operating at different wavelengths.

The spectral bandwidth of the wavelength tunable fiber laser was measured by an optical spectrum analyzer with a resolution of 0.1 nm. Figures 3.4.8(a) and

(b) show the typical optical spectrum of the wavelength tunable fiber laser operating at 2.89 μm in logarithmic and linear scales, respectively. The spectral bandwidth was about 0.32 nm, which is determined by the distance between the collimating lens and the blazed grating, the groove density of the blaze grating, and the fiber core diameter of the gain fiber. The spectral linewidth of the wavelength tunable laser can be reduced by increasing the distance between the collimating lens and the blazed grating and using a grating with larger groove number.
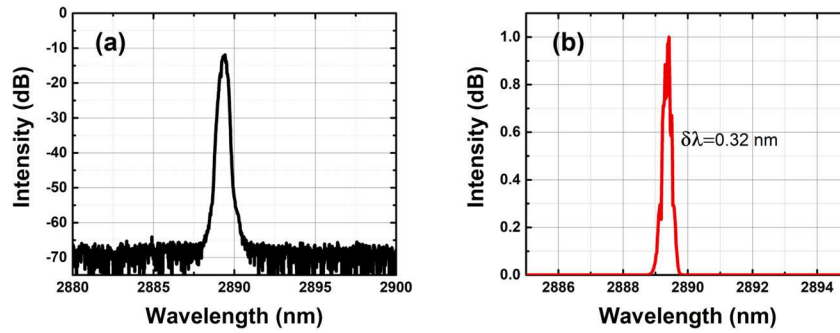
Fig. 3.4.8. Measured optical spectrum of the wavelength tunable Dy^{3+}/Er^{3+} co-doped ZBLAN fiber laser operating at 2889 nm with intensity plotted in (a) logarithmic scale, and (b) linear scale.

The output power as a function of the launched pump power for the wavelength tunable 4.5-m Dy^{3+}/Er^{3+} co-doped ZBLAN fiber laser operating at different wavelengths was measured and is shown in Figure 3.4.9. It is clear that the wavelength tunable laser has different pump thresholds and slope efficiencies as it operates at different wavelengths. The slope efficiencies and pump thresholds are summarized in Table 3.4.1. The 3 μm laser has the highest efficiency because the 4.5-m Dy^{3+}/Er^{3+} co-doped ZBLAN fiber has the largest gain

around 3 µm as shown by the ASE spectrum. The 2.785 µm laser produced by Er^{3+} has the lowest efficiency of 0.56%, which is even much less than that of a single Er^{3+}-doped ZBLAN fiber laser, because it suffers from high loss caused by the energy transfer from Er^{3+} to Dy^{3+} and the strong absorption of Dy^{3+} at this wavelength. When the laser wavelength was tuned to 2.85 µm, the laser efficiency increased to 1.52% because the laser emission was produced by Dy^{3+}.   The laser efficiency increased with increasing operating wavelength until reaching a maximum of 3.28% at 3 µm and then decreased with increasing operating wavelength due to the reduced gain at long wavelengths. A slope efficiency of 1.23 % was measured for the wavelength tunable fiber laser operating at 3.2 µm. The pump threshold of the 4.5-m Dy^{3+}/Er^{3+} co-doped ZBLAN fiber laser, however, decreased as the operating wavelength increased from 2.85 µm to 3.1 µm. The pump threshold of the wavelength tunable laser operating at 2.85 µm was 12 W and decreased to a minimum value of 5.77 W at 3.1 µm, where the blazed grating has the maximum reflection. Further increasing the laser wavelength led to an increase of the pump threshold due to the decreasing emission cross-section. Because the laser emission below 2.8 µm result only from the $^4I_{11/2}$ -$^4I_{13/2}$ transition of Er^{3+}, the pump threshold of the 2.785 µm laser was 8.2 W, which is smaller than that of the 2.85 µm laser that is produced by the $^6H_{13/2}$ - $^6H_{15/2}$ transition of Dy^{3+}.
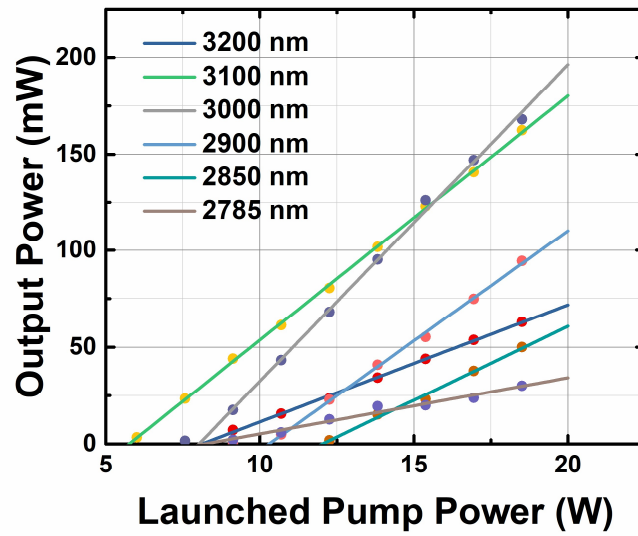
Fig. 3.4.9. The output power as a function of launched pump power for the 4.5-m wavelength tunable Er³⁺/Dy³⁺ co-doped fiber laser operating at different wavelengths.

Table 3.4.1. Slope efficiencies and thresholds of the 4.5-m wavelength tunable Er³⁺/Dy³⁺ co-doped ZBLAN fiber laser operating at different wavelengths.

Wavelength (nm)	Slope Efficiency (%)	Threshold (W)
2785	0.56	8.20
2850	1.52	12.03
2900	2.26	10.28
3000	3.28	8.02
3100	2.53	5.77
3200	1.23	8.28

The output power at different wavelengths of the 4.5-m wavelength tunable Dy³⁺/Er³⁺ co-doped ZBLAN fiber laser was measured at pump powers of 15.4 W and 18.5 W, respectively, and is shown in Figure 3.4.10. The output power increases with increasing operating wavelength until it reaches a maximum at 3

μm and then decreases with increasing operating wavelength above that. A maximum output power of 168 mW at 3 μm was obtained at a pump power of 18.5 W. Higher output power can be obtained with higher pump power, but increases the likelihood of fiber damage due to the thermal management issues at the pumping end. It is also worth noting that the wavelength tunable 4.5-m Dy^{3+}/Er^{3+} co-doped ZBLAN fiber laser cannot operate at 2740 nm or a shorter wavelength at the two pump power levels due to the reduced gain of singly Er^{3+}-doped ZBLAN fiber laser. The output power of the laser at 2740 nm at different pump power levels was measured and is shown in Figure 3.4.11. It is clear that the output increased with the increasing pump power until reaching a maximum value of 10 mW at a pump power of 11.32 W. Further increase of the pump power led to a rapid decrease of the output power and the 2740 nm lasing vanished as the pump power exceeded 13 W. Nevertheless, the operating wavelength of the 4.5-m Dy^{3+}/Er^{3+} co-doped ZBLAN fiber laser can be tuned to 2709 nm at low pump power. The Dy^{3+}/Er^{3+} co-doped ZBLAN fiber laser has wavelength tuning behavior similar to that of a single Er^{3+}-doped ZBLAN fiber laser, confirming that Er^{3+} in the co-doped system can be forced to lase individually.   However, the efficiency of the Dy^{3+}/Er^{3+} co-doped ZBLAN fiber laser is much smaller than that of that of singly Er^{3+}-doped fiber lasers because Dy^{3+} has large absorption in the 2700nm region. The efficiency of a wavelength tunable Dy^{3+}/Er^{3+} co-doped ZBLAN fiber laser can be further improved by optimizing the doping levels of Dy^{3+} and Er^{3+}.
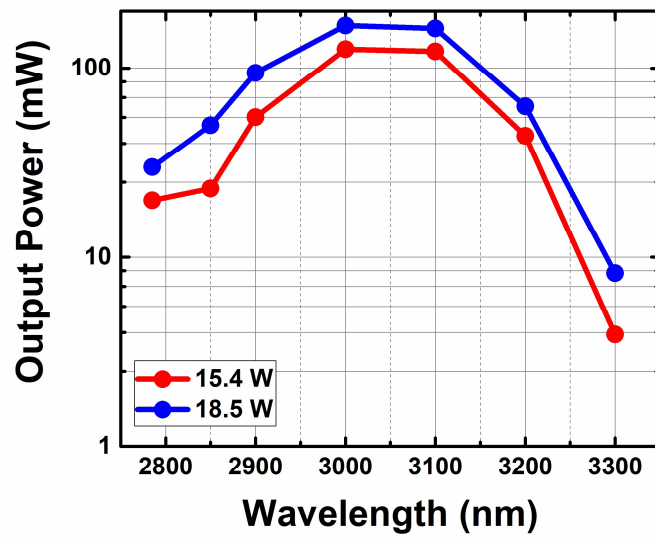
Fig. 3.4.10. Output power of the 4.5-m wavelength tunable Dy³⁺/Er³⁺ co-doped fiber laser operating at different wavelengths pumped at 15.4 W and 18.5 W.
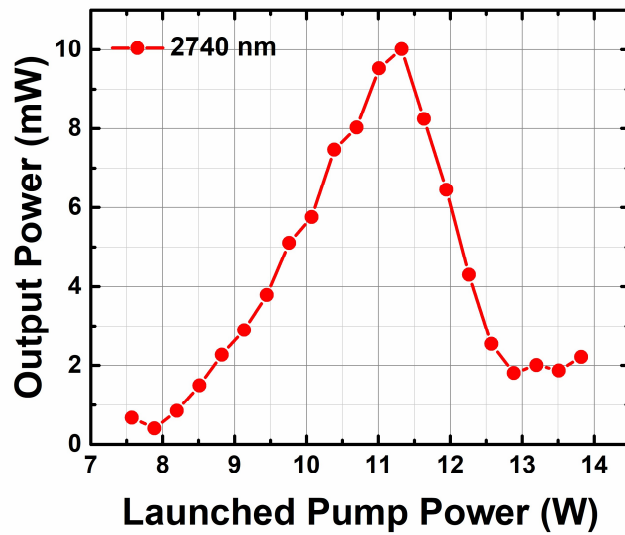
Fig. 3.4.11. Output power as a function of launched pump power for the 4.5-m wavelength tunable Dy³⁺/Er³⁺ co-doped fiber lasers operating at 2740 nm.

3.5 Chapter summary.

In conclusion, we have demonstrated widely wavelength tunable Dy^{3+}/Er^{3+} co-doped fiber lasers using 0.25 mol.% $Dy^{3+}/$ 4 mol.% Er^{3+} co-doped ZBLAN fiber. A continuous wavelength tunable range of nearly 700 nm was achieved. The efficiency and wavelength tunable range of Dy^{3+}/Er^{3+} co-doped fiber lasers can be further improved by optimizing the doping levels of Dy^{3+} and Er^{3+}. A more powerful wavelength-tunable laser in the 2.7-3.4 μm can be obtained by using higher pump power with improved thermal management or by using fiber amplifiers.

Chapter 4. Compact CNT Mode-locked Ho³⁺-doped Fluoride Fiber Laser at 1.2 μm

In previous chapters, we have discussed fluoride fiber lasers operating in the mid-infrared region. However, fluoride fiber lasers also have significant performance in the infrared region. In this chapter, we are going to introduce a mode-locked fiber laser operating at 1.2 μm. A diode laser pumped carbon nanotube mode-locked Ho³⁺-doped fluoride fiber laser at 1.2 μm is demonstrated in this chapter. Stable mode-locked pulses with an average power of 1 mW at a repetition rate of 18.47 MHz were obtained at a pump power of 348 mW. The pulse energy and peak power of this mode-locked laser oscillator were about 54 pJ and 12.6 W, and increased to 2.41 nJ and 0.54 kW, respectively, by using a 15-cm Ho³⁺-doped fluoride fiber amplifier. The pulse duration was measured to be 4.3 ps with an autocorrelator.

4.1 Introduction and background.

Laser sources operating in the 1.2 μm wavelength region have attracted increasing interest for a variety of applications including molecular spectroscopy, medical treatment, oxygen remote sensing, noninvasive medicine and biomedical diagnostics [123-126]. In recent years, fiber lasers have become excellent laser platforms due to their advantages including low manufacturing and maintenance cost, high reliability and compactness, excellent beam quality, high power scalability and heat dissipation capability. Several fiber lasers in this wavelength

region have been demonstrated by use of Raman scattering of silica fiber and radiative emission of bismuth ions [128-131]. However, long fibers (10s-100s meter) had to be used in these demonstrations due to the low unit gains of Raman fibers and bismuth-doped fibers. It is well known that ZBLAN (ZrF_4-BaF_2-LaF_3-AlF_3-NaF) glass is the most stable heavy metal fluoride glass allowing high concentration doping of rare-earth ions and thus high unit gains can be obtained with highly doped ZBLAN fibers. On the other hand, rare-earth ions doped in ZBLAN allow a number of laser transitions that are non-radiative in silica glass because of the low phonon energy of ZBLAN and their long radiative lifetimes [127]. Holmium (Ho^{3+}) doped ZBLAN can emit efficiently at 1.2 μm through the transition from the upper level $^5I_6$ to the lower level $^5I_8$ besides other radiative transitions yielding mid-infrared emissions at 2 μm and 3 μm [132]. Most recently, several Ho^{3+}-doped ZBLAN fiber lasers at 1.2 μm have been demonstrated with either continuous-wave (CW) or Q-switched laser output [127, 133-136].

Owing to the high unit gain of highly Ho^{3+}-doped ZBLAN fiber, a single frequency distributed Bragg reflector all-fiber laser at 1.2 μm with a spectral line width less than 100 kHz has been demonstrated [133] and a 2.4-W CW fiber laser with a slope efficiency of 42% at 1.19 μm has been recently achieved with only a 10 cm gain fiber [134]. Q-switched operation of Ho^{3+}-doped fiber lasers has also been successfully demonstrated with graphene and semiconductor saturable absorbers [135, 136], however, the shortest pulse obtained so far is 800 ns. Much shorter pulses and higher peak power are in great demand for various

applications. Therefore, mode-locked Ho[3+]-doped ZBLAN fiber lasers are attractive for achieving ultrashort pulses at 1.2 μm. Mode-locked operation of Ho[3+]-doped ZBLAN fiber laser at 1.2 μm was first demonstrated with a nonlinear polarization rotation (NPR) technique [137] and 47 ps pulses at a repetition rate of 1.77 MHz were obtained. However, the NPR technique is generally sensitive to environment and small perturbations. In contrast, a saturable absorber exhibiting high transmission at high power density can usually provide reliable and robust mode-locked laser performance. Carbon nanotubes (CNTs) have been used as excellent saturable absorbers for the mode-locked operation of a variety of lasers [138-141] due to their advantages including ultrafast recovery time (~100 fs), broad absorption bandwidth, chemical stability and ease of incorporating with fibers. Various CNT mode-locked fiber lasers in the 1.55 μm and 2μm region have also been reported [139, 142-145]. In this chapter, we report a CNT mode-locked Ho[3+]-doped ZBLAN fiber laser at 1.2 μm. Sub-5 ps pulses in the 1.2 μm region were obtained for the first time, to the best of our knowledge. This laser provides us an excellent platform to study the mode-locking of a fiber laser with small net dispersion in the normal region.

The absorption and emission cross-sections of Ho[3+] ions corresponding to the 1.2 μm transitions were obtained by measuring the absorption and the fluorescence of Ho[3+]-doped ZBLAN glass and are shown in Figure 4.1.1. Ho[3+] has an absorption band around 1150 nm, which is very close to the desired laser wavelength 1.2 μm. In addition, an 1150 nm pump can easily be achieved with

semiconductor lasers or Raman fiber lasers. Therefore, 1150 nm lasers are the ideal pump sources for 1.2 µm lasers.

The energy-level diagram of Ho^{3+} is shown in the inset of Figure 4.1.1. Electrons in the ground state $^5I_8$ are pumped by 1150 nm to the excited state $^5I_6$. The 1.2 µm emission is generated through the transition from the excited state $^5I_6$ to the ground state $^5I_8$. In a low-concentration Ho^{3+}-doped ZBLAN glass, the lifetime of the $^5I_6$ state is about 3.5 ms, which is much shorter than the 12 ms lifetime of the $^5I_7$ state. Therefore, the competitive 2.9 µm emission is usually self-terminated due to population accumulation in the $^5I_7$ state. In addition, the branching ratio of 9:1 between the two transitions $^5I_6 \rightarrow {}^5I_8$ and $^5I_6 \rightarrow {}^5I_7$ is also advantageous for 1.2 µm emission. Therefore, Ho^{3+}-doped ZBLAN is a promising high-efficiency gain medium for the 1.2 um fiber lasers.
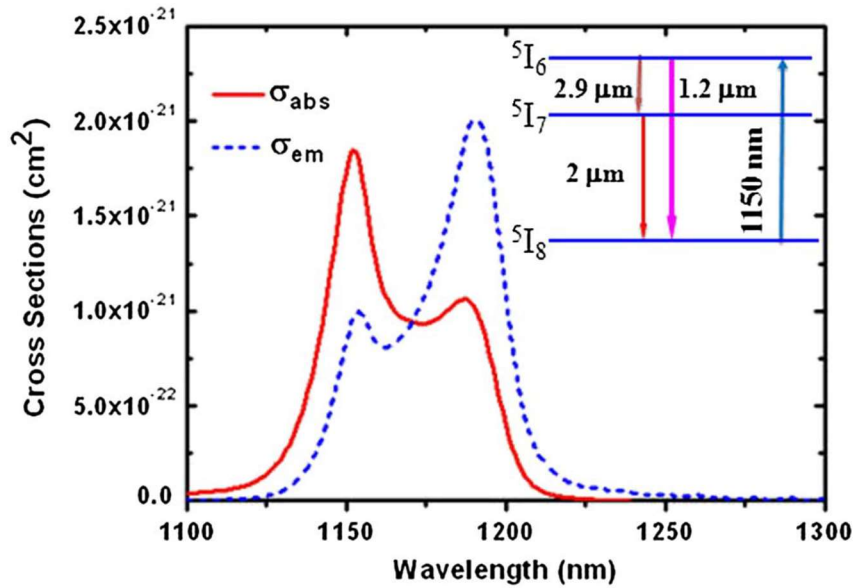
Fig. 4.1.1. (Color online) Absorption and emission cross-sections of Ho^{3+} ions in ZBLAN glass. (Inset: energy level diagram and transitions related to the 1.2 µm emission) [146].

4.2 Experimental setup.

The schematic of the experimental setup for the CNT mode-locked fiber ring-cavity laser is shown in Figure 4.2.1. A 10-cm long 3 mol.% Ho^{3+}-doped ZBLAN fiber was used as the gain fiber, which has a core diameter of 5.3 μm and cladding diameter of 125 μm. The numerical aperture of the fiber core is 0.14. A Vytran splicer was used to fabricate the gain chain by splicing a Ho^{3+}-doped ZBLAN fiber to two pieces of Hi1060 silica fibers. The Ho^{3+}-doped ZBLAN fiber chain was pumped by two polarization-combined 1150 nm semiconductor lasers via a filter-based wavelength division multiplexer (WDM1). A fused-taper-based WDM (WDM2) was used to remove the residual 1150 nm pump laser and served as a spectral filter for the mode-locked operation in the normal dispersion region as well. The 1190 nm port of WDM2 was spliced to a fiber-optic carbon nanotube (CNT) saturable absorber, which has a linear transmission of about 40%. A fused fiber coupler with a coupling ratio of 30/70 was used as the output coupler. An optical isolator (Isolator 2) was connected to the 30% output port of the 30/70 coupler to avoid the any reflection back to the ring cavity. Another isolator (Isolator1) was connected to the 70% port of the 30/70 coupler and the signal port of WDM1 to form the ring cavity and ensure unidirectional propagation of the laser. Pulse trains of the mode-locked laser were detected by an InGaAs avalanche photodetector (Thorlabs, APD130C) and measured by an oscilloscope (Tektronix, TDS1012) and a radio-frequency (RF) spectrum analyzer (ADVANTEST, R3131A). The output spectrum was measured with an optical spectrum analyzer (ANDO, AQ6317).
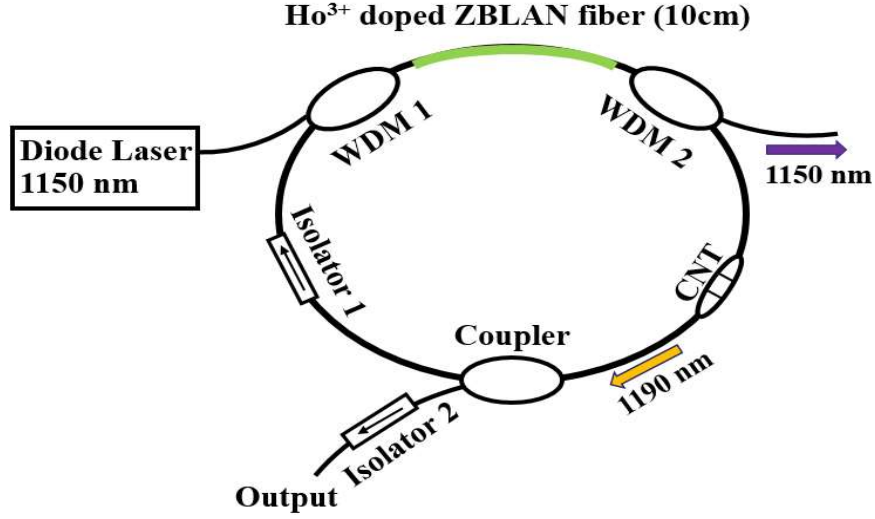
Fig. 4.2.1. Schematic of the experimental setup for a CNT mode-locked Ho^{3+}-doped ZBLAN fiber laser at 1.2 m

Saturable absorbers with proper absorption and modulation are crucial for the self-starting and stable mode-locked operation of a laser system. We have selected single-walled CNT particles with a diameter of 1.4 nm ± 0.1 nm and a length of 0.5-0.6 μm to make the saturable absorbers. Firstly, 5 milligrams of CNT powder was poured into 10 ml 0.1% sodium dodecyl sulfate aqueous solution. After ultrasonic processing, 5 ml of upper strata CNT solution was extracted. Then the upper strata CNT solution was mixed with polyvinyl alcohol (PVA) aqueous solution (2 mg/10ml) in different proportions. The CNT/PVA solutions with different proportions were poured into cuvettes to form films. The CNT/PVA films were cut into 1 mm × 1 mm pieces and put between two surfaces of fiber connectors to make a fiber-based CNT saturable absorbers. CNT saturable absorbers with linear transmissions from 20% to 80% were fabricated. Figure 4.2.2(a) shows the transmission of a CNT with a linear transmission of about 40%

at 1190 nm, which was selected for the development of a mode-locked laser system in the 1.2 µm region. The nonlinear transmission of this CNT saturable absorber was tested with the Ho^{3+}-doped ZBLAN fiber laser at 1.2 µm reported here. Figure 4.2.2(b) shows the measured transmission of this CNT saturable absorber as a function of the laser fluence. The saturated transmission of the CNT saturable absorber is about 73% at a laser fluence of 1.8 mJ/cm^2. The modulation depth of the CNT saturable absorber is 33%, which was found to be enough to mode-lock the Ho^{3+}-doped fiber laser very easily.
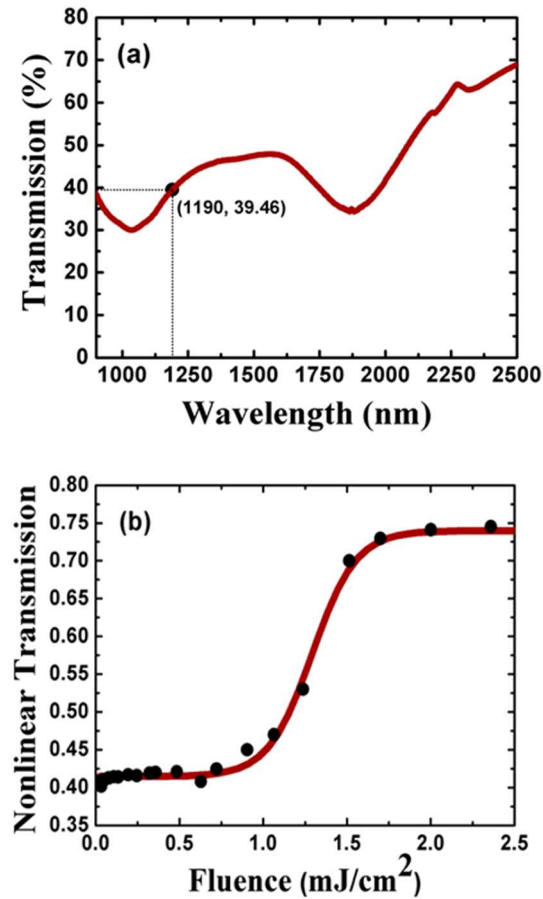
Fig. 4.2.2. (a) Linear transmission of a CNT saturable absorber vs wavelength.(b) Nonlinear transmission of a CNT saturable absorber measured at 1190nm .

4.3 Experimental results

Stable mode-locked operation of the ring cavity fiber laser started at a pump power of 335 mW and was maintained until the pump power reached 441 mW, with stable pulses disappearing when the pump power was higher than that. When the pump power was 348 mW, the laser output power was 1 mW. The pulse train of the CNT mode-locked Ho^{3+}-doped ZBLAN fiber laser was measured by an oscilloscope and is shown in Figure 4.3.1. The output spectrum of the laser is shown in Figure 4.3.2 The central wavelength of the laser is 1192 nm and the 3-dB bandwidth of the laser is about 0.48 nm. Due to the small total dispersion of the fiber cavity ($0.12ps^2$), the spectrum of this normal dispersion mode-locked laser exhibits different features from mode-locked Yb^{3+} fiber lasers in the 1 μm region. There are two side peaks beside the main laser peak, which doesn't have a flat top, being more similar to that of an anomalous dispersion mode-locked fiber laser. RF spectra of this laser measured over a frequency range of 300 MHz and 50 kHz (centered on 18.47 MHz) are shown in Figure 4.3.3 (a) and (b), respectively. The repetition rate of the mode-locked laser is 18.47 MHz, which is consistent with a ring cavity length of 10.8 m. Over 70 dB signal-to-noise ratio and very narrow bandwidth of the RF spectrum confirms the stable mode-locked operation of this fiber laser. The pulse energy of the mode-locked laser is about 54 pJ.
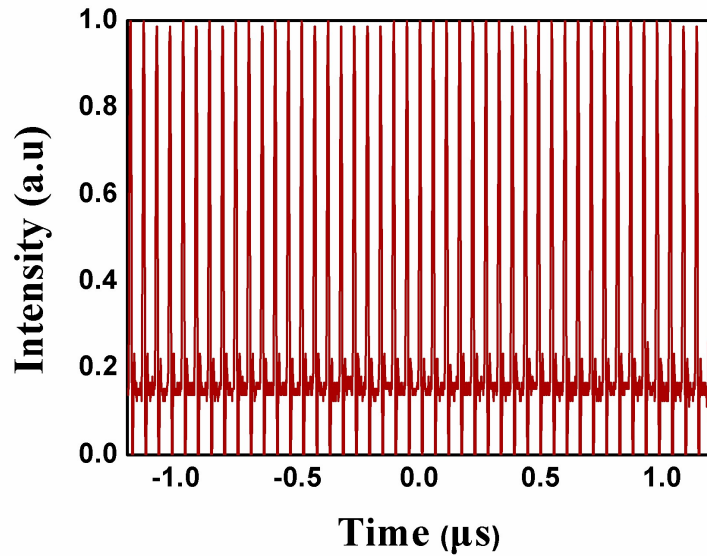
Fig. 4.3.1. Pulse trains of a CNT mode-locked Ho^{3+}-doped ZBLAN fiber laser.
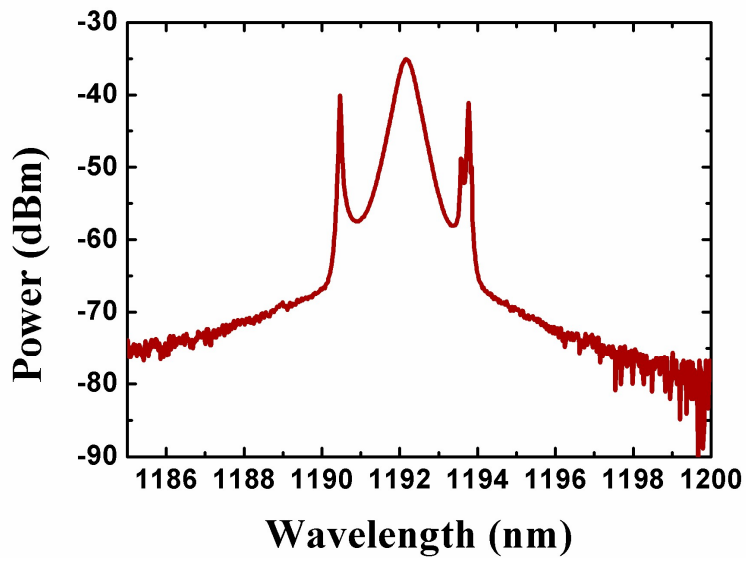
Fig. 4.3.2. Optical spectrum of a CNT mode-locked Ho^{3+}-doped ZBLAN fiber laser.
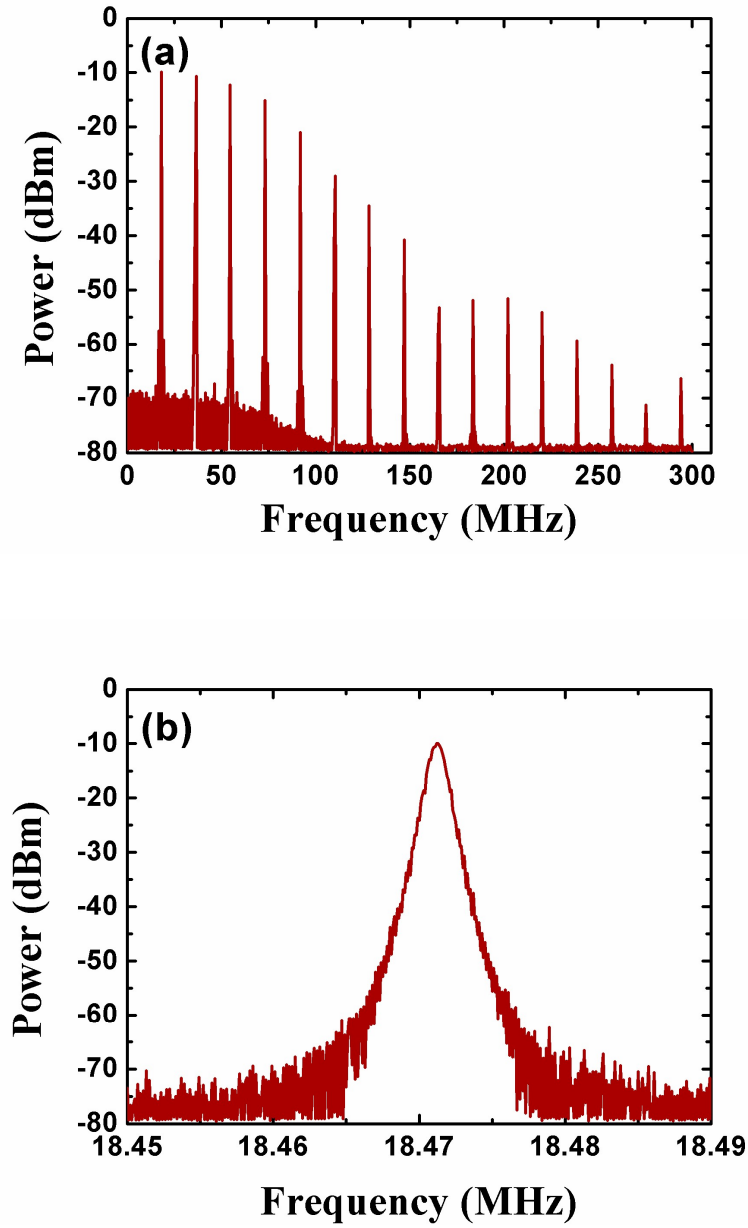
Fig. 4.3.3. Radio-frequency spectra of a CNT mode-locked Ho^{3+}-doped ZBLAN fiber laser measured over (a) a frequency range of 300 MHz and (b) a small frequency range of 40 kHz centered at 18.47 MHz.

An autocorrelator (Femtochrome, FR-103XL) was employed to measure the

pulse width. In order to measure the pulse width with high signal-to-noise ratio,

a 15-cm Ho^{3+}-doped ZBLAN fiber amplifier pumped by a 1150 nm Raman fiber laser was used to increase the average power of the mode-locked laser to 44.5 mW. The peak power of the amplified pulses is about 540 W. The nonlinear distortion of the mode-locked pulse was assumed to be negligible due to the short-length of the fiber amplifier. The autocorrelator trace was recorded with an oscilloscope and is shown in Figure 4.3.4. The full-width at half maximum (FWHM) of the autocorrelator trace is 6.72 ps, corresponding to a pulse width of 4.3 ps assuming the pulse is Gaussian. The time-bandwidth product of this laser is 0.4358, which is very close to the time-bandwidth-product (TBP) of a transform limited pulse, so we conclude that pulses of this compact CNT mode-locked Ho^{3+}-doped fluoride fiber laser were transform limited.
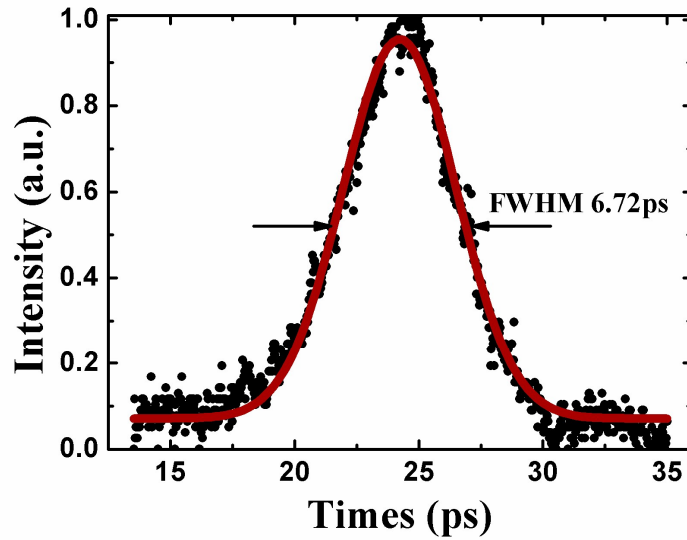
Fig. 4.3.4. Autocorrelation trace of the mode-locked fiber laser.

In conclusion, we have successfully developed a diode-pumped CNT mode-locked Ho^{3+}-doped ZBLAN fiber laser at 1192 nm. Fundamental mode-locking of this laser was obtained at a pump power of 348 mW. The pulse width was measured to be 4.3 ps, which is the shortest pulse width ever obtained for a fiber laser in the 1.2 μm region.

Reference:

[1]. A. Einstein, F. A. Barnes, " On the quantum theory of radiation", Laser Theory, 5-21 IEEE Press, New Your(1972).

[2]. T. H. Maiman, "Stimulated optical radiation in ruby", Nature 187, 493-493 (1960).

[3]. T. H. Maiman, "Optical maser action in ruby", Br. Commun. Electron. 7 674 (1960).

[4]. A. Javan, W.R. Bennett Jr., and D. R. Herriott, "Population inversion and Continuous optical maser oscillation in a gas discharge containing a He-Ne mixture", Phys. Rev. Lett. 6(3), 106 (1961).

[5]. C. K. N. Patel, "Continuous-wave laser action on vibrational–rotational transitions of CO_2", Phys. Rev. 136 (5A), A1187 (1964).

[6]. C. K. N. Patel, "Interpretation of CO_2 optical maser experiments", Phys. Rev. Lett. 12 (21), 588 (1964).

[7]. A. D. White, E. I. Gordon and J. D. Rigden, "Output power of the 6328 Å gas maser", Appl. Phys. Lett. 2 (5), 91 (1963).

[8]. F. G. Houtermans, "Über Massen-Wirkung im optischen Spektralgebiet und die Möglichkeit absolut negativer Absorption für einige Fälle von Molekülspektren (Licht-Lawine)", Helv. Phys. Acta 33, 933 (1960).

[9]. E. I. Gordon and E. F. Labuda, "Gas pumping in continuously operating ion lasers", Bell Sys. Tech. J. 43 (4), 1827 (1964).

[10]. C. J. Koester and E. Snitzer, "Amplification in a fiber laser," Appl. Opt. 3, 1182–1186 (1964).

[11]. S. B. Poole, D. N. Payne, and M. E. Fermann, "Fabrication of low loss optical fibres containing rare-earth ions," Electron. Lett. 21, 737–738 (1985).

[12]. R. J. Mears, L. Reekie, S. B. Poole, and D. N. Payne, "Neodymium-doped silica single-mode fibre laser," Electron. Lett. 21, 738–740 (1985).

[13]. D. S. Funk, J. W. Carlson, and J. G. Eden, "Ultraviolet (381 nm), room temperature laser in neodymium-doped fluorozirconate fibre," Electron. Lett. 30, 1859–1860 (1994).

[14]. J. Y. Allain, M. Monerie, and H. Poignant, "Tunable CW lasing around 610, 635, 695, 715, 885 and 910 nm in praseodymiumdoped fluorozirconate fibre," Electron. Lett. 27, 189–191 (1991).

[15]. R. G. Smart, D. C. Hanna, A. C. Tropper, S. T. Davey, S. F. Carter, and D. Szebesta, "CW room temperature upconversion lasing at blue, green and red wavelengths in infrared-pumped Pr^{3+}-doped fluoride fibre," Electron. Lett. 27, 1307–1309 (1991).

[16]. H. M. Pask, R. J. Carman, D. C. Hanna, A. C. Tropper, C. J. Mackechnie, P. R. Barber, and J. M. Dawes, "Ytterbium-doped silica fiber lasers: versatile sources for the 1–1.2 μm region," IEEE J. Sel. Top. Quantum Electron. 1, 2–13 (1995).

[17]. J. Nilsson,W. A. Clarkson, R. Selvas, J. K. Sahu, P. W. Turner, S. U. Alam, and A. B. Grudinin, "High power wavelength tunable cladding pumped rare-earth-doped silica fiber lasers," Opt. Fiber Technol. 10, 5–30 (2004).

[18]. P. F. Moulton, G. A. Rines, E. V. Slobodtchikov, K. F. Wall, G. Frith, B. Samson, and A. L. G. Carter, "Tm-doped fiber lasers: fundamentals and power scaling," IEEE J. Sel. Top. Quantum Electron. 15, 85–92 (2009).

[19]. X. Zhu and N. Peyghambarian, "High power ZBLAN glass fiber lasers: review and prospect," Adv. Optoelectron. 2010, 501956 (2010).

[20]. N. S. Prasad and M. Devi, in 11th International HITRAN Conference, The Harvard-Smithsonian Center for Astrophysics (Cambridge, 2010), pp. 16–18.

[21]. A. S. Yusupov, S. E. Goncharov, I. D. Zalevskii, V. M. Paramonov, and A. S. Kurkov, "Raman fiber laser for the drug-free photodynamic therapy," Laser Phys. 20, 357 (2010).

[22]. F. Anquez, E.Courtade, A.Sivery, P.Suret,and S.Randoux, "A high-power tunable Raman fiber ring laser for the investigation of singlet oxygen production from direct laser excitation around 1270 nm," Opt. Express 18, 22928 (2010).

[23]. M. Wanner, M. Avram, D. Gagnon et al., "Effects of non-invasive, 1,210 nm laser exposure on adipose tissue: Results of a human pilot study," Lasers Surg. Med. 41, 401 (2009).

[24].M. C. Pierce, S. D. Jackson, M. R. Dickinson, T. A. King, and P. Sloan, "Laser-tissue interaction with a continuous wave 3-μm fibre laser : Preliminary studies with soft tissue," Lasers in Surgery and Medicine: The Official Journal of the American Society for Laser Medicine and Surgery, 26(5): 491-495 (2000).

[25]. D. E. McCumber, "Einstein relations connecting broadband emission and absorption spectra", Phys. Rev. 136 (4A), A954 (1964).

[26]. T. Qiu, L. Li, A. Sch¨ulzgen, et al., "Generation of 9.3-W multimode and 4-W single-mode output from 7-cm short fiber lasers," IEEE Photonics Technology Letters, vol. 16, no. 12, pp. 2592–2594 (2004).

[27]. A. Sch¨ulzgen, L. Li, V. L. Temyanko, S. Suzuki, J. V. Moloney, and N. Peyghambarian, "Single-frequency fiber oscillator with watt-level output power using photonic crystal phosphate glass fiber," Optics Express, vol. 14, no. 16, pp. 7087– 7092 (2006).

[28]. R. E. Slusher, G. Lenz, J. Hodelin, J. Sanghera, L. B. Shaw, and I. D. Aggarwal, "Large Raman gain and nonlinear phase shifts in high-purity As2Se3 chalcogenide fibers," Journal of the Optical Society of America B, vol. 21, no. 6, pp. 1146–1155 (2004).

[29] J. S. Sanghera, I. D. Aggarwal, L. B. Shaw, et al., "Nonlinear properties of chalcogenide glass fibers," Journal of Optoelectronics and Advanced Materials, vol. 8, no. 6, pp. 2148– 2155 (2006).

[30]. K. Ohsawa, T. Shibata, K. Nakamura, and S. Yoshida, "Fluorozirconate glasses for infrared transmitting optical fibers," in Proceedings of the 7th European Conference on Optical Communication (1981),

[31]. P. France, M. G. Drexhage, J.M. Parker, M. W. Moore, S. F. Carter, and J. V.Wright, Fluoride Glass Optical Fibers, Blackie and Son, London, UK, (1990).

[32]. T. Kanamori and S. Sakaguchi, "Preparation of elevated NA fluoride optical fibers," Japanese Journal of Applied Physics, vol. 25, no. 6, pp. L468–L470 (1986).

[33]. J. Meijer, "Laser beam machining (LBM), state of the art and new opportunities," J. Mater. Process. Technol. 149, 2–17 (2004).

[34]. T. Tamaki, "Laser micro-welding of transparent materials by a localized heat accumulation effect using a femtosecond fiber laser at 1558 nm," Opt. Express 14, 10461– 10468 (2006).

[35]. M. Mielke, D. Gaudiosi, K. Kim, M. Greenberg, X. Gu, R. Cline, X. Peng, M. Slovick, N. Allen, M. Manning, M. Ferrel, N. Prachayaamorn, and S. Sapers, "Ultrafast fiber laser platform for advanced materials processing," J. Laser Micro/ Nanoeng. 5, 53–58 (2010).

[36]. A. Tuennermann, S. Nolte, and J. Limpert, "Femtosecond vs picosecond laser material processing," Laser Tech. J. 7, 34–38 (2010).

[37]. D. Creeden, P. A. Ketteridge, P. A. Budni, S. D. Setzler, Y. E. Young, J. C. McCarthy, K. Zawilski, P. G. Schunemann, T. M. Pollak, E. P. Chicklis, and M. Jiang, "Mid-infrared ZnGeP2 parametric oscillator directly pumped by a pulsed 2 micron Tm-doped fiber laser," Opt. Lett. 33, 315–317 (2008).

[38]. C. Kieleck, M. Eichhorn, A. Hirth, D. Faye, and E. Lallier, "High-efficiency 20–50 kHz mid-infrared orientationpatterned GaAs optical parametric oscillator pumped by a 2 micron holmium laser," Opt. Lett. 34, 262–264 (2009).

[39]. N. Leindecker, A. Marandi, R. L. Byer, K. L. Vodopyanov, J. Jiang, I. Hartl, M. Fermann, and P. G. Schunemann, "Octavespanning ultrafast OPO with 2.6–6.1 μm instantaneous bandwidth pumped by femtosecond Tm-fiber laser," Opt. Express 20, 7046–7053 (2012).

[40]. P. E. Britton, D. Taverner, K. Puech, D. J. Richardson, P. G. R. Smith, G. W. Ross, and D. C. Hanna, "Optical parametric oscillation in periodically poled lithium niobate driven by a diode-pumped Q-switched erbium fiber laser," Opt. Lett. 23, 582–584 (1998).

[41]. C. Gu, M. Hu, L. Zhang, J. Fan, Y. Song, C. Wang, and D. T. Reid, "High average power, widely tunable femtosecond laser source from red to mid-infrared based on an Yb-fiber-laserpumped optical parametric oscillator," Opt. Lett. 38, 1820– 1822 (2013).

[42]. J. M. Dudley, L. Provino, N. Grossard, H. Maillotte, R. S. Windeler, B. J. Eggleton, and S. Coen, "Supercontinuum generation in air-silica microstructured fibers with nanosecond and femtosecond pulse pumping," J. Opt. Soc. Am. B 19, 765–771 (2002).

[43]. C. R. Phillips, C. Langrock, J. S. Pelc, M. M. Fejer, J. Jiang, M. E. Fermann, and I. Hartl, "Supercontinuum generation in quasi-phase-matched LiNbO3 waveguide pumped by a Tmdoped fiber laser system," Opt. Lett. 36, 3912–3914 (2011).

[44]. S. Fan, H. Takeuchi, T. Ouchi, K. Takeya, and K. Kawase, "Broadband terahertz wave generation from a MgO:LiNbO3 ridge waveguide pumped by a 1.5 μm femtosecond fiber laser," Opt. Lett. 38, 1654–1656 (2013).

[45]. W. Shi, M. Leigh, J. Zong, Z. Yao, D. T. Nguyen, A. Chavez- Pirson, and N. Peyghambarian, "High power all fiber based narrow linewidth single mode fiber laser pulses in the C-band and frequency conversion to THz generation," IEEE Sel. Top. Quantum Electron. 15, 377–384 (2009).

[46]. A. Piper, A. Malinowski, K. Furusawa, and D. J. Richardson, "High power high brightness mJ Q-switched ytterbium-doped fiber laser," Electron. Lett. 40, 928–929 (2004).

[47]. O. Schmidt, J. Rothhardt, F. Roser, S. Linke, T. Schreiber, K. Rademaker, J. Limpert, S. Ermeneux, P. Yvernault, F. Salin, and A. Tunnermann, "Millijoule pulse energy Q-switched short-length fiber laser," Opt. Lett. 32, 1551–1553 (2007). 1 October 2014 / Vol. 53, No. 28 / APPLIED OPTICS 6565

[48]. Q. Fang, Y. Qin, B. Wang, and W. Shi, "230 Waverage power all fiber based actively Q-switched fiber master oscillator power amplifier," Appl. Opt. 52, 6744–6747 (2013).

[49]. L. Pan, I. Utkin, and R. Fedosejevs, "Passively Q-switched ytterbium-doped double-clad fiber laser with a Cr4+:YAG saturable absorber," IEEE Photon. Technol. Lett. 19, 1979–1981 (2007).

[50]. T. Tsai, Y. Fang, Z. Lee, and H. Tsao, "All fiber passively Qswitched erbium laser using mismatch of mode field areas and a saturable-amplifier pump switch," Opt. Lett. 34, 2891–2893 (2009).

[51]. J. Liu, S. Wu, Q. Yang, and P. Wang, "Stable nanosecond pulse generation from a graphene-based passively Qswitched Yb-doped fiber laser," Opt. Lett. 36, 4008–4010 (2011).

[52]. K. T. Vu, A. Malinowski, and D. J. Richardson, "Adaptive pulse shape control in a diode-seeded nanosecond fiber MOPA system," Opt. Express 14, 10996–11001 (2006)..

[53]. P. Perez-Millan, A. Diez, M. V. Andres, D. Zalvidea, and R. Duchowicz, "Q-switched all-fiber laser based on magnetostriction modulation of a Bragg grating," Opt. Express 13, 5046–5051 (2005).

[54]. M. Leigh, W. Shi, J. Zong, J. Wang, S. Jiang, and N. Peyghambarian, "Compact single frequency all fiber Q-switched laser at 1 μm," Opt. Lett. 32, 897–899 (2007).

[55]. K. Kieu and M. Mansuripur, "Active Q-switching of a fiber laser with a microsphere resonator," Opt. Lett. 31, 3568– 3570 (2006).

[56]. L. F. Mollenauer and R. H. Stolen, "Soliton laser", Opt. Lett. 9 (1), 13 (1984).

[57].J. G. Fujimoto, A. M. Weiner, and E. P. Ippen, "Generation and measurement of optical pulses as short as 16 fs", Appl. Phys. Lett. 44, 832 (1984).

[58]. R. L. Fork et al., "Compression of optical pulses to six femtoseconds by using cubic phase compensation", Opt. Lett. 12 (7), 483 (1987).

[59]. H. A. Haus, "Mode-locking of lasers", J. Sel. Top. Quantum Electron. 6 (6), 1173 (2000).

[60]. T. Hu, D. D. Hudson, S. D. Jackson, "Actively Q-switched 2.9 μm Ho^{3+} Pr^{3+} doped fluoride fiber laser", Opt. Lett., 37, 2145-2147 (2012).

[61]. D. J. Coleman, T. A. King, D. K. Ko, et al, "Q-switched operation of a 2.7 μm cladding-pumped Er3+/Pr3+ codoped ZBLAN fibre laser", Opt. Commun., 236, 379-385 (2004).

[62]. S. Tokita, M. Murakami, S. Shimizu, et al, "12 W Q-switched Er: ZBLAN fiber laser at 2.8 μm", Opt. Lett., 36, 2812-2814 (2011).

[63]. M. Gorjan, M. Marinček, M. Čopič, "High-power pulsed diode-pumped Er:ZBLAN fiber laser", Opt. Lett., 36, 1923-1925 (2011).

[64]. C. Wei, X. Zhu, R. A. Norwood, et al., "Passively Q-Switched 2.8-Nanosecond Fiber Laser", IEEE PHOTONICS TECH L, 24,1741-1744 (2012).

[65]. T. Hu, D. D. Hudson, S. D. Jackson, "Actively Q-switched 2.9 μm Ho^{3+}/Pr^{3+} doped fluoride fiber laser", Opt. Lett., 37, 2145-2147 (2012)

[66]. J. Li, T. Hu, S. D. Jackson, "Dual wavelength Q-switched cascade laser", Opt. Lett., 37, 2208-2210 (2012).

[67]. J. Li, T. Hu, S. D. Jackson, "Q-switched induced gain switching of a two-transition cascade laser", Opt. Express, 20, 13123-13128 (2012).

[68]. J. Li, D. D. Hudson, Y. Liu, et al., "Efficient 2.87 μm fiber laser passively switched using a semiconductor saturable absorber mirror", Opt. Lett., 37, 3747-3749 (2012).

[69]. C. Wei, X. Zhu, et al. "Passively continuous-wave mode-locked Er^{3+} doped ZBLAN fiber laser at 2.8 μm", Opt. Lett., 37, 3849-3851 (2012).

[70]. A. Haboucha, V. Fortin, M. Bernier, et al., "Fiber Bragg grating stabilization of a passively mode-locked 2.8 μm Er^{3+}: fluoride glass fiber laser", Opt. Lett., 39, 3294-3297 (2014).

[71]. T. Hu, D. D. Hudson, S. D. Jackson, "Stable, self-starting, passively mode-locked fiber ring laser of the 3 μm class", Opt. Lett., 39, 2133-2136 (2014).

[72]. S. Duval, M. Bernier, V. Fortin, et al., "Femtosecond fiber lasers reach the mid-infrared", Optica, 2, 623-626 (2015).

[73]. P. Tang, Z. Qin, J. Liu, et al., "Watt-level passively mode-locked Er^{3+} doped ZBLAN fiber laser at 2.8 μm", Opt. Lett. 40, 4855-4858 (2015).

[74]. Z. Qin, G. Xie, C. Zhao, et al., "Mid-infrared mode-locked pulse generation with multilayer black phosphorus as saturable absorber", Opt. Lett., 41, 56-59 (2016).

[75]. T. Hu, S. D. Jackson, D. D. Hudson, "Ultrafast pulses from a mid-infrared fiber laser", Opt. Lett., 40, 4226-4228 (2015).

[76]. K. Yin, T. Jiang, X. Zheng, et al., "Mid-infrared ultra-short mode-locked fiber laser utilizing topological insulator Bi2Te3 nano-sheets as the saturable absorber", arXiv:1505.06322 (2015).

[77]. G. Zhu, X. Zhu, F. Wang, et al., "Graphene Mode-Locked Fiber Laser at 2.8 μm ", IEEE PHONTONICS TECH L, 28, 7-10 (2016).

[78]. M. E. Doroshenko, P. Koranda, J. Tauer, H. Kofler, E. Wintner, and J. K. Jabczynski, "Mid-infrared Q-switched Er : YAG laser for medical applications," Laser Phys. Lett. 7 498 (2010).

[79]. F. K. Tittel, D. Richter, and A. Fried. "Mid-infrared laser applications in spectroscopy," in Solid-state mid-infrared laser sources, 458-529 (2003).

[80]. M. C. Pierce, S. D. Jackson, M. R. Dickinson, T. A. King, and P. Sloan, "Laser-tissue interaction with a continuous wave 3-μm fibre laser : Preliminary studies with soft tissue," Lasers in Surgery and Medicine: The Official Journal of the American Society for Laser Medicine and Surgery, 26(5): 491-495 (2000).

[81]. J. Tafoya, J. W. Pierce, R. K. Jain, B. J. F. Wong, "Efficient and compact high-power mid-IR (~3 um) lasers for surgical applications," Proc. SPIE 5312, Lasers in Surgery: Advanced Characterization, Therapeutics, and Systems XIV, (13 July 2004).

[82]. P. Werle, F. Slemr, K. Maurer, R. Kormann, M. Robert, and J. Bernd, "Near- and mid-infrared laser-optical sensors for gas analysis," Proc. SPIE 4817, Diode Lasers and Applications in Atmospheric Sensing, (23 September 2002);

[83]. M. C. Brierley and P. W. France, "Continuous wave lasing at 2.7 μm in an erbium-doped fluorozirconate fiber," Electronics Letters, 24(15), pp. 935–937 (1988).

[84]. Q. Ren, V. Venugopalan, K. Schomacker, T. F. Deutsch, T. J. Flotte, C. A. Puliafito, and R. Birngruber, "Mid-infrared laser ablation of the cornea: a comparative study," Lasers Surg. Med. 12, 274–281 (1992).

[85]. H. A. Wigdor and J. T. Walsh, Jr., J. D. Featherstone, S. R. Visuri, D. Fried, and J. L. Waldvogel, "Lasers in dentistry," Lasers Surg. Med. 16, 103–133 (1995).

[86].L. I. Deckelbaum, "Cardiovascular applications of laser technology," Lasers Surg. Med. 15, 315–341 (1994).

[87]. J. Kampmeier, S. Schafer, G. E. Lang, and G. K. Lang, "Comparison of free-running vs. Q-switched Er: YAG laser photorefractive keratec- tomy (scanning mode) in swine eyes," J. Refract. Surg. 15, 563–571 (1999).

[88].M. C. Brierley and P. W. France, "Continuous wave lasing at 2.7 μm in an erbium-doped fluorozirconate fiber," Electronics Letters, 24(15), pp. 935–937 (1988).

[89].Stuart D. Jackson, Terence A. King, and Markus Pollnau, "Diode-pumped 1.7-W erbium 3-μm fiber laser," Opt. Lett. 24, 1133-1135 (1999).

[90]. T. Sandrock, D. Fischer, P. Glas, M. Leitner, and W. Wrage, "Diode-pumped 1-W Er-doped fluoride glass M-profile fiber laser emitting at 2.8 m," Opt. Lett. 24, pp. 1284-1286 (1999).

[91]. B. Srinivasan, J. Tafoya, and R. K. Jain, "High-power "Watt-level" CW operation of diode-pumped 2.7 m fiber lasers using efficient cross-relaxation and energy transfer mechanisms," Opt. Express 4, pp. 490-495 (1999).

[92]. X. Zhu and R. Jain, "10-W-level diode-pumped compact 2.78 um ZBLAN fiber laser," Opt. Lett. 32(1), 26-28 (2007).

[93]. S. Tokita, M. Murakami, S. Shimizu, M. Hashida, and S. Sakabe, "Liquid-cooled 24 W mid-infrared Er : ZBLAN fiber laser," Opt. Lett. 34(20), 3062-3064 (2009).

[94]. S. Tokita, M. Hirokane, M. Murakami, S. Shimizu, M. Hashida, and S. Sakabe, "Stable 10 W Er:ZBLAN fiber laser operating at 2.71–2.88μm," Opt. Lett. 35(23), 3943-3945 (2010).

[95]. Yigit Ozan Aydin, Vincent Fortin, Réal Vallée, and Martin Bernier, "Towards power scaling of 2.8 μm fiber lasers," Opt. Lett. 43, 4542-4545 (2018).

[96]. V. Fortin, M. Bernier, S. T. Bah, and R. Vallée, "30 W fluoride glass all-fiber laser at 2.94 μm," Opt. Lett. 40(12), 2882-2885 (2015).

[97]. M. R. Majewski, R. I. Woodward, and S. D. Jackson, "Dysprosium-doped ZBLAN fiber laser tunable from 2.8 μm to 3.4 μm, pumped at 1.7 μm," Opt. Lett. 43(5), 971-974 (2018).

[98]. S. D. Jackson, "Single-transverse-mode 2.5-W holmium-doped fluoride fiber laser operating at 2.86 μm," Opt. Lett. 29(4), 334-336 (2004).

[99].Y. H. Tsang, A. E. El-Taher, T. A. King, and S. D. Jackson, "Efficient 2.96 μm dysprosium-doped fluoride fibre laser pumped with a Nd:YAG laser operating at 1.3 μm," Opt. Express 14(2), 678-685 (2006).

[100]. R. I. Woodward, M. R. Majewski, G. Bharathan, D. D. Hudson, A. Fuerbach, and S. D. Jackson, "Watt-level dysprosium fiber laser at 3.15 μm with 73% slope efficiency," Opt. Lett. 43(7), 1471-1474 (2018).

[101]. V.Fortin, F. Jobin, M. Larose, M. Bernier, and R. Vallée, "10-W-level monolithic dysprosium-doped fiber laser at 3.24 μm," Opt. Lett. 44(3), 491-494 (2019).

[102]. M. R. Majewski, R. I. Woodward, and S.D. Jackson," Dysprosium-doped ZBLAN fiber laser tunable from 2.8 μm to 3.4 μm, pumped at 1.7 μm." Opt. Lett. 43(5), 971-974 (2018).

[103]. R. I. Woodward, M. R. Majewski and S.D. Jackson, "Mode-locked dysprosium fiber laser: Picosecond pulse generation from 2.97 to 3.30 μm,"APL Photonics 3(11), 116106 (2018).

[104]. M. R. Majewski, M. Z. Amin, T. Berthelot, and S. D. Jackson," Directly diode-pumped mid-infrared dysprosium fiber laser," Opt. Lett. 44(22), 5549-5552 (2019).

[105]. J. Wang, X. Zhu, M. Mollaee, J. Zong, and N. Peyhambarian, "Efficient energy transfer from Er^{3+} to Ho^{3+} and Dy^{3+} in ZBLAN glass,"Opt. Express 28(4), 5189-5199 (2020).

[106]. J. Mei, K. Zhong, M. Wang, Y. Liu, D. Xu, W. Shi, Y. Wang, J. Yao, R. A. Norwood, and N. Peyghambarian, "Widely-tunable high-repetition-rate terahertz generation in GaSe with a compact dual-wavelength KTP OPO around 2 μm," Opt. Express 24, 23368-23375 (2016).

[107]. T. Xing, L. Wang, S. Hu, T. Cheng, X. Wu, and H. Jiang, "Widely tunable and narrow-bandwidth pulsed mid-IR PPMgLN-OPO by self-seeding dual etalon-coupled cavities," Opt. Express 25, 31810-31815 (2017).

[108]. K. Huang, J. Gan, J. Zeng, Q. Hao, K. Yang, M. Yan, and H. Zeng, "Observation of spectral mode splitting in a pump-enhanced ring cavity for mid-infrared generation," Opt. Express 27(8), 11766-11775 (2019).

[109]. K. Huang, Y. Wang, J. Fang, H. Chen, M. Xu, Q. Hao, M. Yan, and H. Zeng, "Highly efficient difference-frequency generation for mid-infrared pulses by passively synchronous seeding," High Power Laser Sci. Eng. 9, E4 (2021).

[110]. G. J. Wagner, T. J. Carrig, R. H. Page, K. I. Schaffers, J. Ndap, X. Ma, and A. Burger, "Continuous-wave broadly tunable Cr2+:ZnSe laser," Opt. Lett. 24(1), 19-21 (1999).

[111]. V.V. Fedorov; S.B. Mirov; A. Gallian; D.V. Badikov; M.P. Frolov; Y.V. Korostelin; V.I. Kozlovsky; A.I. Landman, Y. P. Podmar'kov, V. A. Akimov, and A. A. Voronov, "3.77–5.05

μm Tunable Solid-State Lasers Based on Fe2+-Doped ZnSe Crystals Operating at Low and Room Temperatures," IEEE J. Quantum Electron. 42 (9), 907-917 (2006).

[112]. M. Razeghi, W. Zhou, S. Slivken, Q. Lu, D. Wu, and R. McClintock, "Recent progress of quantum cascade laser research from 3 to 12 μm at the Center for Quantum Devices [Invited]," Appl. Opt. 56(31), H30-H44 (2017).

[113]. A. Bauer,F. Langer, M. Dallner, M. Kamp, M. Motyka, G. Sęk, K. Ryczko, J. Misiewicz, S. Hofling, and A. Forchel,   "Emission wavelength tuning of interband cascade lasers in the 3–4 μm spectral range, " Appl. Phys. Lett. 95(25), 251103 (2009).

[114]. X. Zhu, N. Peyghambarian. "High-power ZBLAN glass fiber lasers: review and prospect," Adv. OptoElectron. 2010 (2010).

[115]. N. J. C. Libatique, J. Tafoya, N. K. Viswanathan, R. K. Jain and A. Cable, "Field-usable diode-pumped 120 nm wavelength-tunable CW mid-IR fibre laser." Electron. Lett. 36(9), 791-792 (2000).

[116]. X. Zhu, and R. Jain, "Compact 2 W wavelength-tunable Er: ZBLAN mid-infrared fiber laser." Opt. Lett. 32(16), 2381-2383 (2007).

[117]. S. Tokita, M. Hirokane, M. Murakami, S. Shimizu, M. Hashida, and S. Sakabe, "Stable 10 W Er:ZBLAN fiber laser operating at 2.71–2.88μm," Opt. Lett. 35(23), 3943-3945 (2010).

[118]. D. Hudson, E. Magi, L. Gomes, and S. D. Jackson, "1W diode-pumped tunable Ho3+, Pr3+-doped fluoride glass fibre laser." Electron. Lett. 47(17), 985-986 (2011).

[119]. W. Li, H. Wang, T. Du, B. Xu, Z. Cai, H. Xu, and Z. Luo, "Compact self-Q-switched, tunable mid-infrared all-fiber pulsed laser," Opt. Express 26(26), 34497-34502 (2018).

[120]. M. R. Majewski and S. D. Jackson, "Tunable dysprosium laser." Opt. Lett. 41(19), 4496-4498 (2016).

[121]. M. R. Majewski, R. I. Woodward and S. D. Jackson, "Dysprosium-doped ZBLAN fiber laser tunable from 2.8 μm to 3.4 μm, pumped at 1.7 μm." Opt. Lett. 43(5), 971-974 (2018).

[122]. J. Wang, X. Zhu, R. A. Norwood, and N. Peyghambarian, "Beyond 3 μm Dy^{3+}/Er^{3+} co-doped ZBLAN fiber lasers pumped by 976 nm laser diode," Appl. Phys. Lett. 118(15), 151101 (2021).

[123]. N. S. Prasad and M. Devi, in 11th International HITRAN Conference, The Harvard-Smithsonian Center for Astrophysics (Cambridge, 2010), pp. 16–18.

[124]. A. S. Yusupov, S. E. Goncharov, I. D. Zalevskii, V. M. Paramonov, and A. S. Kurkov, "Raman fiber laser for the drug-free photodynamic therapy," Laser Phys. 20, 357 (2010).

[125]. F. Anquez, E.Courtade, A.Sivery, P.Suret,and S.Randoux, "A high-power tunable Raman fiber ring laser for the investigation of singlet oxygen production from direct laser excitation around 1270 nm," Opt. Express 18, 22928 (2010).

[126]. M. Wanner, M. Avram, D. Gagnon et al., "Effects of non-invasive, 1,210 nm laser exposure on adipose tissue: Results of a human pilot study," Lasers Surg. Med. 41, 401 (2009).

[127]. X. Zhu, J. Zong, R. A. Norwood , A. Chavez-Pirson , N. Peyghambarian , N. Prasadl., "Holmium-doped ZBLAN fiber lasers at 1.2 μm," Proc. SPIE 8237, 823727 (2012).

[128]. L. Zhang, H. Jiang, S. Cui, J. Hu, and Y. Feng, "Versatile Raman fiber laser for sodium laser guide star," Laser.Photon.Rev. 8, pp.889–895 (2014).

[129]. S. Kivistö, J. Puustinen, M. Guina, R. Herda, S.Marcinkevicius, E. Dianov, and O. Okhotnikov, "Pulse dynamics of a passively mode-locked Bi-doped fiber laser," Opt. Express, 18, pp. 1041–1048 (2010).

[130]. B. Chapman, E. Kelleher, S. Popov, K. Golant, J. Puustinen, O. Okhotnikov, and J. R. Taylor., "Picosecond bismuth-doped fiber MOPFA for frequency conversion," Opt. Lett. 36, 3792 (2011).

[131]. X. Yang, L. Zhang, H. Jiang, T. Fan, Y. Feng, "Actively mode-locked Raman fiber laser," Opt. Express 23, 19831 (2015).

[132]. X. Zhu, G. Zhu, C. Wei, L. Kotov, J. Wang, M. Tong, R. A. Norwood, and N. Peyghambarian., "Pulsed fluoride fiber lasers at 3 μm," J. Opt. Soc. Amer. B 34, A15-A28 (2017)

[133]. X. Zhu, J. Zong, A. Miller, K. Wiersma, R. A. Norwood, N. Prasad, A. Chavez-Pirson, and N. Peyghambarian., "Single-frequency Ho^{3+}-doped ZBLAN fiber laser at 1200nm," Opt. Lett. 37, 4185 (2012).

[134]. X.Zhu, J. Zong, K.Wiersma, R. A. Norwood, N. Prasad, M. Obland, A. Chavez-Pirson, and N. Peyghambarianl., "Watt-levelshort-length holmium-doped ZBLAN fiber lasers at 1.2 μm," Opt. Lett., 39, 1533 (2014).

[135]. S. Liu, X. Zhu, G. Zhu, K. Balakrishnan, J. Zong, K. Wiersma, A. Chavez-Pirson, R. A. Norwood, and N. Peyghambarian., "Graphene Q-switched Ho^{3+}-doped ZBLAN fiber laser at 1190nm," Opt. Lett., 40, 147 (2015).

[136]. Y. Wang, X. Zhu, J. Zong, K. Wiersma, A. Chavez-Pirson, C. Sheng, R. A. Norwood, and N. Pegyhambarian, "SESAM Q-switched fiber laser at 1.2 µm," in CLEO, OSA: STh4O.8 (2016).

[137]. X. Yang, L. Zhang, Y. Feng, X. Zhu, R. A. Norwood, N. Peyghambarian, "Mode-Locked Ho^{3+}-Doped ZBLAN Fiber Laser at 1.2 µm," J. Lightw. Technol. 34, 18 (2016)

[138]. S. Y. Set, H. Yaguchi, Y. Tanaka, M. Jablonski,"Lase rmode-locking using a saturable absorber incorporating carbon nanotubes," J. Lightw. Technol. 22, 51 (2004).

[139]. S. Y. Set, H. Yaguchi, Y. Tanaka, M. Jablonski, "Ultrafast fiber pulsed lasers incorporating carbon nanotubes," IEEE J. Sel. Topics Quantum Electron. 10, 137 (2004).

[140]. S. Yamashita, Y. Inoue, K. Hsu, S. Y. Set, M. Jablonski, H. Yaguchi, T. Kotake, K. Sato, "A 2-cm-long fiber Fabry–Perot mode-locked laser incorporating carbon nanotubes," in CLEO, San Francisco, CA, 2004, Paper CTuD7.

[141]. S. Yamashita, Y. Inoue, S. Maruyama, Y. Murakami, H. Yaguchi, M. Jablonski, and S. Y. Set, "Saturable absorbers incorporating carbon nanotubes directly synthesized onto substrates and fibers and their applications to mode-locked fiber lasers," Opt. Lett. 29, 1581 (2004).

[142]. M. Solodyankin, E. Obraztsova, A. Lobach, A. Chernov, A. Tausenev, V. Konov, and E. Dianov, "Mode-locked 1.93µm thulium fiber laser with a carbon nanotube absorber" Opt. Lett. 33, 1336 (2008)

[143]. D. Popa, Z. Sun, T. Hasan, W. Cho, F. Wang, F. Torrisi, A. Ferrari,"74-fs nanotube-mode-locked fiber laser," Appl. Phys. Lett. 101, 153107 (2012)

[144]. G. Sobon, A. Duzynska, M. Swiniarski, J. Judek, J. Sotor, M. Zdrojek,"CNT-based saturable absorbers with scalable modulation depth for Thulium-doped fiber lasers operating at 1.9 µm," Scientific Reports 7, Article number: 45491 (2017)

[145]. S.Yong-Won, S.Y. Set, S. Yamashita, C. Gosh, T. Kotake,"1300-nm pulsed fiber lasers mode-locked by purified carbon nanotubes,"   IEEE photonics technology letters 17, 8 1623-1625 (2005).

[146]. X. Zhu, J. Zong, A. Miller, K. Wiersma, R. A. Norwood, N. S. Prasad, A. Chavez-Pirson, and N. Peyghambarian, "Single-frequency Ho^{3+}-doped ZBLAN fiber laser at 1200 nm," Opt. Lett. 37, 4185-4187 (2012).